REPORT DOCUMENTATION PAGE

1. AGENCY USE ONLY (Leave blank)	2. REPORT DATE April 2001	3. REPORT TYPE AND DATES COVERED Final Report, 2001

4. TITLE AND SUBTITLE
Transient Application, Recirculating Pool Fire, Agent Effectiveness Screen: Final Report, NGP Project 3A/2/890

5. FUNDING NUMBERS
N/A

6. AUTHOR(S)
William Grosshandler, Anthony Hamins, Kevin McGrattan, and Cary Presser

7. PERFORMING ORGANIZATION NAME(S) AND ADDRESS(ES)

Building and Fire Research Laboratory
National Institute of Standards and Technology
Gaithersburg, Maryland

Chemical Science and Technology Laboratory
National Institute of Standards and Technology
Gaithersburg, Maryland

8. PERFORMING ORGANIZATION REPORT NUMBER
N/A

9. SPONSORING / MONITORING AGENCY NAME(S) AND ADDRESS(ES)
SERDP
901 North Stuart St. Suite 303
Arlington, VA 22203

10. SPONSORING / MONITORING AGENCY REPORT NUMBER
N/A

11. SUPPLEMENTARY NOTES

12a. DISTRIBUTION / AVAILABILITY STATEMENT
Approved for public release: distribution is unlimited.

12b. DISTRIBUTION CODE
A

13. ABSTRACT *(Maximum 200 Words)*
In this study, a laboratory-scale facility has been developed to screen the suppression effectiveness of agents that are delivered in a transient fashion such as solid propellant gas generators. The transient application, recirculating pool fire (TARPF) agent effectiveness screen features a propane fire stabilized behind an obstruction, which is known to be a highly challenging suppression configuration. The character of the flame and the impact of the air flow, fuel flow, obstruction geometry, and rate of agent addition on the amount of material needed for importance of the injection process on the flow field and the transport of the agent downstream is examined, and a simple mixing model is used to explain the observed trend of decreasing suppressant mole fraction with increasing injection duration, even for agents as different as CF_3Br and N_2. Direct numerical simulation of the suppression event is shown to successfully predict the quantity and rate of N_2 required to extinguish the flame based upon a published global reaction fate for premixed propane/air flame propagation.

14. SUBJECT TERMS
SERDP, SERDP Collection, fire suppression, halon alternatives, aircraft fire

15. NUMBER OF PAGES
85

16. PRICE CODE
N/A

17. SECURITY CLASSIFICATION OF REPORT	18. SECURITY CLASSIFICATION OF THIS PAGE	19. SECURITY CLASSIFICATION OF ABSTRACT	20. LIMITATION OF ABSTRACT
unclass	unclass	unclass	UL

20020913 086

Transient Application, Recirculating Pool Fire, Agent Effectiveness Screen: Final Report, NGP Project 3A/2/890

William Grosshandler, Anthony Hamins, and Kevin McGrattan
Building and Fire Research Laboratory
and
Cary Presser
Chemical Science and Technology Laboratory
National Institute of Standards and Technology
Gaithersburg, MD 20899

April, 2001

4 TITLE AND SUBTITLE Transient Application, Recirculating Pool Fire, Agent Effectiveness Screen: Final Report, NGP Project 3A/2/890	5 FUNDING NUMBERS
6 AUTHOR(S) William Grosshandler, Anthony Hamins, Kevin McGrattan and Cary Presser	

7 PERFORMING ORGANIZATION NAME(S) AND ADDRESS(ES) National Institute of Standards and Technology Gaithersburg, MD 20899	8 PERFORMING ORGANIZATION REPORT NUMBER

9 SPONSORING/MONITORING AGENCY NAME(S) AND ADDRESS(ES) The Department of Defense Strategic Environmental Research and Development Program	10. SPONSORING/MONITORING AGENCY REPORT NUMBER

11 SUPPLEMENTARY NOTES

12a DISTRIBUTION/AVAILABILITY STATEMENT	12b DISTRIBUTION CODE

13 ABSTRACT (Maximum 200 words)

In this study, a laboratory-scale facility has been developed to screen the suppression effectiveness of agents that are delivered in a transient fashion such as solid propellant gas generators. The transient application, recirculating pool fire (TARPF) agent effectiveness screen features a propane fire stabilized behind an obstruction, which is known to be a highly challenging suppression configuration. The character of the flame and the impact of the air flow, fuel flow, obstruction geometry, and rate of agent addition on the amount of material needed for importance of the injection process on the flow field and the transport of the agent downstream is examined, and a simple mixing model is used to explain the observed trend of decreasing suppressant mole fraction with increasing injection duration, even for agents as different as CF_3Br and N_2. Direct numerical simulation of the suppression event is shown to successfully predict the quantity and rate of N_2 required to extinguish the flame based upon a published global reaction rate for premixed propane/air flame propagation.

(*Appendix A is also identified in NISTIR 6733)

14 SUBJECT TERMS fire suppression, halon alternatives, aircraft fires	15 NUMBER OF PAGES 85
	16. PRICE CODE

17 SECURITY CLASSIFICATION OF THIS REPORT UNCL	18. SECURITY CLASSIFICATION OF THIS PAGE UNCL	19. SECURITY CLASSIFICATION OF ABSTRACT UNCL	20 LIMITATION OF ABSTRACT none

EXECUTIVE SUMMARY[*]

Because of its many positive attributes, halon 1301, or trifluorobromomethane (CF_3Br), has been used as a fire extinguishing agent in many applications including aircraft, ships, and specialized structures. Due to its high ozone depletion potential, however, world-wide production was halted in 1994. In the search for a long-range replacement, novel types of extinguishing agents and delivery mechanisms are under development. To gauge the suitability of a replacement agent, methods are needed to evaluate the material's suppression effectiveness under conditions that relate to field applications.

In this study, a laboratory-scale facility has been developed to screen the suppression effectiveness of agents that are delivered in a transient fashion such as solid propellant gas generators. The transient application, recirculating pool fire (TARPF) agent effectiveness screen features a propane fire stabilized behind an obstruction, which is known to be a highly challenging suppression configuration. The character of the flame and the impact of the air flow, fuel flow, obstruction geometry, and rate of agent addition on the amount of material needed for suppression are evaluated for N_2, CF_3Br, and a solid propellant gas generator (SPGG). The importance of the injection process on the flow field and the transport of the agent downstream is examined, and a simple mixing model is used to explain the observed trend of decreasing suppressant mole fraction with increasing injection duration, even for agents as different as CF_3Br and N_2. Direct numerical simulation of the suppression event is shown to successfully predict the quantity and rate of N_2 required to extinguish the flame based upon a published global reaction rate for premixed propane/air flame propagation.

Important Findings:

- The minimum mole fraction of agent for suppression, normalized by the cup burner value, correlates with $[1 - \exp(-\Delta t/\tau)]^{-1}$, where Δt is the injection time interval and τ characterizes the mixing time behind the obstacle in the flow.
- The general character of the flame and its extinction by a thermal gaseous agent is captured by a direct numerical simulation of the flow based upon single-step chemistry, and numerical experiments have corroborated the simple correlation of the experimental data for N_2.
- The measured difference between the decrease in agent storage bottle pressure and the arrival of the agent at the fire highlight the importance of determining the agent concentration locally and the difficulty in relating changes in bottle pressure to actual mixing conditions.
- For the first time, both compressed and solid-propellant generated gases can be compared side by side, and the effect on performance of different formulations, particle loadings and burning rates for various SPGG designs can be unambiguously discriminated.
- When the temperature of a hot surface downstream of the pool is above 800 °C, the flame, following suppression, will reignite and stabilize on the hot surface. At a temperature below 800 °C, the number of reignitions approaches zero. This result is in contrast to when the hot surface is located between the stabilizing step and the fuel pool, in which a delayed reignition can be observed at temperatures as low as 400 °C.
- The effectiveness of suppression with a liquid agent is dependent upon how well the droplets are entrained into the flame zone downstream of the stabilizing obstacle.

---

[*]The content of this report is the same as that found in NISTIR 6733 (see bibliography).

ACKNOWLEDGEMENTS

DISCLAIMER

TABLE OF CONTENTS

INTRODUCTION

The Fire Suppression Problem

Water sprinklers are commonly chosen to automatically protect buildings and their contents against fire because sprinklers are highly reliable, inexpensive to install and maintain, and water is non-toxic and friendly to the environment. Alternatives to water suppression are usually required if the situation calls for a very rapid response, if the primary fuel source is a gas or an evaporating liquid, if the protected space contains electrically energized or other water sensitive equipment, or if the application is weight and volume limited. Until recently, one would most likely find halon 1301, or trifluorobromomethane (CF_3Br), as the fire extinguishing agent alternative to water, especially if people had a chance of being exposed at the time of discharge. Due to its high ozone depletion potential, however, world-wide production of CF_3Br was halted in 1994.

In spite of almost a decade of significant research activity, no single chemical or suppression system has been identified that has all the positive attributes of halon 1301. Depending upon the application, one or another candidate system may appear to hold promise. Full-scale suppression testing is always essential to demonstrate acceptability, in spite of the fact that the full-scale tests are strongly influenced by the initial and boundary conditions surrounding the fire and suppression event. Complex, non-linear relationships among the agent, the flow field, and the fire cannot be unraveled from these full-scale suppression tests because critical parameters cannot be controlled tightly enough and the number of tests is constrained by cost, time, safety and environmental considerations.

The U.S. Department of Defense is committed to reducing its dependence on halon 1301 and has made great strides in this direction by eliminating non-essential uses, totally revamping its fire suppression system certification and recycling procedures, and replacing halon systems with alternative technologies where possible. There remain some applications where no substitute chemical or system has been judged satisfactory, and several others where the alternatives identified to date are saddled with serious deficiencies. One of these applications is for military aircraft, which are particularly vulnerable to fire during combat and also need in-flight fire protection during routine missions, a need shared by the commercial fleet.

The amount of a gaseous agent required to extinguish fires in full-scale engine nacelles varies greatly with the geometry of the test fixture and the manner in which the flame is stabilized. It has been observed that if the test is designed to allow fuel to collect behind obstacles in the vicinity of a hot surface, a significantly higher mass of agent is necessary for sustained suppression [1]. The superior performance of chemically acting agents such as CF_3Br and CF_3I relative to a hydrofluorocarbon alternative like HFC-125 is also accentuated in some of these tests. Full-scale testing carried out by the Navy using two different fixtures, each meant to simulate fires in the F/A-18 engine nacelle, led to different conclusions regarding the amount and relative performance of both HFC-125 and solid propellant gas generator (SPGG) fire suppressants [2].

The complexity and unpredictability of full-scale tests can be traced to two factors: flame stabilization, and agent mixing. Flame stability is governed by local geometry, surface temperature, and fuel and air flow patterns. Flame extinction will occur if the agent is entrained into the flame zone in sufficient concentration, if the fuel and air flows are disrupted enough by the agent discharge process, or by a combination of the two effects. Entrainment and localized flame stretch are, in turn, controlled by the way the fire suppression system is designed and by the location of the fire relative to the discharge nozzle.

Figure 1 shows a full-scale mock-up of an F-22 engine nacelle built by the Air Force Research Laboratory at Wright-Patterson AFB, which was used to test the suppression effectiveness of HFC-125 and SPGG as compared to Halon 1301 [3]. When the engine mock-up is slid in on its rails,
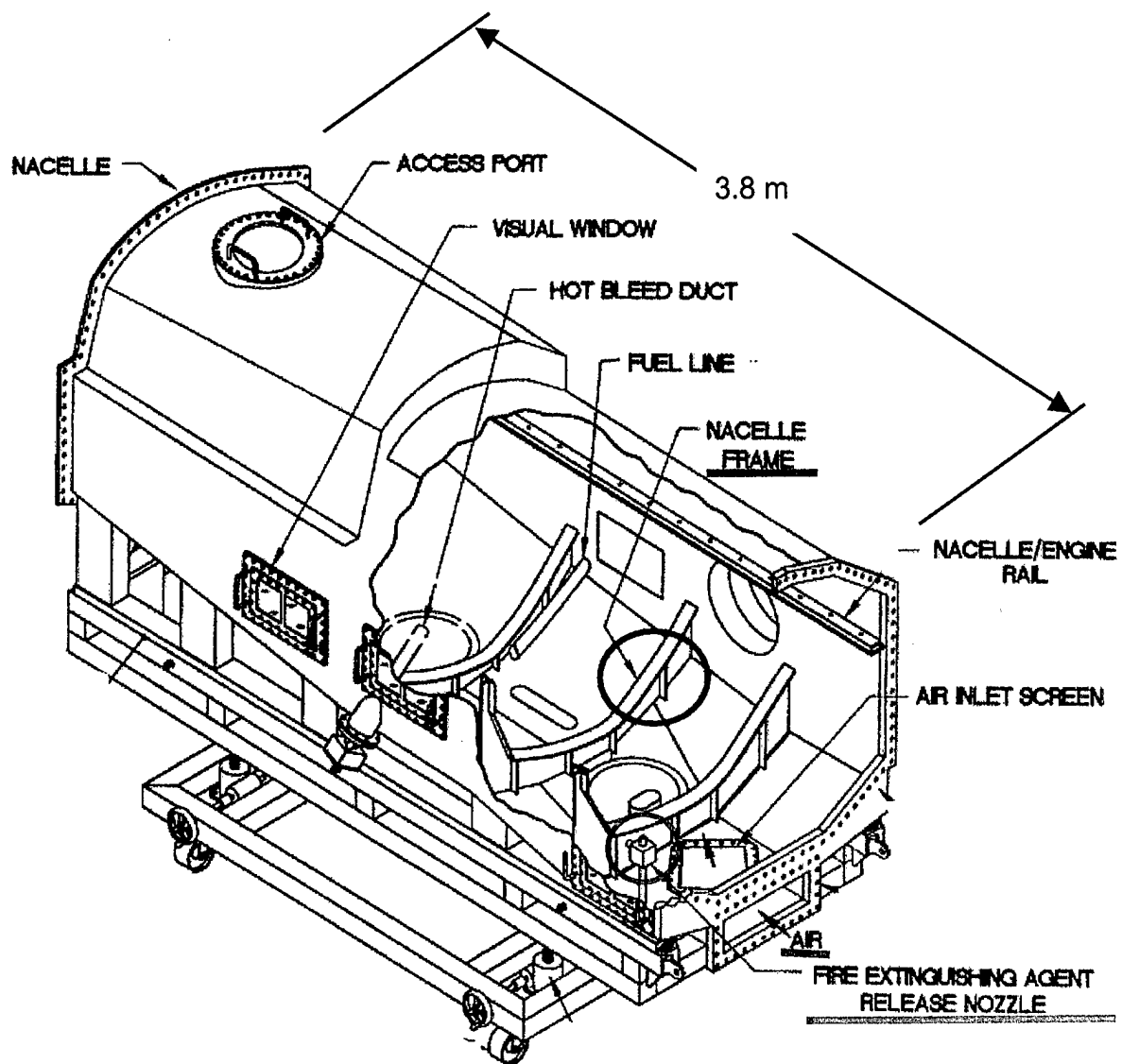
Figure 1. Full-scale F-22 Engine Nacelle Simulator at WPAFB [3, Hamins et al, 1997]

an annular region is formed about the core where flammable vapors can build and leaking fuel can accumulate. Air is brought in through a scoop at the lower right of the structure, it mixes with fuel vapor and/or a spray from a simulated leaking hydraulic, fuel or lubricating oil line, and is ignited by a spark or hot surface such as the bleed-air line. A fire can be stabilized anywhere that the fuel and air mixture is within its flammable limits and the local velocity is below the flame speed. The many obstructions in the flow formed by the nacelle frame, fuel lines, and miscellaneous equipment in the nacelle and on the engine core act as flame holders. The fire extinguishing agent is released into the nacelle near the air inlet. Depending upon the amount of agent released, the rate of agent addition, the presence of hot surfaces or electric arcs, and the location of the fire relative to the injection point, the fire may or may not be fully extinguished. An engine nacelle simulator such as the one in Fig. 1 is useful for demonstrating that a particular agent or system can successfully control full-scale fires, but it is not suited for screening the suppression effectiveness of new compounds, for ranking alternative technologies, or for gaining understanding of fire suppression physics.

Previous Studies
Agent suppression effectiveness for liquid fuel fires such as those described in NFPA 2001 is determined in a laminar diffusion flame using a cup burner [4]. Measurements of suppression effectiveness using a counter-flow burner are preferred for revealing the detailed chemical pathways in the process [5]. In either of these burners the minimum concentration for suppression is found by increasing the agent flow slowly until a critical mole fraction is achieved in the oxidizer stream and flame extinction is observed. In practice, however, agents designed to replace CF_3Br are discharged rapidly, not quasi-statically. Solid propellant gas generators, for example, typically discharge in 10 ms to 500 ms. A robust and repeatable means to evaluate the effectiveness of different formulations and application rates requires a non-conventional screening device.

Hirst and Sutton [6] developed a wind tunnel to explore the impact of step height, air flow, and pressure on the blow-out of a jet fuel pool fire stabilized behind a backward facing step. Hirst et al. [7] studied the suppression of these types of fires using various halons, and concluded that a liquid pool burning in a flow behind an obstacle is the most difficult fire to extinguish. This was born out in full-scale tests done later [8]. Experiments by Hamins et al. [9], in cooperation with Walter-Kidde Aerospace, were conducted in a wind tunnel scaled down from the earlier work by Hirst to examine the performance of HFC-125 and HFC-227ea. Investigations at the Air Force Research Laboratory [10] as part of the Next Generation Program (NGP) sought to determine the detailed structure during suppression of a non-premixed methane/air flame stabilized behind a step. The changing character of the flame with step height and air velocity was examined, along with the amount of halon 1301 required to suppress the flame as a function of the flow parameters and injection interval.

A turbulent spray burner was designed in earlier work at NIST [11] to simulate an engine nacelle spray fire resulting from a ruptured fuel or hydraulic fluid line. In this apparatus, the agent release and mixing process were well controlled and the air flow was maintained constant with a sonic orifice. This arrangement allowed the agent to be discharged without disrupting the incoming air. The turbulent spray burner was used with both gaseous and powdered agents. Hamins et al. [9] redesigned the burner to include a heated disk in the center of the flow downstream of the fuel nozzle. They showed that the concentration of nitrogen necessary to extinguish a turbulent propane flame increased substantially with surface temperature. The same trend, but to a lesser degree, was observed with hydrofluorocarbons.

Previous studies have demonstrated the effectiveness of SPGGs and their hybrids in full-scale fire suppression experiments [12, 3]. Solid propellant gas generators undergo rapid solid-phase reactions producing inert gases, principally carbon dioxide, water vapor, and nitrogen, as well as particulates composed of inorganic salts. Each component individually behaves as a fire suppressant. For many applications, particulate use is unacceptable and the SPGG hardware is typically designed to filter particulate mass during deployment. Hybrid generators are particularly attractive for some special situations such as inhabited spaces or cold temperature applications [13]. The hybrids use the hot inert

3

SPGG exhaust to vaporize and expel a secondary suppressant, typically a liquid, such as water or a low boiling point halocarbon, through a nozzle [12].

Objectives
The research reported here addresses the issues mentioned above for which a full-scale facility is not suited; i.e., screening the fire suppression effectiveness of new chemical compounds, ranking alternative technologies, and gaining understanding of fire suppression physics. The specific objectives put forth in the original proposal were to provide a well-characterized test fixture for screening the effectiveness of agents to suppress and prevent re-ignition of a turbulent, obstructed flame; to allow evaluation of the impact of transient agent delivery on flame extinguishment; and to provide a means to screen the effects of new and currently available agents on solid and liquid fuel surfaces.

Full funding for the three year period was to deliver the following products:

- a well-characterized bench-scale suppression screen for comparing the performance of gaseous agents and dispersed fluid mists in suppressing and preventing re-ignition of a turbulent, obstructed flame burning either gaseous or condensed fuels;
- documentation on the screen apparatus including detailed design information and experimental procedures, with round-robin testing among interested partners to insure utility of the documentation;
- an evaluation of the impact of transient agent delivery on flame extinguishment; and
- development of a means to screen the effects of new agents on condensed (solid and liquid) fuel surfaces.

The focus of the research deviated a bit from what was originally proposed, in some instances due to budget reductions and in others due to discovery.

- Solid fuels were not examined because there was no evidence that they posed a greater threat than propane in this scenario.
- A formal round-robin was not established, but work conducted during the same period at the University of Maryland (see below) and the Air Force Research Laboratory helped to support the conclusions drawn in the current study.
- The design for the liquid mist agent delivery system was not finalized due to the complexity of the process, although the general direction for such a system and its likely capabilities were revealed.
- More emphasis was placed on the deployment of an SPGG suppression effectiveness screen.

As part of the initial cost-sharing commitment, NIST gave a grant to the University of Maryland to examine fluid mechanical and heat transfer phenomena that cause an engine nacelle fire to be particularly difficult to suppress [14]. The objectives of that study were to evaluate the stability of a recirculation zone behind a backward-facing step under conditions expected in an aircraft engine nacelle, and to evaluate the effects of the flow structure on a propane diffusion flame established downstream of the step to characterize a "worst case" fire scenario. The final report from that grant is included as Appendix B to this document.

4

EXPERIMENTAL FACILITY

A Transient Application, Recirculating Pool Fire (TARPF) suppression facility has been developed in the current study to screen different agents and prototype systems, and as an indicator of full-scale performance. The TARPF agent suppression screen is designed to reproduce the most difficult fire situation and to allow control of critical agent discharge parameters, including agent discharge rate and duration, air flow, and obstacle geometry. The performance of gaseous agents, aerosols and solid-propellant gas generators can be examined.

Wind Tunnel and Burner

The TARPF is a small wind tunnel consisting of a number of sections, as shown schematically in Fig. 2. The main portion of the tunnel is 2.5 m long with a square cross section 92 mm on a side. (Refer to Appendix A for detailed mechanical drawings of key components of the facility.) Air, supplied by a compressor rated for a maximum flow of 180 g/s at 1.0 MPa, can be delivered to the tunnel at speeds, averaged over the 92 mm square cross section, up to 17 m/s. Flow is monitored using a calibrated sonic orifice and a piezoelectric pressure transducer. A heater is available to increase the inlet air temperature to above 200 °C. A honeycomb flow straightener and mixing screens are located a meter upstream of the test section. The burner consists of a sintered bronze plate, 92 mm wide by 190 mm long. Propane is the primary fuel used, which can be supplemented with a JP-8 spray. The expanded relative uncertainty* in the flows of fuel and air are ± 5 % of the measured value, based upon the manufacturers' specifications for the metering orifice and mass flow controllers.

Stainless steel baffles between 10 mm and 55 mm high are located upstream of the burner. A ramp can also be inserted to form a 25 mm high backward-facing step, as seen in Fig. 2. A 25 mm high vee-shaped obstruction can be located downstream of the propane pool to form a cavity and a second anchoring position for the flame. An ethane torch located below the vee and external to the tunnel is used to heat the surface temperature up to 900 °C for reignition studies. The fire is initiated by a spark across two protruding electrodes located on the side wall of the test section 20 mm above the surface of the burner and 20 mm downstream of the step. Heat release rates assuming complete combustion are up to 10 kW. The flame is viewed from above and the side through 6 mm thick Pyrex windows by a 30 Hz video camera to record the suppression process. For some experiments, a high-speed digital camera (1000 Hz) is used to investigate the flame dynamics. A photograph of the TARPF with a close up of a typical flame taken through the window is shown in Fig. 3.

Gaseous Agent Discharge

The fire suppressing agent is injected downstream of the air metering orifice. Since the air flow is choked by the metering orifice, the introduction of the agent can be accomplished without altering the total air flow. This is particularly critical when trying to distinguish chemical from physical modes of extinction. Mixing of the agent with the air is facilitated by injecting the agent through two opposed radial ports into the reduced diameter entrance region. (See Appendix A for details on the injector design.)

---

* The expanded relative uncertainty on all dimensions and independent parameters described in this report is ± 50 % of the highest significant place reported, with a coverage factor of 2 [15], unless otherwise stated.
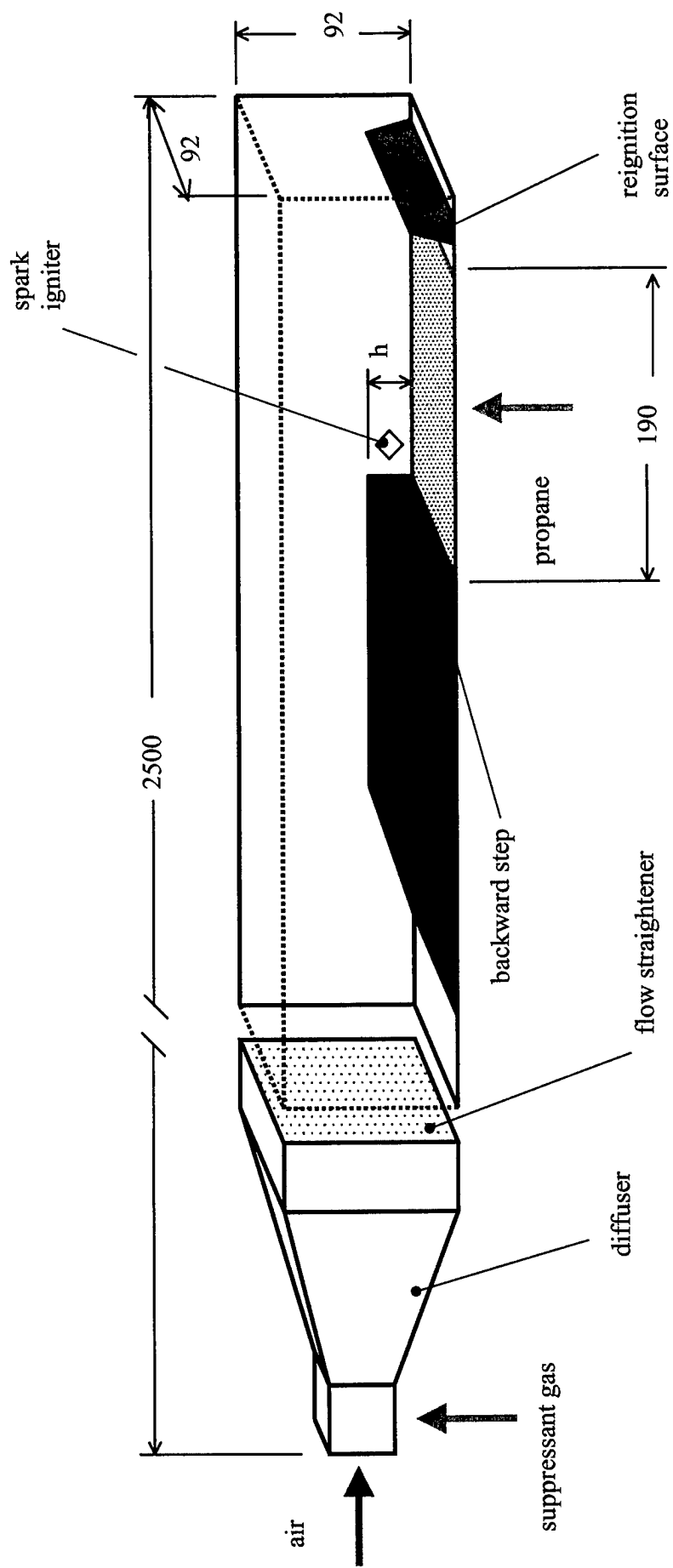
Figure 2. Schematic of step-stabilized pool fire apparatus. Dimensions are in millimeters.

6
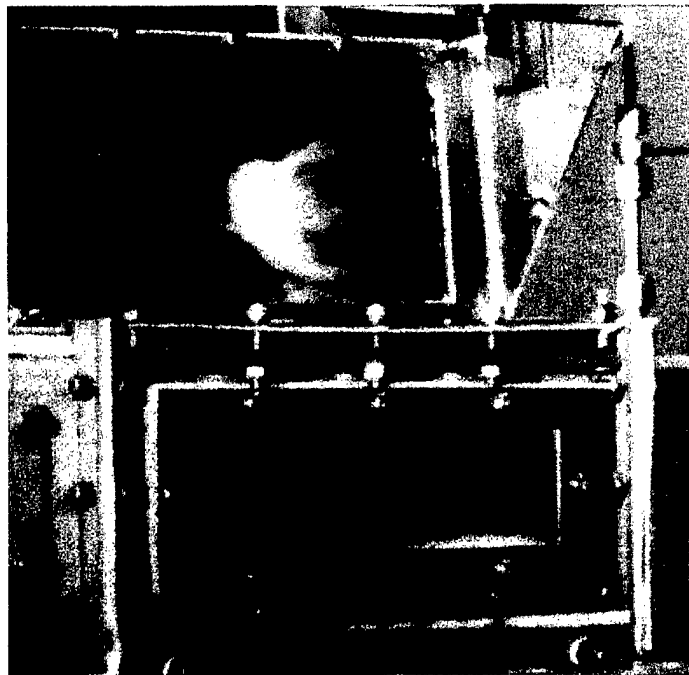
Figure 3. Photograph of TARPF with close-up of baffle-stabilized propane flame.
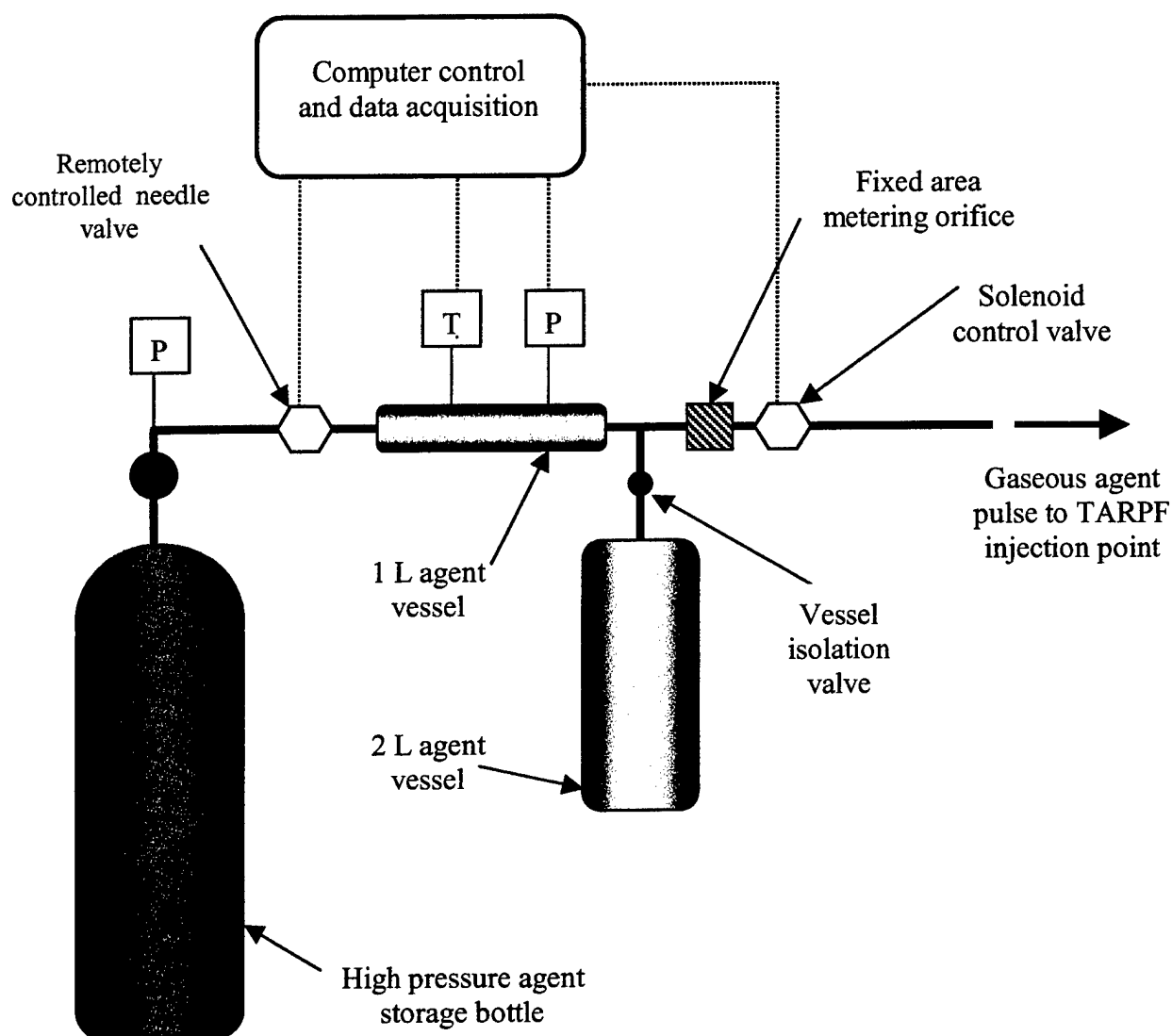
Figure 4. Schematic diagram of gaseous agent injection system.

Nitrogen (0.99995 volume fraction pure), CF₃Br (commercial grade), and HFC-125 (commercial grade) are stored as gases in one and two liter stainless steel vessels with the pressure monitored by a high-speed (1 ms response) piezoelectric transducer, and the temperature measured with a chromel-alumel (76 mm diameter) thermocouple. An electronic timer controls the interval (10 ms to 1000 ms) that a solenoid valve on the agent vessel remains open. The agent passes through a 6 mm diameter orifice before it is injected through two opposed radial ports into the air passage upstream of the diffuser. A computer monitors the flow controllers, pressure transducers, and thermocouples, and sends a signal to the electronic timer to open and close the solenoid valve while releasing the flow of suppressant. Figure 4 shows schematically the elements of the gaseous injection system.

The mass of the gaseous agent released is determined from the change in pressure and temperature in the storage vessels. The expanded uncertainty in the calculated mass is ± 2 %, with a minimum absolute uncertainty of 0.12 g attributable to the resolution of the pressure transducer. The discharge rate and duration are controlled by the initial agent pressure and an electronically actuated solenoid valve. Figure 5 is a pressure trace taken during a typical nitrogen discharge. The initial pressure is set to 0.96 MPa with an electronically controlled metering valve located between a standard
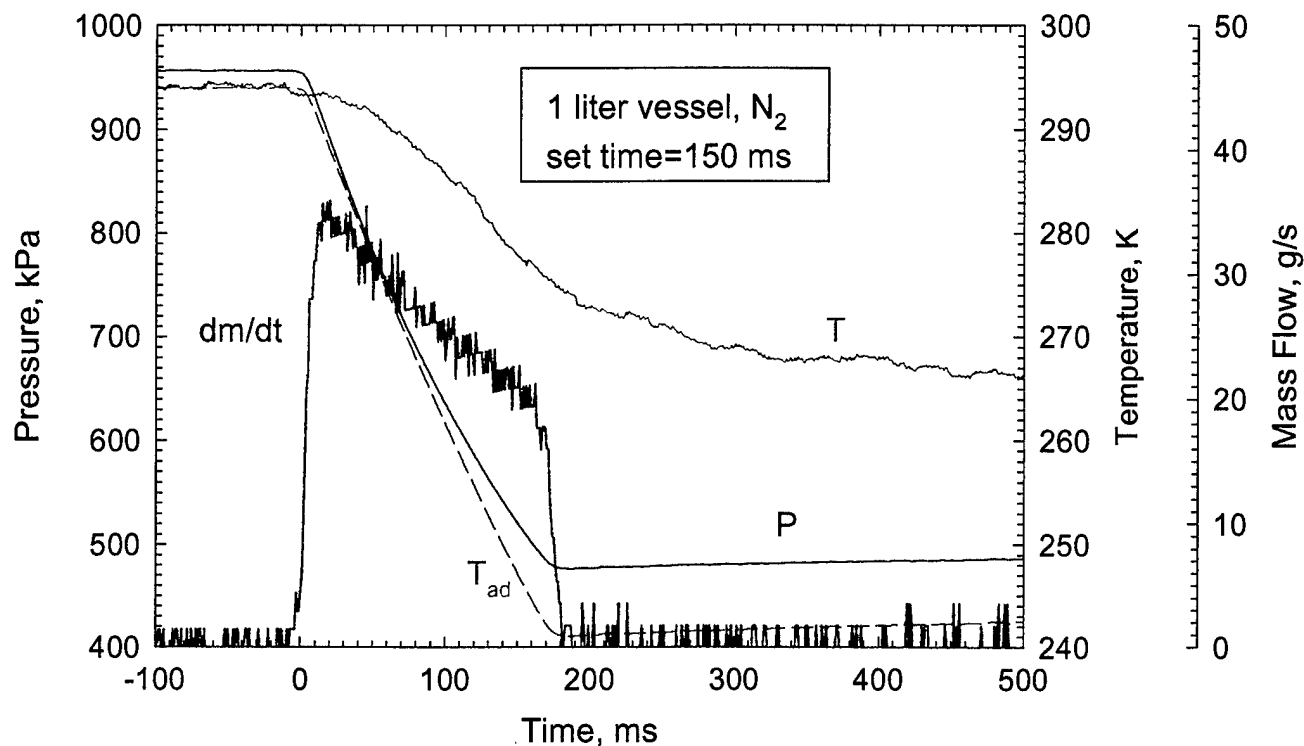
Figure 5. Storage vessel pressure trace and temperature during discharge of nitrogen into TARPF.

high pressure nitrogen gas bottle and the stainless steel agent bottle. The computer acquires background data on the initial state for one second, at which point the electric solenoid valve is opened to allow nitrogen to enter the wind tunnel. An electronic timer closes the valve after the desired interval. Pressure and temperature in the agent bottle are measured at a frequency of 1000 Hz during the discharge process. The piezoelectric pressure transducer is able to follow the change within about 5 kPa, but the thermocouple is too slow. To determine the instantaneous mass discharge (dm/dt in Fig. 5), the nitrogen is assumed to be an ideal gas with the expansion inside the bottle occurring isentropically. The temperature of the thermocouple is recorded to within 1 °C. However, the actual gas temperature could differ by tens of degrees since the thermocouple bead adjusts much more slowly due to its thermal inertia. The gas temperature is more appropriately estimated by the theoretical adiabatic value, T_{ad}. Assuming errors propagate in a normal fashion, the uncertainty of dm/dt is estimated to be $\pm$ 2 g/s.

Three observations can be made from the shape of the discharge curve in Fig. 5: (i) the discharge data are much noisier than the pressure data, because they rely on the gradient of pressure; (ii) the measured interval (about 180 ms) is longer than the 150 ms interval set in the electronic timer, due to the inertia of the solenoid valve; and (iii) the discharge rate at the start of the process is markedly higher than the average rate.

Aerosol Agent Control
Aerosol agents require a totally different injection system than what has been described above or used previously. Yang et al. [16, 1999] developed a means to accurately meter alternative liquid agents using a nebulizer, but their screening device operated in a continuous rather than impulsive mode. Commercial

9
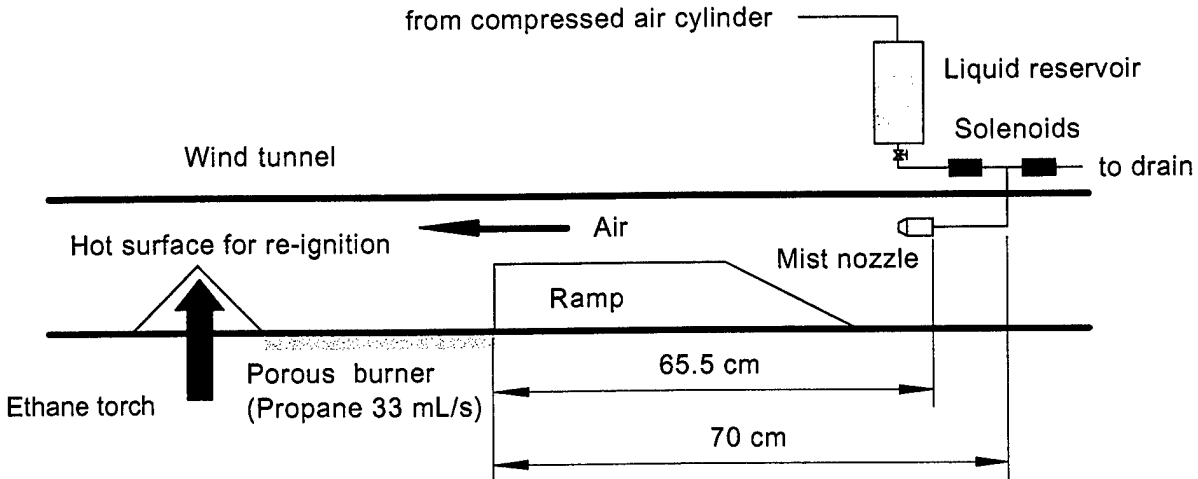
Figure 6. Liquid aerosol agent injection system.

fuel injectors were considered but the flow rates and injection duration were not adjustable over the range and with the precision necessary for the current application.

Figure 6 shows the aerosol injection system developed for the TARPF. Several kinds of atomizers were used to introduce and fully disperse misted agents into the upstream air passage under various conditions, including the introduction of aerosol at different locations along the tunnel air passage, different atomizer operating conditions such as different spray angles, liquid flow rates, and transient duration times. The liquid dispensing system consists of a liquid reservoir, a compressed air cylinder, two computer-controlled solenoids, and a hollow-cone atomizer. The atomizer was positioned equi-distanced vertically between the ramp and the upper wall of the wind tunnel, and at discrete locations along the air passage from 65.5 cm upstream of the propane porous burner to a location downstream near the ramp. Several different atomizers were used while trying to obtain a well-dispersed spray of droplets in the air passage. The atomizers were operated at line pressures that varied between 0.27 MPa and 0.69 MPa in an attempt to affect the quality of atomization. The atomizers were commercially manufactured to the following: (1) a nominal spray angle of 70° when operated at 1.03 MPa with a flow rate of 1.9 mL/s, and (2) a nominal spray angle of 60° when operated at 0.69 MPa with a flow rate of 1.1 mL/s. Operating these atomizers at nominal pressures normally results in a fully developed spray, and thus an increase above the nominal condition has a small effect on further reducing droplet size. When positioned at upstream locations, the spray appeared to fill the entire air passage cross section.

To initiate a mist for a fixed duration, the data acquisition system activated the solenoid that was connected to the reservoir. At the end of the discharge, the solenoid is deactivated to terminate the flow to the atomizer. The second solenoid leading to a drain is simultaneously activated to prevent any residual flow to the nozzle and dripping from the nozzle.

Liquid Fuel Injector/Hot Surface Arrangement
To investigate different re-ignition scenarios, a hot surface obstruction was set up immediately downstream of the propane porous burner (see Fig. 6). The vee-shaped obstruction was 25 mm in height, the base was 25 mm wide, and was centered across 50 mm of the wind tunnel passage (see Appendix A. for detailed drawings). An S-type thermocouple was place on the external upstream surface of the obstruction. A high-resistance ceramic adhesive (max: 1500 °C) was used to adhere the thermocouple to the Inconel surface, 15.5 mm thick. An ethane torch was supported underneath the obstruction to heat the

10

inner surface to over 1100 °C. A mass flow controller was used to regulate the obstruction surface temperature. A stream of JP-8 droplets was used to provide a source of re-ignition for the propane flame by directing the droplets directly onto the heated obstruction after flame suppression. The droplet array was generated from a 0.14 mm sapphire orifice that was pressure fit into a 3.1 mm tube. The tube was inserted into the wind tunnel passage from the top wall at a position 25 mm upstream of the flame stabilizing obstacle. The end of the tube (3.8 mm) was bent 90° into the direction of the air stream, and was centered between the passage top wall and face of the ramp. The JP-8 was forced through the injector with nitrogen back pressure at 170 kPa. The low back pressure and several sintered filters (with a pore size of 7 μm and 2 μm) were used to help prevent clogging of the injector. Initially, piezo-electric crystals were used to initiate droplet breakup, but impingement of the fuel on the heated obstruction was difficult due to entrainment of the individual droplets into the high-velocity air flow. Impingement was achieved successfully by directing the non-atomized fuel stream on the heated obstruction. The JP-8 injection time (controlled by a solenoid valve), and flow rate were varied in order to optimize the impingement process. The impingement of the fuel onto the obstruction surface resulted in a significant decrease in the surface temperature and thus care was taken to compensate for this effect during experiments.

SPGG Facility and Operation

Gas generators are manufactured in discrete units using specific chemical formulations and orifice sizes that are designed based on the particular application. Unlike a compressed gas or aerosol discharge, the TARPF operator can control neither the total mass discharged nor the injection time interval of the SPGG. To accommodate this limitation, a custom discharge chamber was designed to allow the operator to select the fraction of the SPGG discharge that is injected into the flame zone. The hardware was designed to allow standard size gas generators (which contain significantly more material than is required for suppression in the TARPF) to be evaluated by repeating the test sequence with identical gas generators and incrementally increasing the fraction of SPGG effluent allowed to flow into the TARPF air stream. The SPGG effluent (gas and particulate) passes through a metering orifice and is injected into the air stream using the same manifold as for the compressed gaseous agents. (Refer to Fig. 8a.) The flow through the bypass port is discarded into a laboratory exhaust hood. The pressure in the discharge chamber is monitored by a 1 ms response piezoelectric transducer and the temperature is measured with a 76 μm type K thermocouple. A computer monitors the pressure transducer and thermocouple.

Figure 7 shows a photograph of the TARPF and the location of the SPGG injection system; Figure 8a is a schematic diagram of the SPGG injection system; and Fig. 8b is a close-up photograph. The discharge chamber is made of stainless steel with an internal volume of approximately 200 mL. There are four main ports on the discharge chamber as seen in Fig. 8: (1) a port with a ¾ NPT female thread connecting to the gas generator cartridge holder, (2) a variable area metering orifice (1.6 mm to 6.4 mm diameter) to limit the flow into the TARPF, (3) a bypass port tapped for a 2 NPT nipple, and (4) a 19 mm port for mounting a pressure relief blow-out diaphragm. A housing made of 6 mm thick steel (seen in Fig. 8) encloses the entire injection system as a precaution against a premature or explosive discharge

Appendix A contains detailed fabrication diagrams of the discharge chamber assembly. The main chamber body (76 mm x 76 mm x 100 mm) is sandwiched between a cartridge inlet plate and a metering orifice outlet plate that limits the flow of effluent into the TARPF. Copper gaskets are used to create a seal between the plates and the chamber. Two 1/8 NPT holes on the side of the main chamber body allow access for pressure and temperature transducers. The SPGG cartridge holder (see Fig. 8) is mounted vertically facing upward to Port 1 with a 3/4 NPT nipple. The holder is made of steel pipe 229 mm long and 50 mm in diameter. The lower cap was designed to accommodate the SPGG hardware and ignition wiring. (Refer to the appendix for details.)

SPGG Injection System
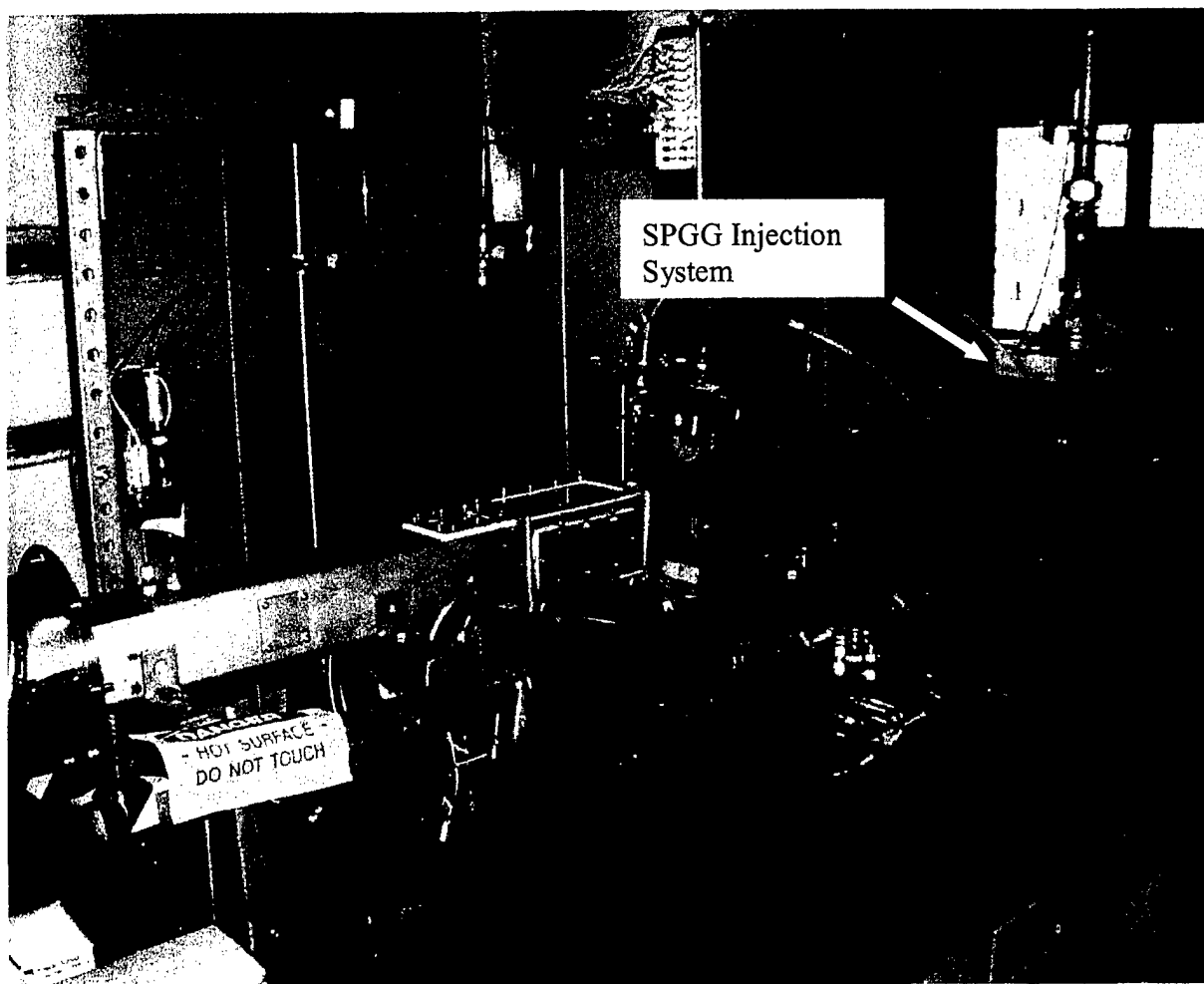
Figure 7. Photograph of TARPF showing location of SPGG injection system.

The fraction of the SPGG effluent injected into the TARPF was varied by selecting the size of Ports 3 and 4 (the pressure relief port). The combined area is referred to here as the bypass area. In an arrangement similar to that of Port 1, two plates could be attached to Port 3, allowing variation of the effective opening area (51 mm, 38 mm, or 25.4 mm). In many of the experiments, Port 4 was left open to maximize the bypass area.

The mass of the SPGG injected into the TARPF is determined from the total mass discharged and the bypass area ratio, equal to the ratio of the area of the metering orifice to the combined area of the metering orifice and the bypass area. The expanded uncertainty in the calculated mass is ± 2 %, with a minimum absolute uncertainty of 0.12 g attributable to the resolution of the pressure transducer. From the temperature and pressure measurements, the rate of suppressant addition to the incoming air, dm/dt, can be estimated within an expanded uncertainty of ± 2 g/s. The concentration of the SPGG in the air flow is determined from the rate of suppressant addition (dm/dt) and the mass flow rate of air. As in the gaseous agent experiments, the rate of air flow is invariant during the agent discharge through the use of a sonic orifice positioned upstream of the agent discharge location, in the air duct.
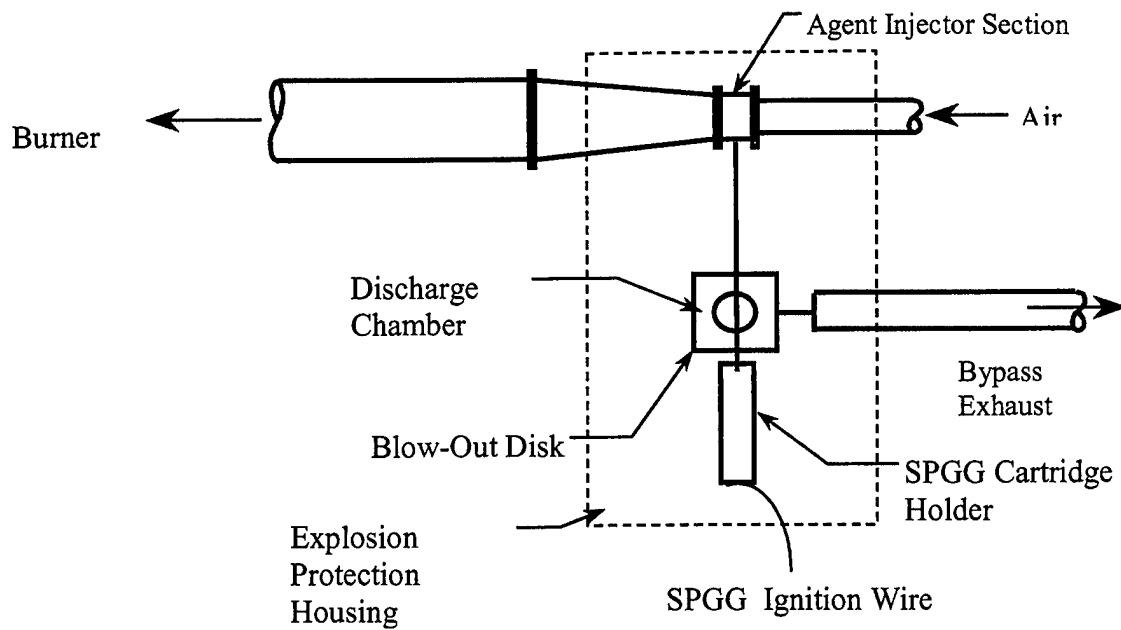
(a.) Schematic diagram of SPGG injection system
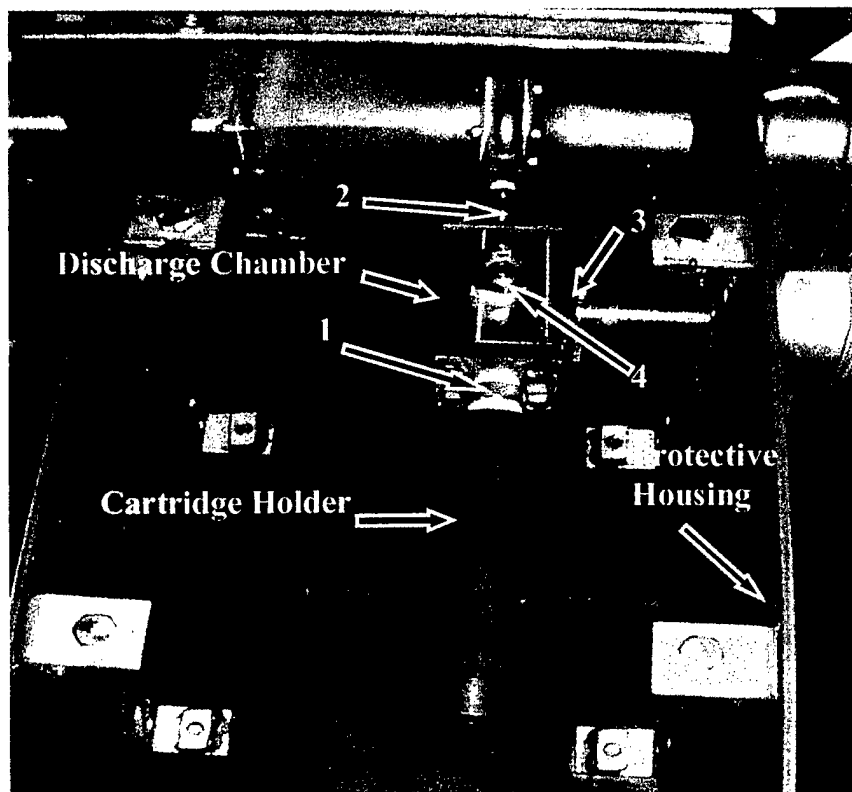
(b) Photograph of injection system with housing cover removed, showing the SPGG cartridge holder, discharge chamber, and ports: (1) SPGG outlet, (2) metering orifice, (3) bypass, and (4) blow-out.

Figure 8. SPGG injection system chamber.

In the current study, identical commercial air-bag hybrid gas generators were used, one in each of fifty experiments. Each generator released 20.7 g $\pm$ 0.1 g. The discharged mass was specified by the manufacturer and confirmed experimentally by weighing the generators before and after each discharge. The agent is composed of twenty grams of compressed argon gas and 0.7 g of a solid propellant, which at equilibrium converts to KCl (s) , H_2O, N_2 and a small amount of gaseous CO_2 [17].

The gas generator was discharged after steady-state fire conditions were achieved in the TARPF. The discharge was controlled by engaging an electronic switch on a control box that completed a circuit leading from a 12 V battery to the electrical connector located on the gas generator. One ampere was required to fire the 40 mg squib, which is an intrinsic part of the gas generator. The squib ignites the solid propellant, which rapidly discharges. The combustion products of the solid propellant propel the gaseous argon from the generator casing, located within the cartridge holder, into the discharge chamber. SPGG cartridges were changed and prepared for the next run in less than four minutes.

NUMERICAL MODELING AND ANALYSIS

To better understand the fluid dynamics of the suppression event, a computational fluid dynamics (CFD) model was used to simulate the baffle or step-stabilized flame in the TARPF facility. Similar numerical studies have been performed in the past few years. Among these, Liou and Hwang [18] used a two-dimensional CFD model to study the residence time of tracer particles within the recirculation zone of a backward-facing step. Weller *et al.* [19] applied a large eddy simulation (LES) model to study a premixed turbulent flame stabilized by a backward-facing step. Here, a low Mach number CFD model is applied to study the suppression event in the TARPF facility. The model is called the Fire Dynamics Simulator (FDS), and the simulations described here were performed with the first publicly released version [20]. The model is typically used to simulate large-scale fires, in which case turbulence is handled with a simple LES model. As applied here, however, the sub-grid scale turbulence model is not used, but rather the coefficients of viscosity, thermal conductivity and mass diffusivity are derived from kinetic theory and empirical extrapolation [21]. Thus, the calculations directly simulate the fluid motion (although not the combustion).

A brief description of the model equations is given below. The full numerical method used to solve the equations is given in Ref. [20]. First, consider the following conservation equations of mass, momentum and energy of a mixture of perfect gases in the low Mach number limit:

Conservation of Mass

$$\frac{\partial \rho}{\partial t} + \nabla \cdot \rho \mathbf{u} = 0 \tag{1}$$

Conservation of Species

$$\frac{\partial}{\partial t}(\rho Y_i) + \nabla \cdot \rho Y_i \mathbf{u} = \nabla \cdot \rho D_i \nabla Y_i + \dot{W}_i \tag{2}$$

Conservation of Momentum

$$\rho \left(\frac{\partial \mathbf{u}}{\partial t} + (\mathbf{u} \cdot \nabla)\mathbf{u} \right) + \nabla p = \rho \mathbf{g} + \nabla \cdot \tau \tag{3}$$

Conservation of Energy

$$\frac{\partial}{\partial t}(\rho h) + \nabla \bullet (\rho h \mathbf{u}) - \frac{Dp}{Dt} = (1 - X_r)\dot{q}''' - \nabla \bullet \mathbf{q} \tag{4}$$

Here, ρ is the density, Y_i the mass fraction, $\dot{W}_i$ the production rate of the ith component of the mixture, $\mathbf{u}=(u,v,w)$ is the velocity vector, p the pressure, $\mathbf{g}$ the gravity vector, h the enthalpy, $\dot{q}'''$ the rate of heat release per unit volume, and X_r the radiative heat loss fraction, taken as 0.20 for methane [22]. The components of the viscous stress tensor τ are

$$\tau_{ij} = \mu \left(\frac{\partial u_i}{\partial x_j} + \frac{\partial u_j}{\partial x_i} - \delta_{ij} \frac{2}{3} \frac{\partial u_k}{\partial x_k} \right) \tag{5}$$

where μ is the dynamic viscosity. The energy flux vector $\mathbf{q}$ is given by

$$\mathbf{q} = -k\nabla T - \sum_i \rho D_i h_i \nabla Y_i \tag{6}$$

where k is the thermal conductivity of the mixture, T is the temperature, and h_i is the enthalpy of the ith component.

The conservation equations are supplemented by an equation of state relating the thermodynamic quantities ρ, p and h. The pressure is first decomposed into three components, a ``background'' pressure p_0, a hydrostatic contribution, $-\rho g z$, and a perturbation to the hydrostatic, $\tilde{p}$. The coordinate z is the vertical spatial component. Using this definition of pressure, the equation of state can be written in a form appropriate for a perfect gas in the low Mach number regime [23]:

$$p_0 = \rho T \mathcal{R} \sum (Y_i / M_i) = \rho T \mathcal{R} / M \tag{7}$$

Here, M_i is the molecular mass of the ith species, M is the average molecular weight of the mixture and $\mathcal{R}$ is the universal gas constant. The pressure p in the state and energy equations is replaced by the background pressure p_0 to filter out sound waves that travel at speeds that are much faster than typical flow speeds expected in fire applications.

A further assumption about the thermodynamic variables is that the constant-pressure specific heat of the ith species $c_{p,i}$ is assumed to be independent of temperature. Under this assumption, the enthalpy can be written as:

$$h = \sum_i h_i Y_i = T \sum_i c_{p,i} Y_i \tag{8}$$

The specific heat for each species can be expressed in terms of the number of internal degrees of freedom active in that molecule.

$$c_{p,i} = \left(\frac{2 + \nu_i}{2} \right) \frac{\mathcal{R}}{M_i} = \left(\frac{\gamma_i}{\gamma_i - 1} \right) \frac{\mathcal{R}}{M_i} \tag{9}$$

If the ratio of specific heats for all the species is assumed to be that of a diatomic molecule ($\nu = 5, \gamma = 7/5$), the equation of state can be rewritten in the form:

$$p_0(t) = \frac{\gamma - 1}{\gamma} \rho h \tag{10}$$

16

The basis of this approximation is that nitrogen will be the dominant species in the simulations. The coefficients of viscosity, thermal conductivity and material diffusivity are approximated from kinetic theory. The viscosity of the lth species is given by

$$\mu_l = \frac{26.69 \times 10^{-7}(M_l T)^{\frac{1}{2}}}{\sigma_l^2 \, \Omega_v} \qquad \frac{kg}{m \, s} \tag{11}$$

where σ_l is the Lennard-Jones hard-sphere diameter (Å) and Ω_v is the collision integral, an empirical function of the temperature T. The thermal conductivity of the lth species is given by

$$k_l = \frac{\mu_l \, c_{P,l}}{Pr} \qquad \frac{W}{m \, K} \tag{12}$$

where the Prandtl number Pr is 0.7. The viscosity and thermal conductivity of a gas mixture are given by

$$\mu = \sum_l Y_l \, \mu_l \quad ; \quad k = \sum_l Y_l \, k_l \tag{13}$$

The binary diffusion coefficient of the lth species diffusing into the mth species is given by

$$D_{lm} = \frac{2.66 \times 10^{-7} T^{3/2}}{M_{lm}^{\frac{1}{2}} \sigma_{lm}^2 \, \Omega_D} \qquad \frac{m^2}{s} \tag{14}$$

where $M_{lm} = 2(1/M_l + 1/M_m)^{-1}$, $\sigma_{lm} = (\sigma_l + \sigma_m)/2$, and Ω_D is the diffusion collision integral, an empirical function of the temperature T [21]. It is assumed that nitrogen is the dominant species in any combustion scenario considered here, thus the diffusion coefficient in the species mass conservation equations is that of the given species diffusing into nitrogen:

$$(\rho D)_l = \rho \, D_{l0} \tag{15}$$

where species 0 is nitrogen.

A simple one-step, finite-rate reaction is used to model the combustion of propane:

$$C_3H_8 + 5 \, O_2 \longrightarrow 3 \, CO_2 + 4 \, H_2O \tag{16}$$
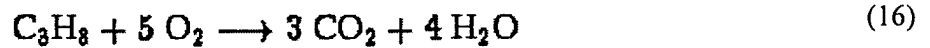
The fuel depletion rate (unit mass / unit time / unit volume) is given by the expression

$$\dot{W}_{C_3H_8} = -\frac{B}{M_{O_2}} \rho^2 \, Y_{C_3H_8}^a Y_{O_2}^b \, e^{-E/RT} \tag{17}$$

The heat release rate term is

17

$$\dot{q}''' = -\dot{W}_{C_3H_8}\,\Delta H \qquad\qquad (18)$$

where ΔH is the heat of combustion. Westbrook and Dreyer [24] suggest values for propane of $B = 8.6\times10^{11}$ cm^3 mol^{-1} s^{-1}, E=126.6 kJ/mol, a=0.1 and b=1.65 for propane. The heat of combustion is assumed to be 46,400 J/g.

Both two and three-dimensional simulations have been performed. The advantage of the two dimensional calculations is that greater spatial and temporal resolution can be exploited. The disadvantage is that the much of the complex structure of the turbulent flame cannot be simulated. Three-dimensional calculations are much costlier to perform, but yield a great deal of information about the flame structure.

The solution of the conservation equations governing the flow in the tunnel is computed on either a two-dimensional, uniformly-spaced grid spanning a plane 552 mm long and 92 mm high, or a three dimensional, uniformly spaced grid spanning a volume 552 mm long, 92 mm wide and 92 mm high. The number of the grids are 576 by 96 and 256 by 48 by 60, respectively. The backward-facing step is approximated with masked grid cells. The reactant flows consist of oxygen, nitrogen and propane. Nitrogen is used to represent the products of combustion simply to reduce the computational time. Propane is introduced into the flow domain through a 190 mm by 92 mm vent in the floor of the tunnel at a uniform rate of 33 mL/s. Air and agent are introduced into the domain 100 mm upstream of the step with a top hat velocity profile. At the outflow boundary a constant ambient pressure is assumed. Ignition is achieved by momentarily heating up a small patch on the floor of the tunnel just downstream of the step. At all other wall locations, the temperature is maintained at 200 °C.

Presented in Fig. 9 are sequences of images separated in time by 0.01 s that are taken from simulations that illustrate the dynamics of the suppression event. Figure 9a is a 2-D simulation of flow (moving left to right) over a 25 mm step. The darkness of the image reflects the extent of local heat release. Figure 9b is a 3-D simulation of a flame stabilized on a 25 mm baffle that is undergoing a successful suppression. In both Figs. 9a and 9b the top images show the flame just prior to discharge of nitrogen into the air stream. Upon injection, the flame is disturbed by a large vortex generated by the pressure pulse. Due to the low Mach number approximation, the gas upstream of the step is essentially incompressible, and the velocity jump from 2.1 m/s to 5.7 m/s is conveyed to all points in the flow domain in 0.02 s, the time of the ramp-up from the base velocity to the injection velocity. Thus, even before the agent arrives at the step, the flame has already been dramatically transformed from its original state. The generation of the large vortex at the step produces a pathway by which the agent can penetrate the region just behind the step, mixing with the gases, cooling and diluting the fuel and oxygen.
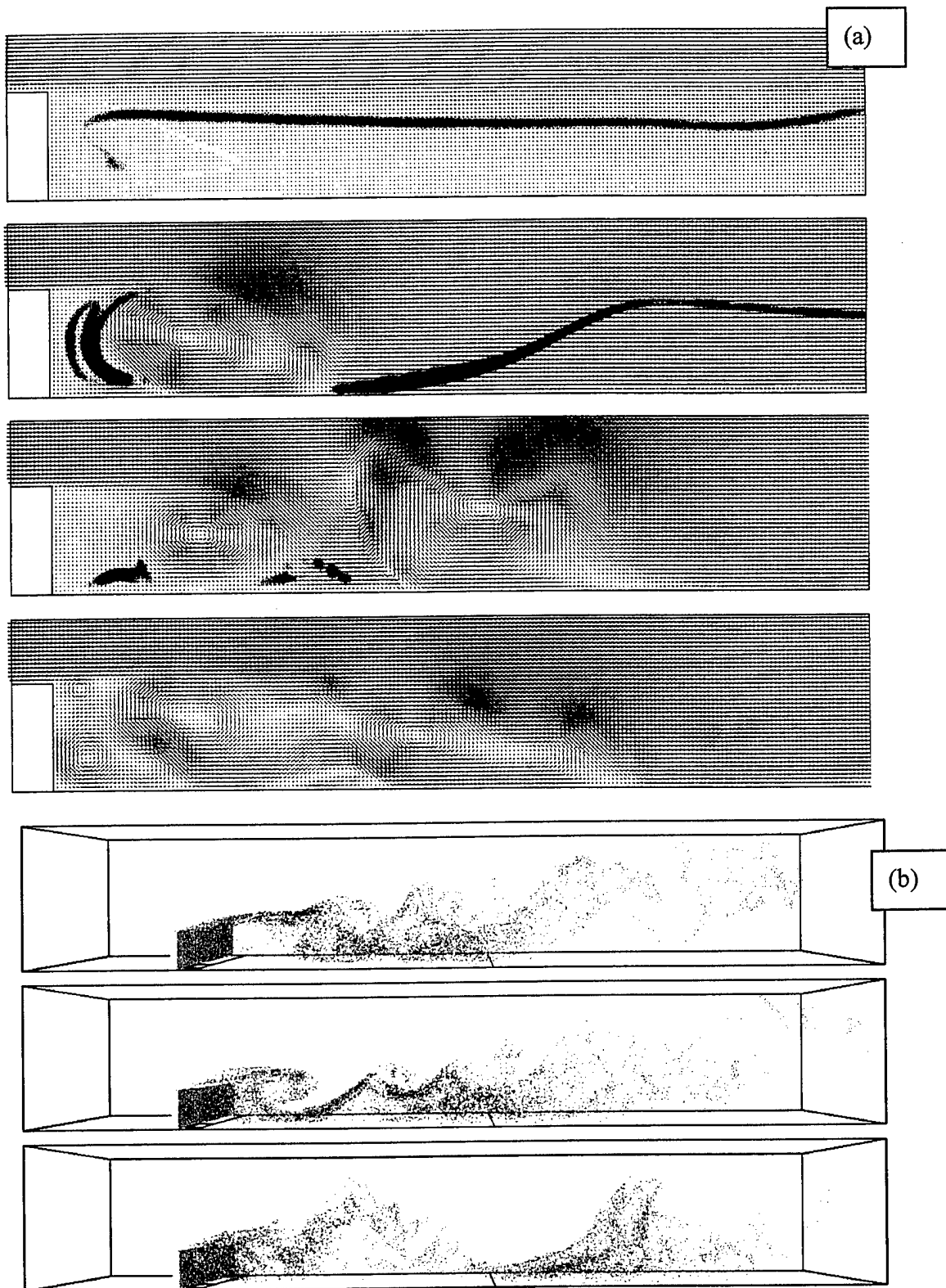
Figure 9. The disruption of a stabilized flame by the injection of nitrogen upstream of 25 mm high obstacle: (a).2-D simulation of flow over step; (b) 3-D simulation of flow over baffle (frames are separated by 0.01 s).

19

EXPERIMENTAL RESULTS

Flow Characterization

The facility was operated over a range of propane and air flows to examine the flame behavior. Blow out can be achieved either by increasing the air flow or decreasing the propane flow. At low air velocities, a fluctuating laminar flame is anchored on the top downstream edge of the step or baffle and extends well downstream of the porous plate. As the velocity increases, the flame becomes turbulent and less luminous. Near blow-out, the orange color disappears and the visible blue flame shrinks. With the backward-facing step installed, an average air velocity above the step of over 23 m/s is necessary to blow out the flame if the propane flow is greater than 33 mL/s (corresponding to a transverse velocity of 1.9 mm/s).

Two air flows were chosen to evaluate the ability of the agents to suppress the propane pool fire stabilized by the backward-facing step. The low and high mean air velocities (just above the step) were 2.1 m/s ± 0.2 m/s and 5.4 m/s ± 0.2 m/s, respectively. Corresponding propane flows of 33 mL/s ± 2 mL/s and 85 mL/s ± 2 mL/s, respectively, were utilized. The low flow condition corresponds to what Takahashi et al. [10] describe as regime I suppression (rim-stabilized flame), and the high flow is transitional between regimes I and II (intermittent turbulent flame).

The velocity distribution of the air 76 mm upstream of the burner was measured with a 3 mm diameter pitot tube at seven locations across the duct. Figure 10 compares the results with and without the flame present for the high flow condition. The velocity profiles are seen to be flat within 5 % over the central three-fourths of the duct. The boundary layer above the step appears to be less than 7 mm thick. The presence of the flame tends to increase the pitot probe signal, which is likely due to a combination of preheating the air upstream by the flame, acceleration in the flow due to partial blockage of the duct caused by the expanding combustion gas, and a possible shift in electrical output due to heating of the pitot probe and transducer.

The facility is designed to introduce suppressant impulsively without altering the air flow. This is achieved by maintaining a choked condition for the air independent of modest changes in downstream pressure generated by the injection process. The pitot tube was used to measure the instantaneous flow 76 mm ahead of and 5 mm above the backward step during the discharge of C_2HF_5 into the air stream for the two different air flow conditions (without fuel flowing). The dashed lines in Fig. 11 show the combined effect of the velocity (V) and density (ρ) change, $V(\rho/\rho_o)^{1/2}$, created by the injection process, where ρ_o is the initial density of the air stream. Figure 11a is for the low air flow condition and a high rate of agent discharge; Fig. 11b represents a high air flow with a low rate of agent addition. The pressure, P, in the agent storage vessel is also plotted in Fig. 11, from which the rate of C_2HF_5 mass added, dm/dt, is calculated. The injection interval is 130 ms ± 5 ms for both cases, but the amount of agent added in Fig. 11b is 1/3 the amount added in Fig. 11a because the agent storage volume was 1 L and 3 L, respectively.

The sizable increase in $V(\rho/\rho_o)^{1/2}$ seen in Fig. 11a within 0.10 s of the passage of the acoustic wave results from the slug of air between the injector and the pitot tube being shifted downstream by the addition of agent. High-speed video images of the flame during the discharge corroborate this description. The shift is barely discernable in Fig. 11b since the amount of agent added is small relative to the flow of air. The time that the agent itself arrives at the pitot tube is limited by the bulk convection and the distance the probe is downstream of the point of injection (1.1 m). The times of arrival of the agent at the pitot tube can be estimated to be 0.58 s and 0.24 s for the conditions in Figs. 11a and 11b, respectively. Interpretation of the pitot signal is complicated by the much higher density of C_2HF_5 as compared to air.

An instrument developed by Pitts et al. [25] was used to measure the infrared absorption by C_2HF_5 at a wavelength of 8.7 μm ± 0.1 μm. Figure 11 also contains a plot of the absorptance,

20
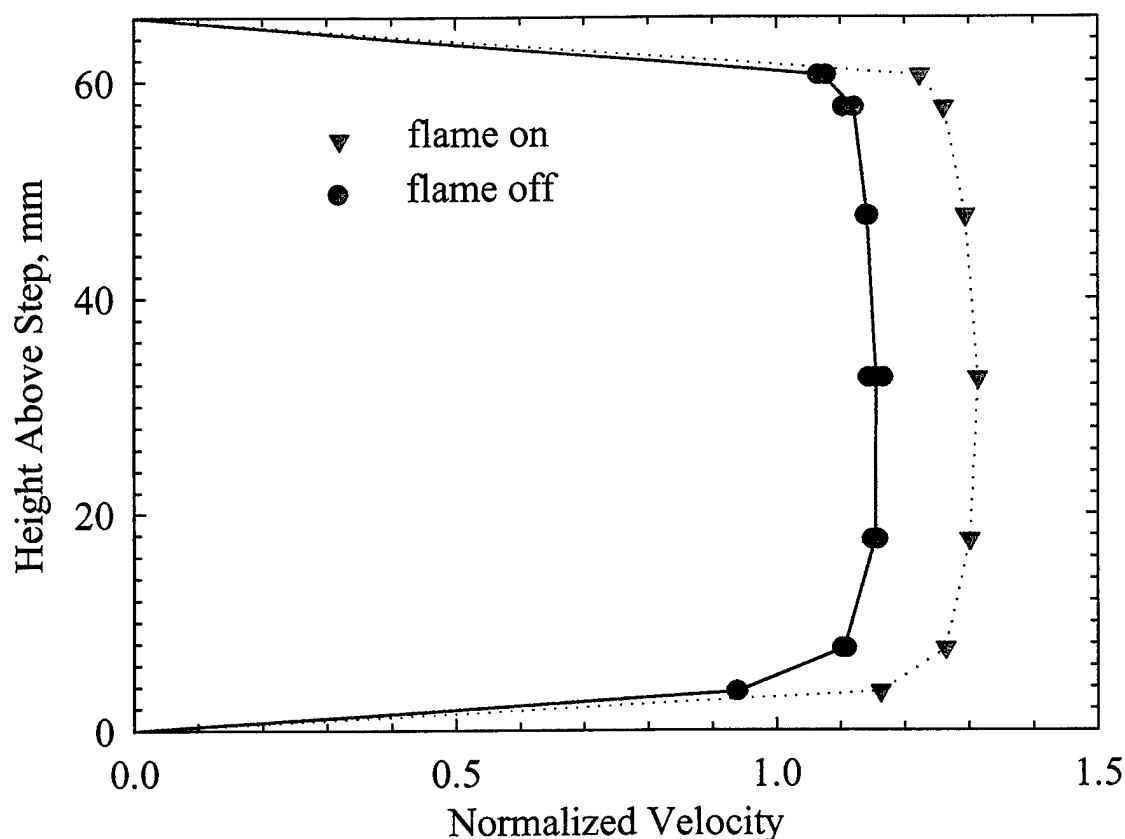
Figure 10. Velocity (normalized by nominal mean) measured upstream of burner, with and without flame lit.

integrated across the width of the duct, during the discharge. The viewing port is 2.3 m downstream of the agent injector and 1.1 m downstream of the pitot tube. The absorptance pulse in Fig. 11b is similar in shape to the rate of discharge, but about 0.1 s wider. Nonuniform mixing of the agent with air as it flows over the step and into the recirculation zone contributes to the long absorptance tail that is evident for over a second in Fig. 11a, although the agent injection duration was only 0.13 s.

The amount of suppressant necessary to extinguish a fire in the TARPF depends upon the fuel and air flows chosen to challenge the suppressant. Figures 12 and 13 show how the amount of nitrogen necessary to extinguish a 25 mm baffle-stabilized flame varies with the flow of air and fuel. The uncertainty in any given value is estimated to be $\pm$ 0.2 g. The filled circles in the figures indicate extinction and the crosses represent no extinction. When the air speed is less than 5 m/s and the fuel flow is fixed at 45 mL/s $\pm$ 2 mL/s, decreasing the speed (see Fig. 12) reduces the amount of nitrogen necessary to extinguish the flame. No flame extinction occurred between 5 m/s and 15 m/s because the amount of nitrogen necessary exceeds the maximum amount contained in the storage vessel. Above 16 m/s, the strain on the flame is sufficient at times to extinguish the flame without the need for any nitrogen. (The dashed lines are included in the figure to assist the eye in identifying the extinction boundaries.) The propane flow does not have much affect on the amount of nitrogen needed to extinguish the flame if the injection interval and air flow are fixed, as shown in Fig. 13. There is a lower limit for the propane (<12 mL/s) that leads to extinction due to heat loss to the burner, even with no nitrogen dilution. The upper limit of propane (120 mL/s) is dictated by the maximum safe operating temperature of the burner; however, since the mass of nitrogen needed to suppress the flame does not

21
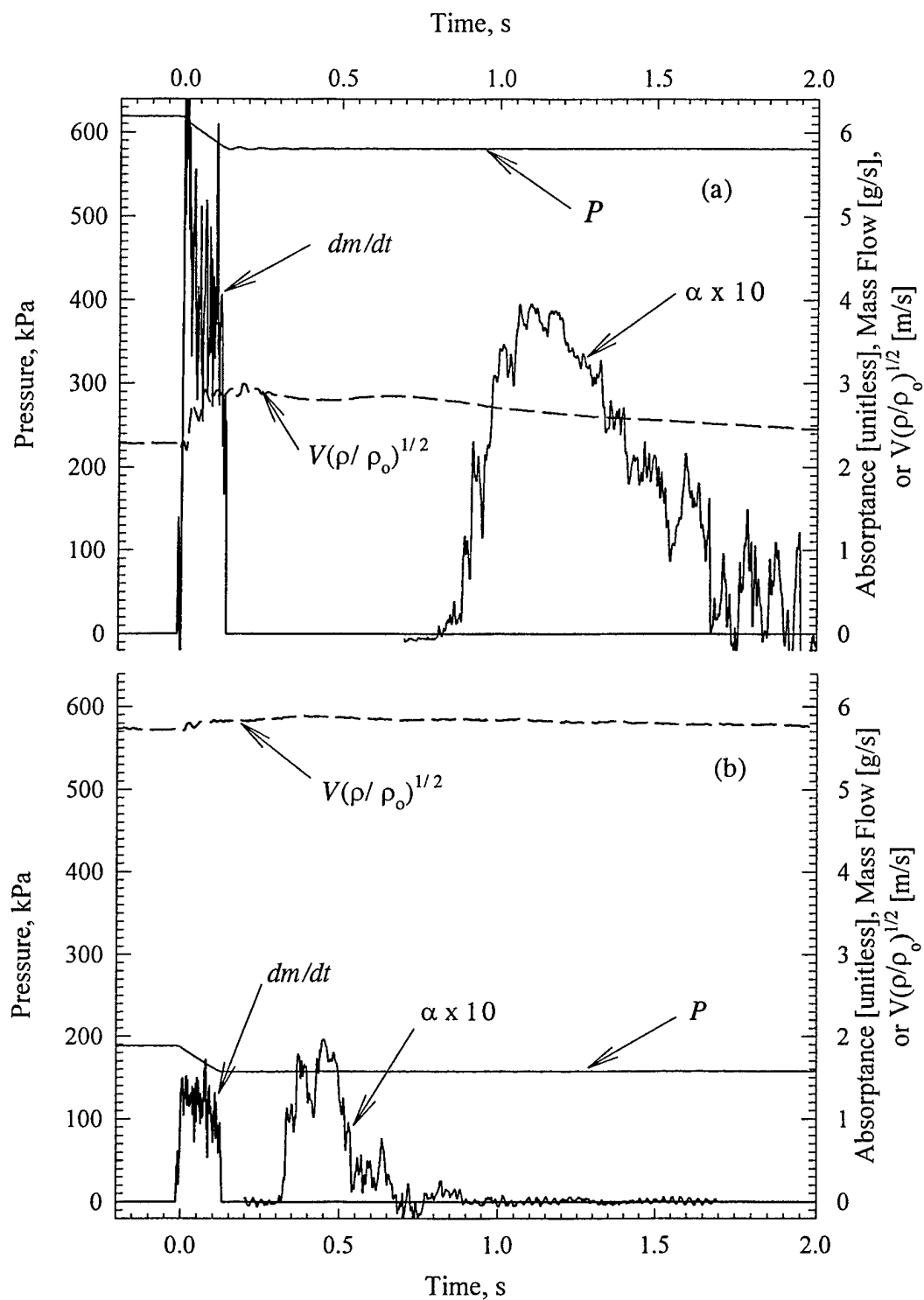
Figure 11. Bottle pressure, agent mass flow, velocity above step, and IR absorptance 1 m downstream of step during 0.125 s discharge of C_2HF_5; (a) low air flow, high agent flow, (b) high air flow, low agent flow.
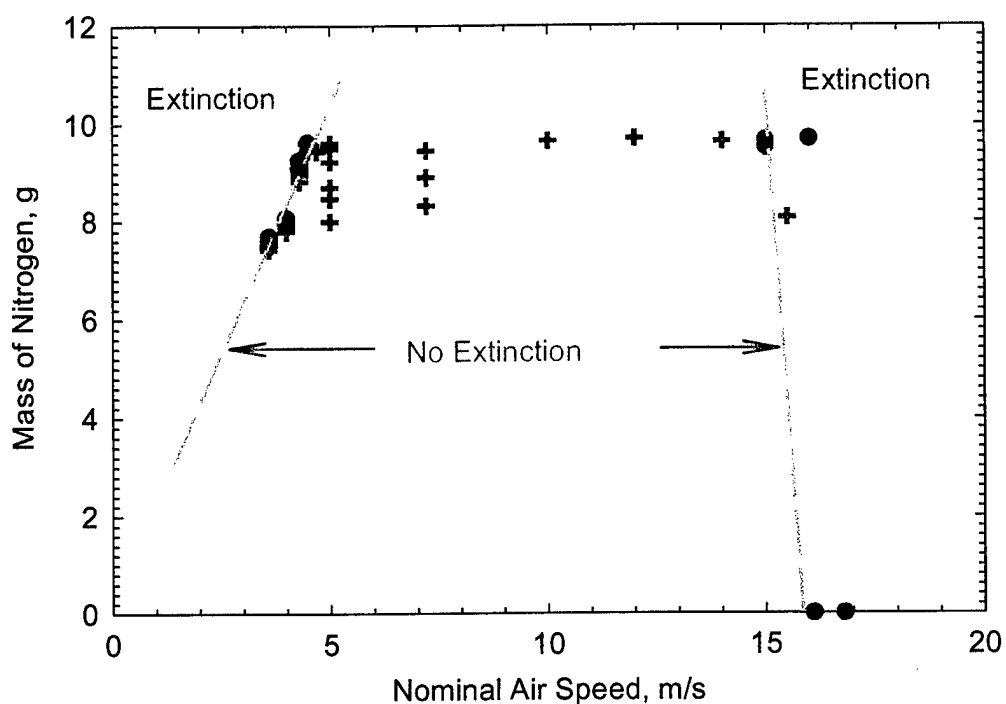
Figure 12. Impact of air speed on extinction of 25 mm baffle-stabilized flame; propane flow is 45 mL/s, nitrogen injection time is 312 ms: circles imply extinction, crosses imply no extinction.
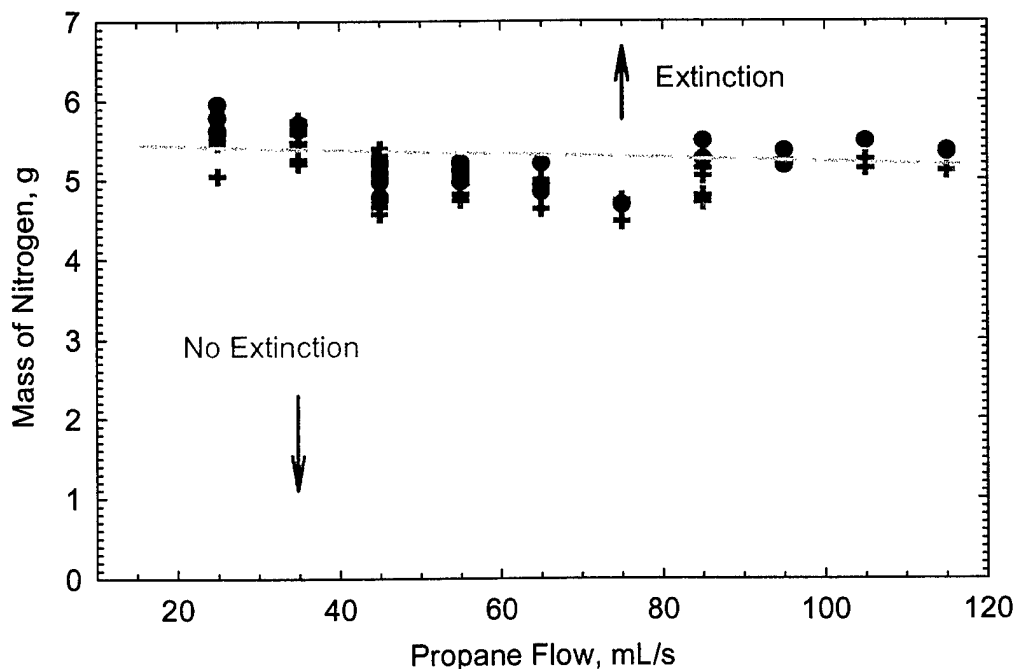
Figure 13. Impact of propane flow on N_2 required for suppression of 25 mm baffle-stabilized flame; air flow is 3.88 m/s, injection time is 185 ms; circles imply extinction, crosses imply no extinction.

23

appear to increase, there is no need to operate the burner at higher fuel flows. (Note: the dip in mass required for propane flows around 75 mL/s is attributed to the low number of experiments conducted in this region.)

The relationship between the total mass of nitrogen required for suppression and the injection time interval is plotted in Fig. 14 for a 3.9 m/s $\pm$ 0.2 m/s air flow, 45 mL/s $\pm$ 2 mL/s propane flow flame stabilized on the 25 mm baffle. The open symbols are experiments that did not extinguish the flame, and the closed symbols are experiments that led to extinction. (The total number of experiments conducted exceeds by a factor of ten the number of data points plotted in this and the following curves; for clarity, only those conditions close to the extinction boundary are included.) As the injection interval increases from 100 ms to 500 ms, the minimum mass required increases over three-fold. The rate of mass addition (calculated by dividing the total mass by the estimated injection interval) decreases with increasing injection interval, as shown in the right-hand figure.

Effect of Obstruction Geometry

The data plotted with squares in Fig. 15 were taken with the ramp placed in front of the 25 mm baffle to form a backward step-stabilized flame, rather than the simple baffle-stabilized flame represented in Fig. 14. The air flow is the same in these two cases but the propane flow is higher, 85 mL/s, in Fig. 15. The addition of the ramp and increase in propane flow do not have much influence on the mass of nitrogen required for suppression. For both the baffle and backward step, just under 6 g of N_2 are required when the injection interval is 200 ms $\pm$ 10 ms. The data plotted as circles in Fig. 15 were taken with the nominal air speed reduced to about 1.5 m/s and the propane flow reduced a proportionate amount to near 33 mL/s. The squares in Fig. 15 represent experiments conducted at the high air and propane flows, and circles represent experiments conducted at the lower flows. Open symbols indicate that the flame was not extinguished, and filled symbols indicate flame extinction. Less than 4 g $\pm$ 0.2 g of N_2 are needed to extinguish this flame if injected over a 200 ms $\pm$ 10 ms interval. The differences in rates of mass addition to suppress the high flow and low flow flames can also be seen at the right in Fig. 15.

Figures 16 and 17 show what happens to the required nitrogen mass and addition rate if the baffle height is decreased to 10 mm or increased to 55 mm (blockage from 11 % to 60 %), respectively. The symbols have the same meaning as in Fig. 15. The short baffle produces a fire which is the easiest to extinguish, and the high baffle the most difficult in terms of the amount and rate of N_2 addition.

The effect of baffle height is not large if the injection interval is at least 150 ms, as can be seen more clearly in Fig. 18. (Note that 6 mm has been added to the height of each obstacle to account for the distance between the floor of the tunnel and the recessed top surface of the burner.) The bottom curve delineates the minimum amount of nitrogen for suppression when the air flow is fixed at its high value and the agent injection interval is maintained at 175 ms $\pm$ 10 ms. The open circles represent the largest mass of N_2 that did not result in extinction for flames stabilized on the different sized baffles; the filled circles are the minimum mass of agent that successfully extinguished the flames. The diamonds are the results for the 25 mm baffle with the ramp in place (backward-facing step). Experiments were also conducted with and without the reignition obstruction shown in Fig. 2. The amount of N_2 necessary for suppression was unchanged.

The rate of mass addition is plotted in the upper curve of Fig. 18 (the triangles are the backward-facing step, and the squares are for the baffles). The data are plotted two ways: the higher value is the rate of nitrogen addition computed during the first 50 ms that the solenoid valve is open (refer to the shape of the dm/dt curve in Fig. 5); the lower value is the average over the entire open interval measured from the pressure trace. The estimated rate of mass addition varies substantially, especially for the 55 mm baffle, depending upon whether the averaging period is the first 50 ms or the entire time that the solenoid remains open.
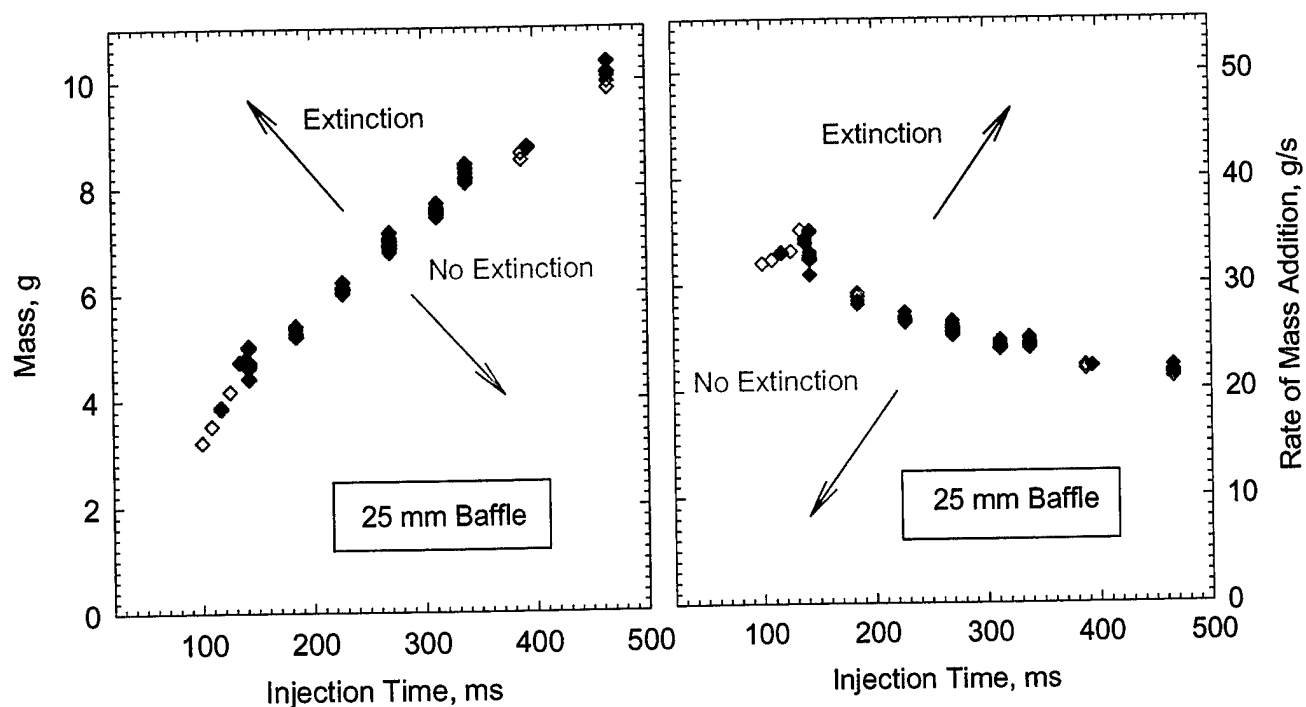
Figure 14. Mass and rate of nitrogen addition required to extinguish 3.88 m/s air flow, 45 mL/s propane flame: filled diamonds, extinction; open diamonds, no extinction.

Figure 15. Mass and rate of nitrogen addition required to extinguish high flow (squares) and low flow (circles) air/propane flames: filled symbols, extinction; open symbols, no extinction.

25
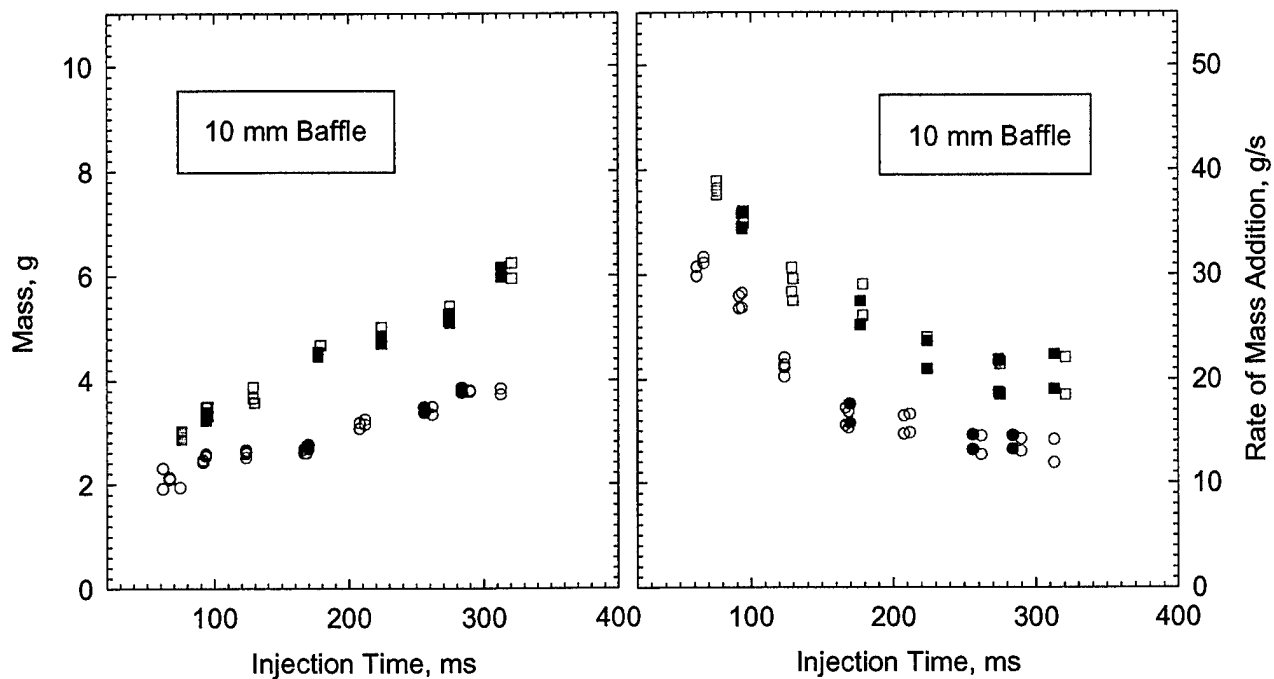
Figure 16. Mass and rate of nitrogen addition required to extinguish high flow (squares) and low flow (circles) air/propane flames: filled symbols, extinction; open symbols, no extinction.

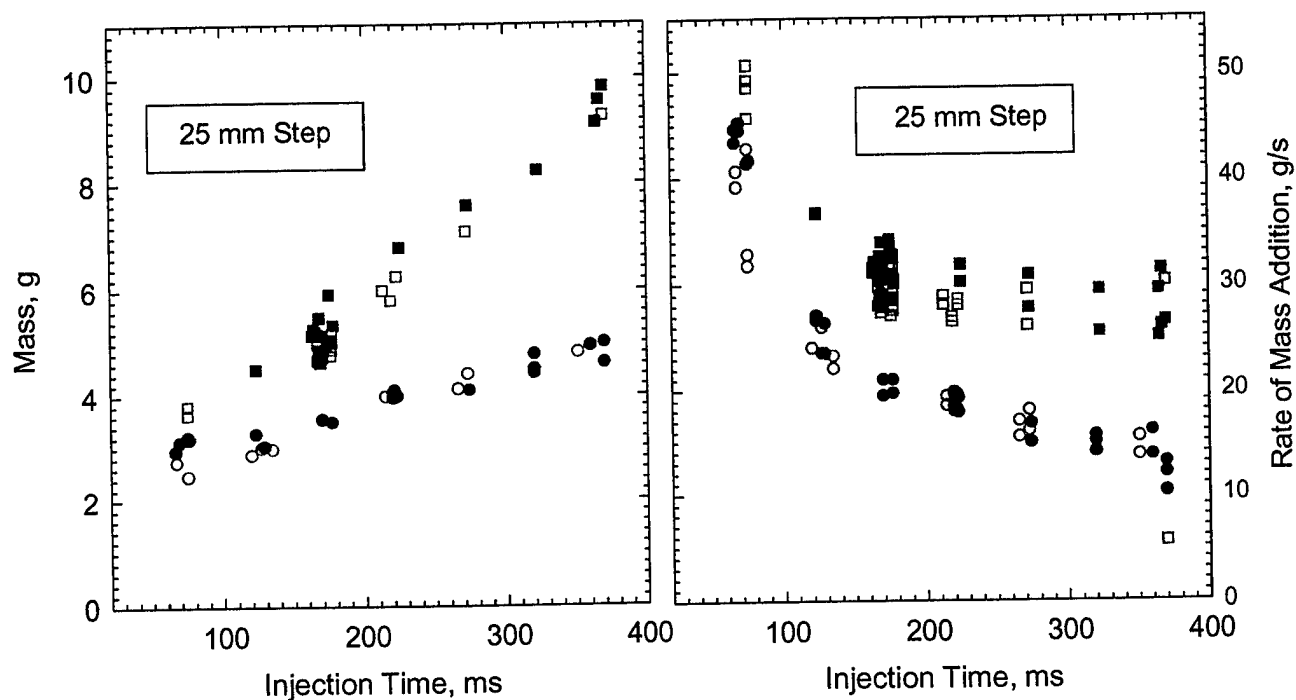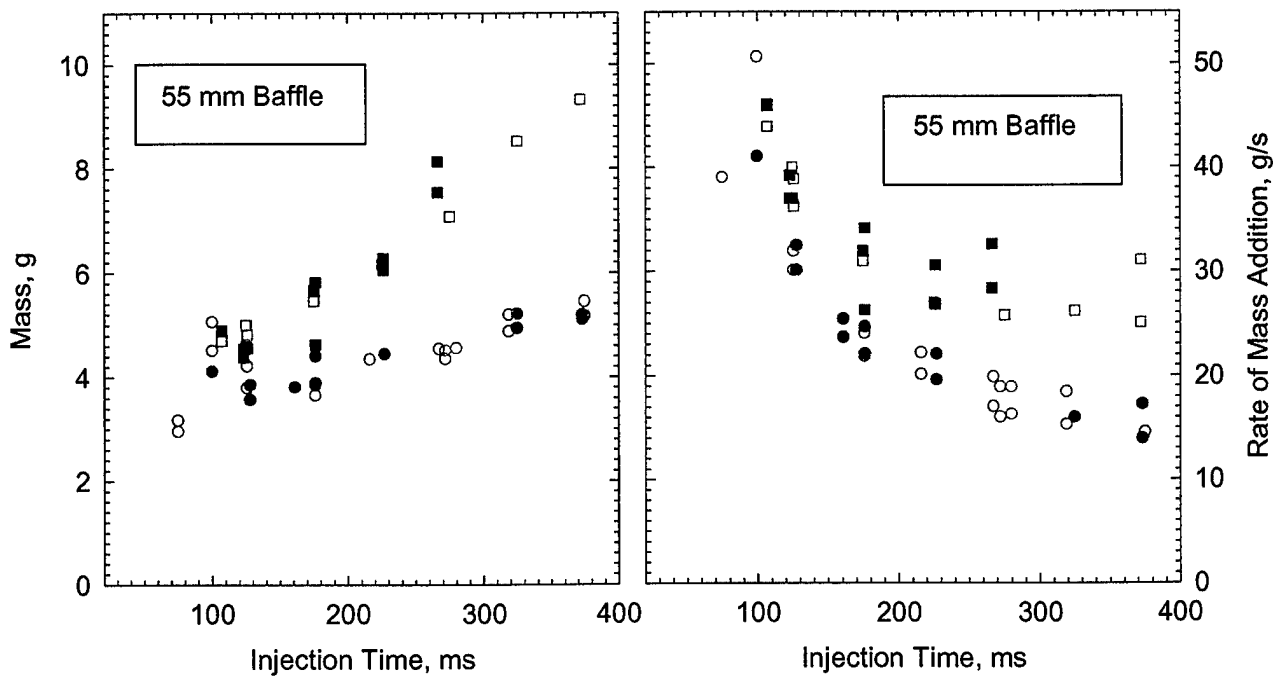Figure 17. Mass and rate of nitrogen addition required to extinguish high flow (squares) and low flow (circles) air/propane flames: filled symbols, extinction; open symbols, no extinction.
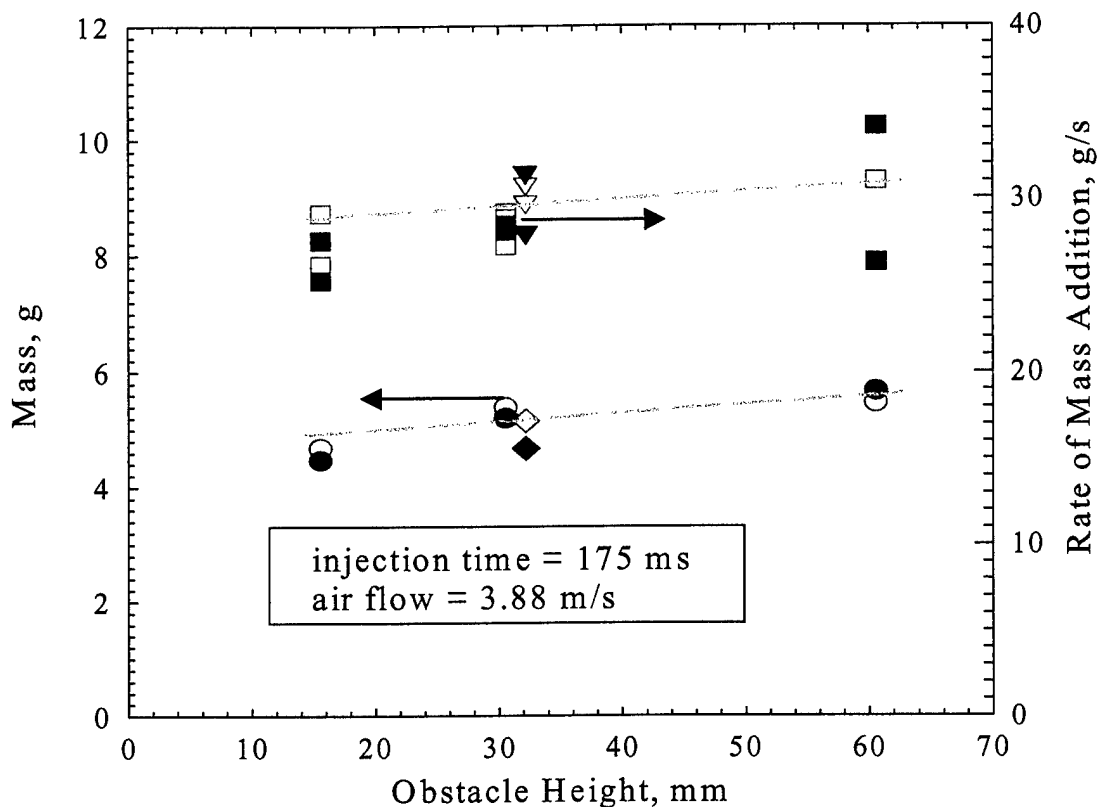
Figure 18. Impact of obstacle height on the total mass and rate of addition of nitrogen required to suppress obstacle stabilized pool fire.

Effect of Type of Gaseous Agent

Figure 19 is a plot of the minimum agent mole fraction that extinguished the fires (X) as a function of the agent injection time interval (Δt) for both N_2 and CF_3Br. The parameter X is defined as the average volume flow of agent during the injection interval divided by the sum of the agent and bulk air flows. The data represent experiments conducted over a range of conditions including air velocities (defined above the obstacles) that varied from 2 m/s to 9 m/s, propane flows from 33 mL/s to 85 mL/s, and baffle heights between 10 mm and 55 mm, in addition to the 25 mm backward step. The open and closed symbols represent the low and high air flow conditions, respectively. Figure 19 shows that X decreases with increasing injection time interval for all obstacle types and both agents. The highest mole fraction requirements were consistently for the low air flow conditions. For some experiments, the value of X was nearly 0.8 for short injection intervals. The most challenging geometric configuration was the 55 mm baffle, followed by the 25 mm obstacles, and the 10 mm baffles. There was little difference in X between the 25 mm step, 25 mm cavity and the 25 mm baffle and those data are presented as one group in Fig. 19.
The effectiveness of CF_3Br was compared to that of N_2 using the 25 mm high backward step. The 1 L storage vessel was used to accentuate the pressure change associated with the small quantities of CF_3Br required for suppression. Only 1.6 g $\pm$ 0.2 g of CF_3Br injected for 100 ms was needed to extinguish the flame under the high air flow conditions (corresponding to X $\cong$ 0.075), as compared to 3.9 g $\pm$ 0.2 g for N_2 as agent (X $\cong$ 0.5) under similar conditions. These results are consistent with numerous studies that show that CF_3Br is a more effective suppressant than N_2 for both free standing and baffle stabilized flames.
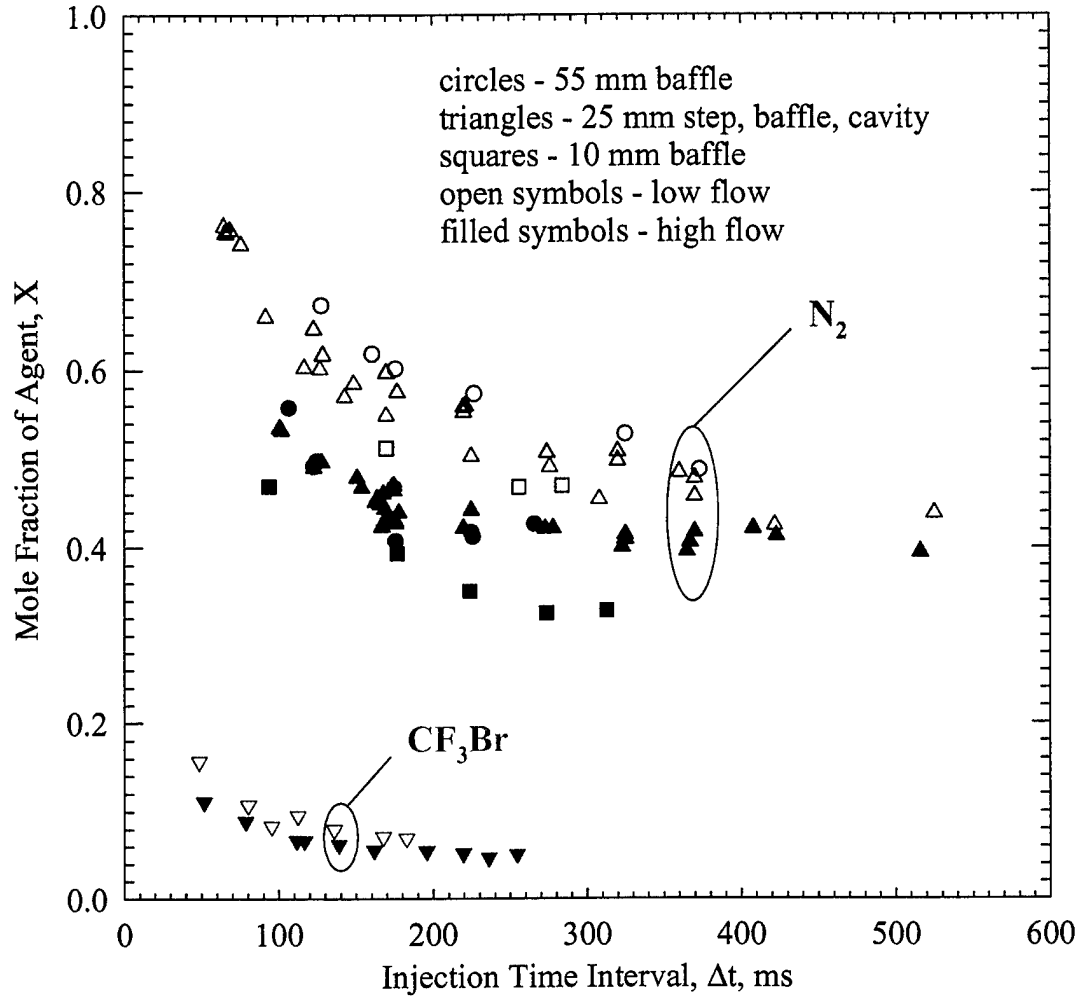
Figure 19. Mole fraction of agents (N_2 and CF_3Br) added to air at extinction boundary for high and low flow conditions, as a function of the injection time interval and obstacle geometry.

Aerosol Agents

The aerosol injection system described earlier was used by Pitts et al. [26] to compare the suppression performance of a water mist and methoxynonafluorobutane in the TARPF to that measured in the steady-state Tsuji burner [16]. The air flow in the tunnel was fixed at 6.67×10^{-3} m^3/s and the porous burner was operated at a propane flow rate of 33 mL/s. The mist discharge duration was varied from 1 s to 10 s. The mass flow rate of the liquid agent, $\dot{m}_{agent}$, can be calculated using the density of the liquid and the calibrated volume flow rate. The mass fraction of the liquid agent, β_{agent}, in the air stream is then

$$\beta_{agent} = \frac{\dot{m}_{agent}}{\dot{m}_{agent} + \dot{m}_{air}} \tag{19}$$

where $\dot{m}_{air}$ is the calculated mass flow rate of air. Note that in writing Eq. (19), it is implicitly assumed that the mist droplets are homogeneously dispersed in the carrier phase (air).

28

A number of suppression experiments were run with the mass fraction of the water calculated to be 0.11. The pool fire stabilized behind the backward-facing step of the ramp could not be completely suppressed under these conditions, although useful observations could be made. Before the mist injection, the flame was luminous and yellow. During the mist injection, the yellow flame was nearly extinguished with pockets of localized blue flame regions. The mist was also observed to have high momentum, which resulted in the major portion of the mist bypassing the flame completely. The duration of the small blue flames coincided with that of the mist application. Once the mist application period was over, the flame regained its original burning intensity and yellow luminosity.

The above observations indicate partial localized flame suppression due to sufficient droplet entrainment into some portions of the mixing layer, but an insufficient number of droplets entrained over time to prevent the flame from flashing back into the previously extinguished zones. In flow experiments conducted with no flame present, the droplets were observed to traverse the burner very rapidly with little entrainment of the mist into the recirculation zone. With a flame, gas expansion effects are enhanced and are expected to further carry the droplets axially past the flame. Although the droplet statistics were not measured, one would expect that the size distribution from these atomizers would cover a range between 1 μm and 200 μm. For droplet entrainment into the recirculation zone behind the ramp to occur, a high concentration of micrometer-sized droplets needs to be dispersed throughout the passage cross section and entrained in the air flow. Apparently, a large enough concentration of small droplets (with a small relative velocity) was unavailable to suppress the flame completely.

In the Tsuji burner experiments, Yang et al. [16] used a droplet delivery system that assured efficient transport of fine liquid droplets to the flame. They found that a calculated water mist mass fraction of 0.03 in the air stream was sufficient to extinguish their laminar counter-flow flame. This is less than 1/3 the mass fraction of water injected into the TARPF without achieving suppression. Thermodynamic estimates of the cooling effect of water suggest that a mass fraction of almost 0.13 is required to bring the equilibrium temperature of a propane/air flame down to 1500 K, which is the extinction temperature found by Pitts et al. [25] for purely thermal agents. Thus, one could argue that a 0.11 mass fraction should not be expected to suppress the TARPF flame.

More experiments and computational modeling are necessary to sort out the discrepancy between the TARPF and Tsuji results to identify the relative importance of droplet entrainment, size distribution, and transient vs. steady-state effects on the mass fraction of water needed to ensure flame extinction. This may best be achieved using an ultrasonic humidifier (producing all droplets less than 2 μm), or twin-fluid atomizer, to inundate the recirculation zone with submicron droplets, as long as the droplets do not pre-vaporize before reaching the flame. Note that entrainment of droplets into the recirculation zone will be dependent on determination of the Stokes number, $St = \rho D^2 \Delta U / 18 \mu \delta$, where ρ is the droplet density, ΔU is the relative velocity between the droplet and surrounding air, μ is the air viscosity, and δ is a characteristic size of a vortex structure formed by the air stream. For values of $St < 1$, droplets will be dispersed with the surrounding stream while for large values of St insufficient time will be available to influence the droplet motion. Thus, entrainment will be optimized for smaller droplets that have little relative velocity to the airflow.

SPGG Results

For the SPGG experiments, the nominal velocity of the air above the backward-facing step was maintained constant at 5.4 m/s; the propane flow was 85 mL/s (at standard temperature and pressure). The pressure build-up in the discharge chamber was measured for a range of bypass areas, as seen in Fig. 20. The high pressures produced in the SPGG discharge chamber and the known area of the metering orifice allow the mass flow of agent added to the air stream of the TARPF to be estimated by assuming that the flow through the orifice is choked. Figure 21 shows the repeatability of the agent injection process with five overlaying mass flow and thermocouple temperature traces. (The thermocouple does

not reflect the true gas temperature, which is expected to be hundreds of degrees Celsius hotter than recorded in the figure.)

The SPGG discharge time was consistently 20 ms $\pm$ 1 ms, which is over three times faster than the shortest N_2 or CF_3Br injection interval, and not much affected by the bypass port area. The bypass ratio (A_{in}/A_{tot}) is the area of the inlet metering orifice (port 2) divided by the total open area available for flow to exit the discharge chamber (ports 2, 3, and 4) The time interval, Δt, is shown in Fig. 22 as a function of the estimated discharge mass. The total mass delivered to the air stream during the discharge process is found by integrating dm/dt over Δt. Excluding the highest and lowest area ratios, the estimated mass delivered can be seen in Fig. 22 to be linearly proportional to the area ratio; however, almost 50 % more mass is estimated than one would expect. The dashed line in Fig. 22 indicates that a 1-to-1 relation would exist if the mass were directly proportional to the area ratio.

There are several factors that contribute to an uncertainty in the estimate of the absolute mass of agent. First, uncertainties in the gas composition and temperature upstream of the metering orifice affect the estimate since the mass is proportional to the square root of the molecular weight divided by the temperature. A factor of two under-estimate in this parameter would cause a 40 % over-estimate in mass, which, if corrected for, would cause the data plotted in Fig. 22 to more closely align with the dotted line. A second source of uncertainty is the complexity of the flow within the discharge chamber created by the jet emanating from the SPGG. The calculation assumes that the upstream flow is steady and parallel to the axis of the metering orifice, but the flow is highly transient and more perpendicular.

Suppression of the propane pool fire with the hybrid gas-generators was found to be successful if at least 1.5 g of agent was injected into the fire; conversely, extinction never occurred when less than 0.7 g was added. The percent of the fires suppressed varied when the agent mass was between these limits, as shown in Fig. 23. The suppression statistics were generated by lumping the mass from thirty-three discharges into bins 0.2 g wide, centered about the data plotted. The solid line is a fit to the data assuming that the shape is sigmoidal. It is apparent from the curve that there is a 50 % chance that suppression will be successful if the amount of agent is 0.9 g $\pm$ 0.1 g, and there is a 90 % success rate for 1.3 g $\pm$ 0.1 g of agent.

Figure 24 is a plot of the mass of agent required for suppression versus the injection time interval. All of the SPGG data are lumped around 20 ms since the injection time was fixed. The N_2 and CF_3Br results extend to much longer injection time intervals. Linear fits to the data yield intercepts of 1.6 g for nitrogen and 1.2 g for halon 1301. The SPGG data fall close to the halon results. The significance of the linear shape and the value of the intercept is unclear; however, the superior performance of the gas generator is undeniable.

The mass fraction of agent, β, is defined as the total mass injected divided by the injection duration, Δt, over the sum of the mass flow of air plus the mass flow of agent. The percentage of occasions that the flame was extinguished is plotted in Fig. 25 as a function of β. All of the fires were extinguished when β was greater than 0.62; none for a mass fraction below 0.49. The definition of β for the SPGG differs somewhat from the definition as applied to the gaseous agents because the mass discharge profiles for SPGG and the gaseous agents are different. Whereas the mass injection rate of the gaseous agents is controllable through selection of the injection hardware, the SPGG mass injection rate is practically dependent on the propellant effluent generation rate (i.e., the propellant burning rate). The character of the mass injection rate, dm/dt, is qualitatively different than that of the gaseous agents. Its value for the SPGG is best represented by the pressure profile shown in Fig. 20, as compared to dm/dt seen in Fig. 5 for gaseous N_2. For the same mass, variation of the discharge profile will lead to variation in agent effectiveness. Optimization of the rate of agent discharge is an area that would benefit from further study, which could be approached from analytic, numerical, and experimental perspectives.
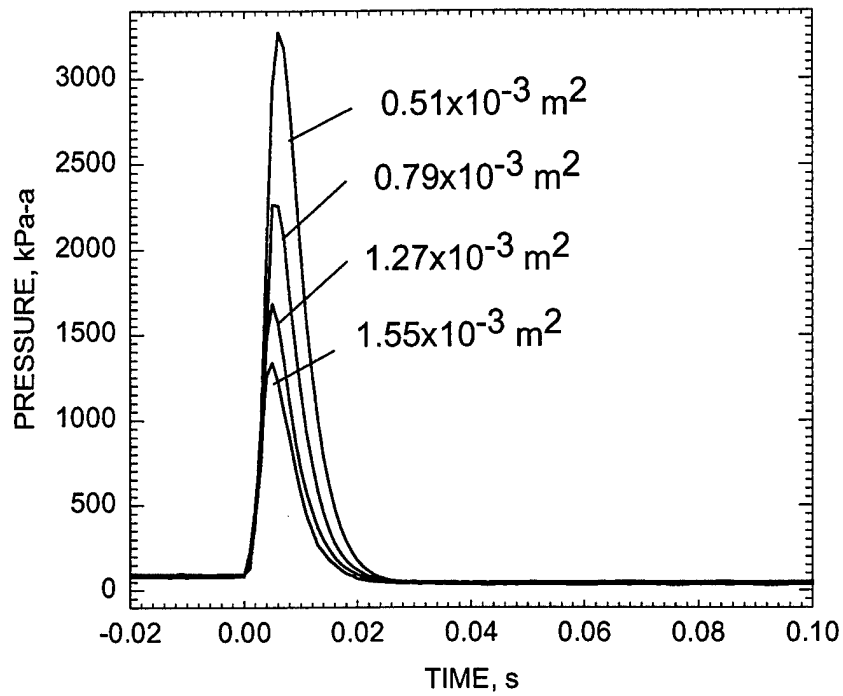
Figure 20. Chamber pressure created by SPGG discharge as a function of bypass area.
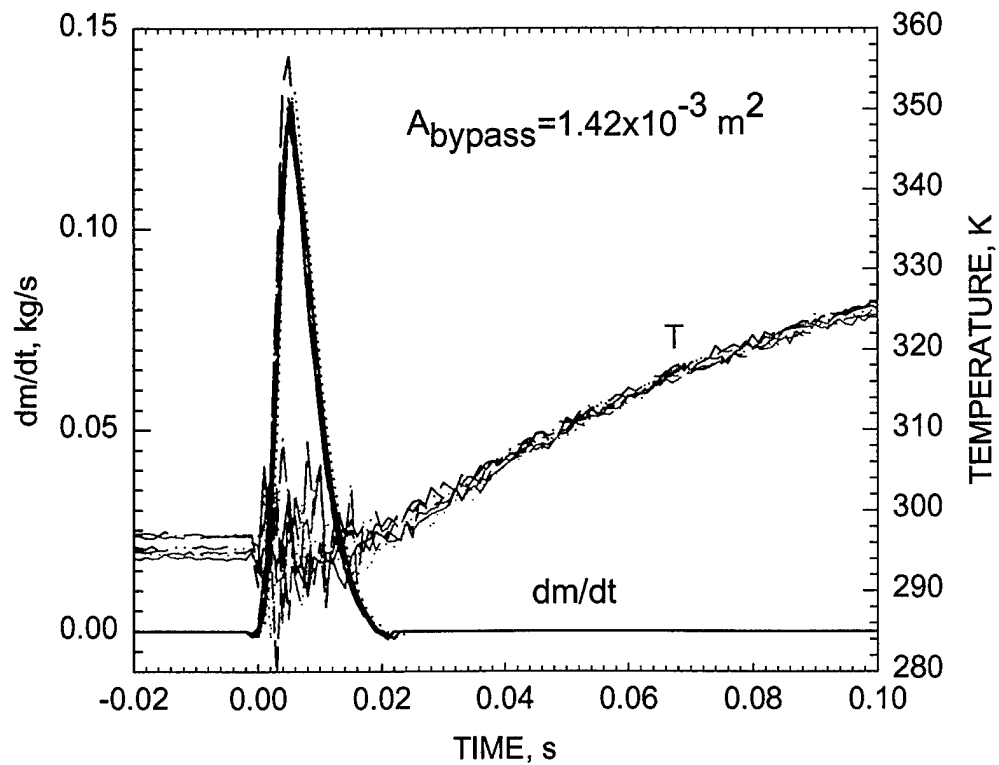
Figure 21. Discharge chamber thermocouple temperature and estimated mass flow of SPGG efluent added to air stream for multiple identical runs.

31
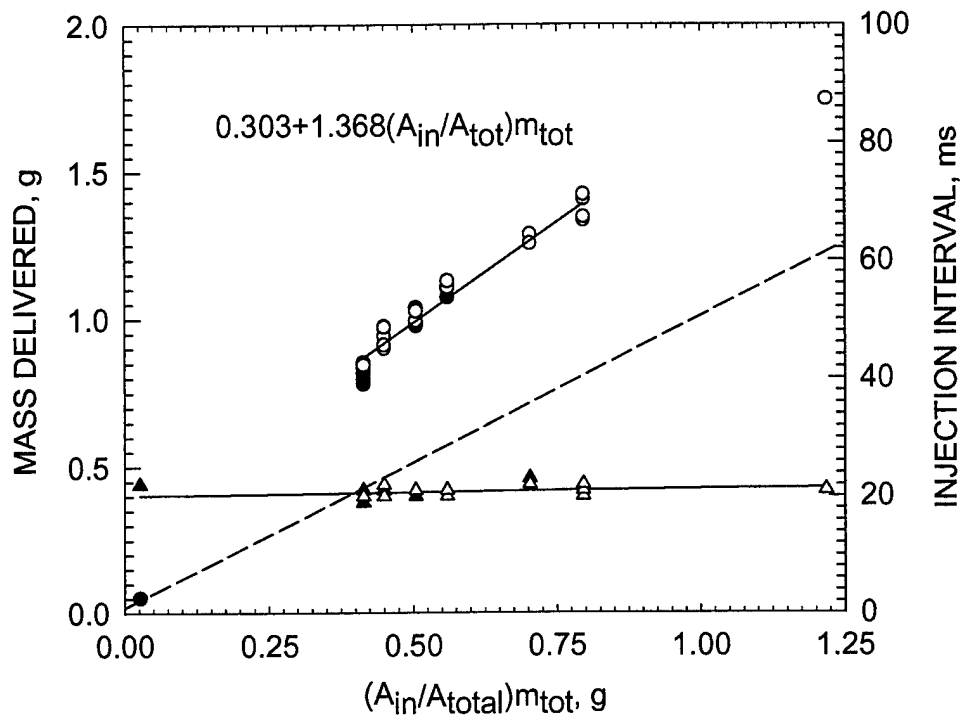
Figure 22. Injection interval (triangles) and calculated mass delivered to flame (circles) as function of area ratio times total mass of gas generated (20.7 g).
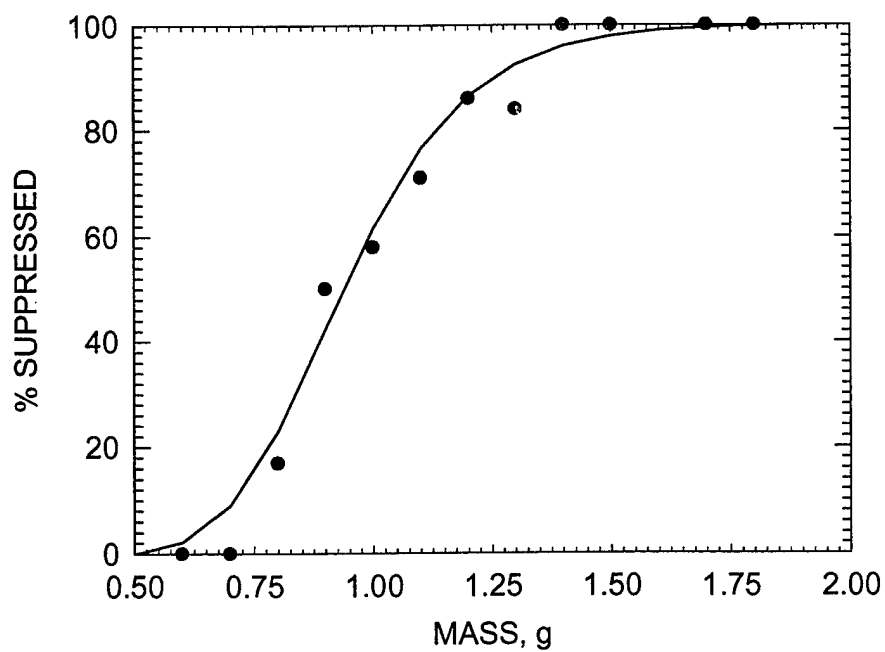
Figure 23. Percent of flames extinguished as a function of mass delivered to flame by SPGG.
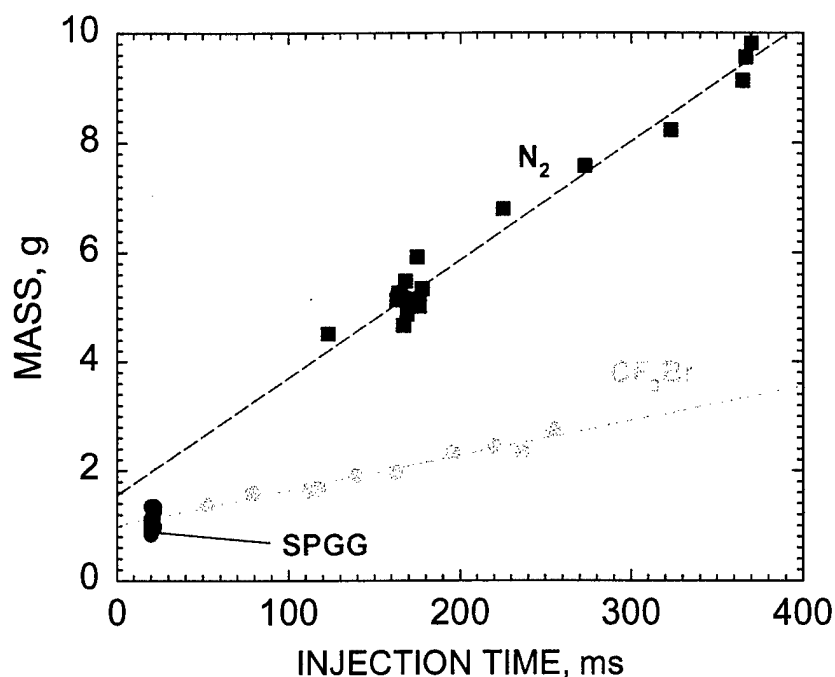
Figure 24. Impact of injection time interval on the mass of agent (CF_3Br, N_2, or SPGG) required to suppress step-stabilized propane pool fire.

Effect of Hot Surface

Figure 2 shows the location of the inverted-vee obstacle placed downstream of the propane pool. An ethane-fueled torch was used to preheat the upstream surface of the obstacle to produce temperatures in excess of 1000 °C as measured by a type-S thermocouple mounted on the exterior face. Pyrometer readings of the interior (i.e., fire-side) surface indicated temperatures were about 50 °C cooler. Experiments were conducted to determine the minimum temperature needed to ignite the propane pool when the air and propane were set to the low flow conditions. Ignition occurred when the hot surface reached temperatures close to 1000 °C.

A spray nozzle was located upstream of the stabilizing step that allowed liquid JP-8 to be sprayed over the propane pool and onto the heated inverted-vee surface. The fuel acted to cool the surface approximately 150 °C below the temperature that had been obtained when only the gaseous propane fuel was flowing. The JP-8 was ignited and formed a flame that stabilized behind the vee when the temperature of the surface exceeded 900 °C.

The procedure used to test for re-ignition of the propane fire was as follows. The propane fire was initiated under the operating conditions of an air flow velocity of 1.5 m/s and a propane flow rate of 33 mL/s, and the obstruction was heated to the temperature desired. The flame was observed to extend past the obstruction. The agent was introduced to the system for three different injection times of 75 ms, 100 ms, and 150 ms, and the occurrence of flame suppression was observed. The cylinder pressure was increased if suppression did not occur, and then the process repeated. The agents tested were nitrogen, HFC125, and CF_3Br. The agent injection time was varied to observed the effect on re-ignition of the propane fuel. The JP-8 stream was then directed against the heated obstruction while the unignited propane still was flowing into the wind tunnel passage. If re-ignition did not occur after 10 s, then the propane flow was terminated. Experiments were repeated with and without the JP-8 stream in order to determine the efficacy of the stream in the re-ignition process. A variety of re-ignition results were

33

observed which depended on the injection time interval of the agent and JP-8 stream. Re-ignition was found to occur when the obstruction was above 900 °C (bright red), and a function of the cooling effect by the agent and JP-8 liquid stream.

The influence of the surface temperature was found to be bi-modal: when the temperature of the hot surface (with the JP-8 and propane flowing) was below about 880 °C ± 10 °C, the amount of agent necessary for suppression was the same as when the surface was unheated; and when the temperature was above 890 °C ± 10 °C, reignition always occurred within about 10 s independent of higher temperatures or the amount of N_2 added. A similar finding resulted when nitrogen was replaced by CF_3Br, although the measured dividing temperature was about 50 °C higher. This difference may have been associated with a build-up of carbon on the hot surface that insulated the fire-side surface from the ethane torch, making an accurate determination of the surface temperature more difficult.

A few experiments were conducted with the temperature reduced to the Leidenfrost point (290 °C for JP-8) to determine if an increase in contact time would compensate for the lower temperature. Ignition of the JP-8 and propane did not occur. Satcunanathan and Zaczek [27] measured the ignition delay of kerosene and Diesel fuels on a hot metal surface and found that ignition could occur in less than one second for a 2 mm diameter droplet, but that the ignition time increased for temperatures between about 500 °C and 550 °C due to surface boiling. No ignition of the JP-8 droplets was observed in the TARPF when the vee-surface temperatures was maintained in the range between 360 °C and 440 °C. However, Jomaas et al. [14] found that ignition of a JP-8 pool fire would occur in their step-stabilized burner for temperatures in the same range. (See Appendix B.)

Data Correlation
The effectiveness of the gaseous agents is compared to that of the SPGG through use of a simple agent mixing model to describe the suppression phenomena. A more detailed description of the model can be found in Grosshandler et al. [28] and Hamins et al. [9]. A characteristic time, τ, for mixing of the agent into the flame zone can be defined in terms of the air and agent volume flows, ($V'_{air} + V'_{agent}$), and the step height, h, as

$$\tau = \gamma h / \{(V'_{air} + V'_{agent})/[(L-h)L]\} \tag{20}$$

where L is the width of the tunnel and γ is an empirical non-dimensional parameter that relates the ratio of the distance that a fluid element travels within the recirculation zone to the obstacle height. Takahashi et al. [10] measured the characteristic mixing time in a similar facility and found γ to be around 40. Evaluating Eq. (20) for the range of flows and baffle heights examined in the current study and using a value of 40 for γ, τ is found to vary between 0.04 s and 0.40 s.

Hamins et al. [9] found that for a specified injection duration it is possible to relate the mole fraction of agent required to achieve extinction, X, to the characteristic mixing time, τ, according to the following relation:

$$X/X^* = [1 - \exp(-\Delta t/\tau)]^{-1} \tag{21}$$

where X^* can be found experimentally by flowing agent continuously into the air stream at increasing rates until extinction occurs. If the air flow is low enough, the value of X^* is expected to be similar to the cup burner extinction requirements [9]. For propane in a cup burner, Trees et al. [5] found the value of X^* to be 0.32 for N_2, 0.41 for Ar, and 0.039 for CF_3Br. Others have found similar results [29]. Figure 26 compares the suppression results for N_2, CF_3Br, and SPGG through use of Eq. (21), where the normalized mole fraction is plotted as a function of the non-dimensional injection interval. For the SPGG results, X^* is assumed to equal the X^* value for argon. While the data do not fall exactly on the model, the trend of the results are well represented by the single curve when one considers run-to-run variations due to the statistics associated with suppression of a turbulent flame. The results show that the
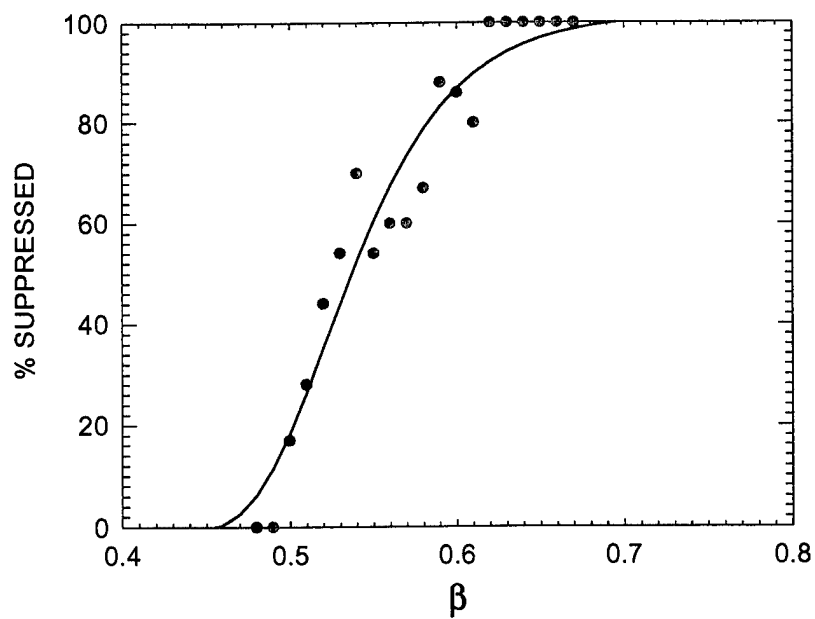
Figure 25. Percent of flames extinguished as a function of the estimated mass fraction of agent.
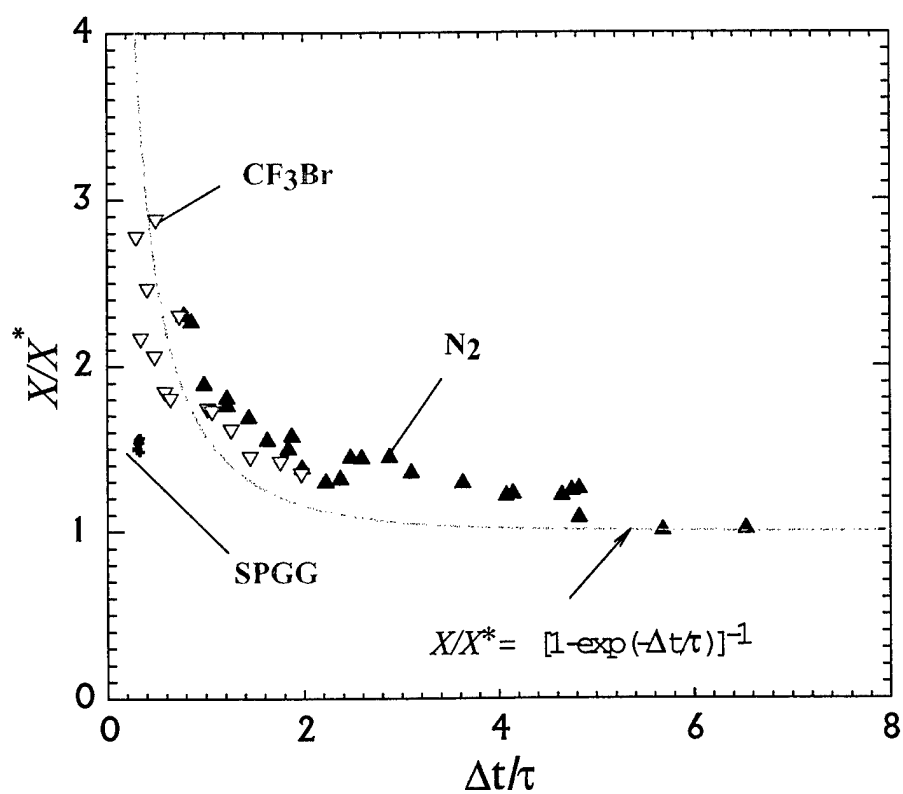
Figure 26. Normalized mole fraction as a function of non-dimensional injection interval, comparing N_2, CF_3Br, and SPGG
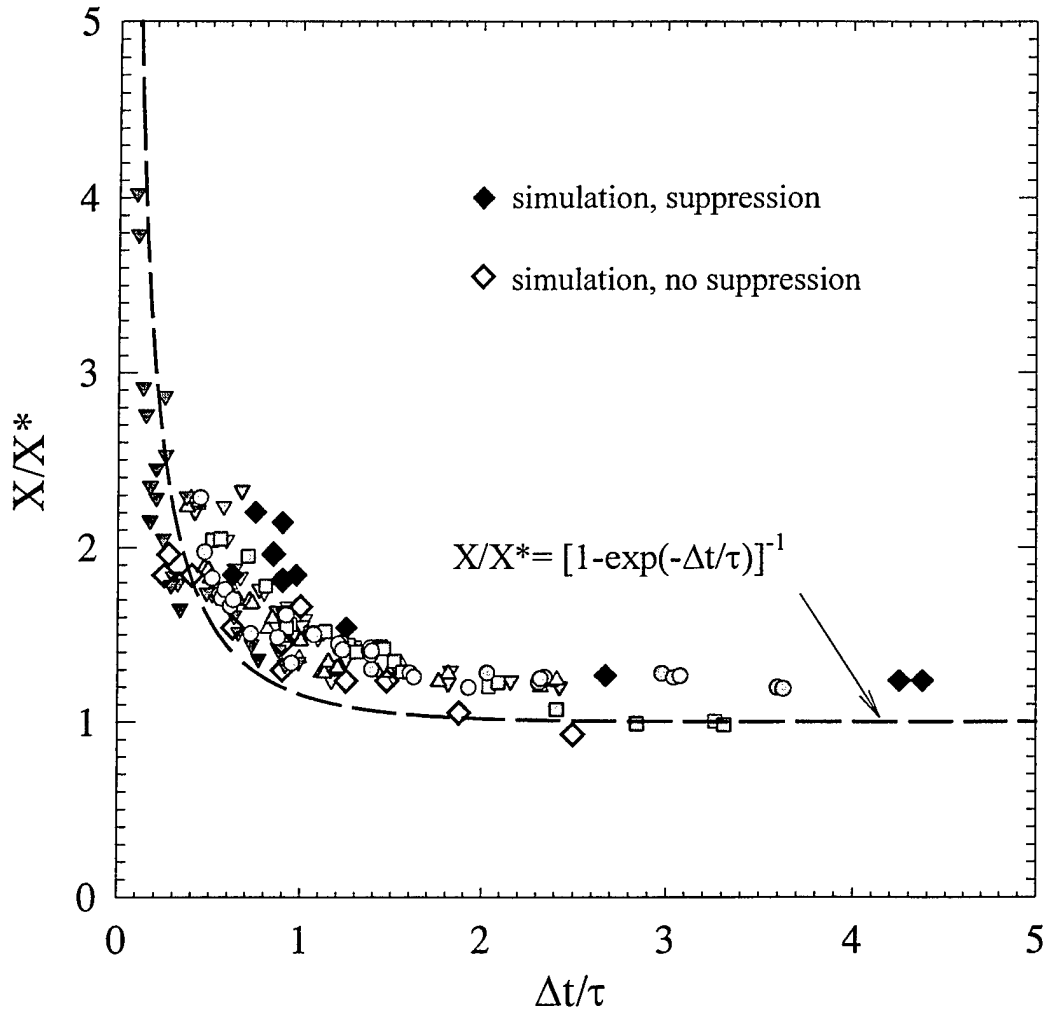
Figure 27. Suppression mole fraction of agent (N_2 or CF_3Br) normalized by cup burner values (X^*) as function of injection time interval normalized by characteristic residence time (τ). Gray symbols: experimental results keyed to Fig. 19; black diamonds: direct numerical simulations with N_2.

effectiveness of the SPGG hybrid significantly exceeds the model predictions.

For laminar diffusion flames strained at intermediate rates, Trees et al. [5] showed that the minimum extinction mole fraction of agent in a counterflow flame decreases from the cup burner value when the strain rate is 50 s^{-1} to much smaller values for a strain rate of 400 s^{-1}. Although the flow in the recirculating region behind a step is much more complicated than in a counterflow flame, the strain rate in the current study should scale with $1/\tau$. When the flow of air is increased sufficiently, the flame becomes strained to the point that agent is not needed for extinguishment (i.e., $\chi^* \to 0$) and the flame blows out. In other words, as the air flow in the TARPF increases, the model represented by Eq. (21) in Fig. 26 must be adjusted not only for changes in τ, but also for changes in the value of χ^*.

A number of direct numerical simulations of N_2 suppressing the step-stabilized flame were conducted assuming a finite reaction rate with one step chemistry. The injection interval and mole

fraction of nitrogen were varied, and the flame structure was followed through the transient period. Either the flame was extinguished, or it was reestablished following the passage of the N_2 pulse. Figure 27 summarizes the results. Open diamonds indicate that no suppression occurred; solid diamonds imply that suppression was successful. The gray symbols refer to the experimental N_2 and CF_3Br data for all geometries examined. The dotted line is Eq. (21).

The computations are able to distinguish regimes of extinction and non-extinction in the case of nitrogen as an agent. The numerical model cannot at present predict what will happen when a chemically active agent like CF_3Br is introduced into the flame. The cooling and dilution of the flame by the agent can be predicted, and hopefully, simplified combustion mechanisms for various chemically-active agents can be developed that will lead to a better understanding of the dynamics of fire suppression.

CONCLUSIONS AND RECOMMENDATIONS

A transient application, recirculating pool fire (TARPF) facility has been built for screening the suppression effectiveness of halon 1301 replacements. The ability to measure the relative effectiveness of alternative agents is key to the development of new fire suppression systems. The physical and chemical properties, and the manner of storage and release of the next generation suppression systems may be quite unlike CF_3Br, but their effectiveness must still be bench-marked against it. The TARPF facility provides the means to screen gaseous agents and solid propellant gas generator concepts in the laboratory for applications in protected spaces involving baffle-stabilized pool fires.

This report represents a comprehensive study, utilizing experimentation, advanced numerical modeling, and analysis to develop and characterize a well-controlled fire suppression facility. Sample experimental results are shown that demonstrate the utility of the facility. Detailed fabrication drawings of the facility are provided in the Appendix of this report. In addition, the experimental procedures are described in detail in the text. Nominal air velocities between 2 m/s and 23 m/s flowing over a backward-facing step were examined. Because the air is metered with a sonic orifice, the injection of agent does not modulate the air flow. The minimum amount of agent for flame extinguishment is substantially and directly affected by the air velocity and the interval of injection. A simple mixing model is useful to explain the observed trend of decreasing suppressant mole fraction with increasing injection duration. A detailed numerical model of the suppression of baffle stabilized fires was developed. The model was successful in simulating the suppression event including a quantitative determination of agent mass requirements.

The facility provides the capability to test solid-propellant gas generators allowing direct comparison of compressed and solid-propellant generated gases for the first time. The capability to test SPGGs under well-controlled laboratory conditions allows evaluation among different propellant formulations, particulate yields, and burning rates for various SPGG designs. Results showed that the effectiveness of the hybrid SPGG exceeded that of CF_3Br and that its effectiveness was significantly greater than expected from the model prediction. Further research could lead to significant improvement of the SPGG as well as traditional agent through enhanced suppressant system design.

Several other research areas require further investigation. These include the effect of the air flow on the steady-state extinction mole fraction of agent, the relationship between agent injection and its concentration history at the flame, and especially the observed differences in the normalized mole fractions of CF_3Br, N_2, and the SPGG for very short injection time intervals.

REFERENCES

[1] Bennett, M.J., Caggianelli, G.M., Kolleck, M.L., and Wheeler, J.A., "Halon Replacement Program For Aviation, Aircraft Engine Nacelle Application Phase II - Operational Comparison of Selected Extinguishants," WL-TR-97-3076, Wright-Patterson Air Force Base, May 1997.

[2] W. Leach, personal correspondence, 1998.

[3] Hamins, A., Cleary, T., and Yang, J., "An Analysis of the Wright-Patterson Full-Scale Engine Nacelle Fire Suppression Experiments," NISTIR 6193, National Institute of Standards and Technology, Gaithersburg, MD, November 1997.

[4] "Clean Agent Fire Extinguishing Systems," NFPA 2001, National Fire Protection Association, Quincy, MA, 2000.

[5] Trees, D., Seshadri, K., and Hamins, A.M., "Exp. Studies of Diffusion Flame Extinction with Halogenated and Inert Fire Suppressants," in Halon Replacements - Technology and Science, A. Miziolek and W. Tsang (eds.), ACS Symposium Series 611, Am.Chem. Soc., 1995.

[6] Hirst, R. and Sutton, D., *Combust. Flame 5*, 319 (1961).

[7] Hirst, R., Farenden, P.J., and Simmons, R.F., *Fire Tech. 12*, 266 (1976).

[8] Hirst, R., Farenden, P.J., and Simmons, R.F., *Fire Tech. 13*, 59 (1977).

[9] Hamins, A., Cleary, T., Borthwick, P., Gorchov, N., McGrattan, K., Forney, G., Grosshandler, W., Presser, C., and Melton, L., "Suppression of Engine Nacelle Fires," chap. 9 in *Fire Suppression Syst. Performance of Alter. Agents in Aircraft Engine and Dry Bay Lab. Simulations*, NIST SP 890: Vol. II, Gann, R.G. (ed.), DoC, Washington, DC, Nov. 1995.

[10] Takahashi, F., Schmoll, W.J., Strader, E.A., and Belovich, V.M., "Suppression of a Nonpremixed Flame Stabilized by a Backward-Facing Step," *Combust. Flame 122*, 105-116 (2000).

[11] Hamins, A, Gmurczyk, G., Grosshandler, W., Rehwoldt, R., Vazquez, I., Cleary, T., Presser, C., and Seshadri, K., "Flame Suppression Effectiveness", Chapter 4 in *Evaluation of Alternative In-flight Fire Suppressants for Full-scale Simulated Aircraft Engine Nacelles and Dry Bays*, (Grosshandler, W.L., Gann, R.G., and Pitts, W.M., eds.) NIST SP 861, National Institute of Standards and Technology, Gaithersburg, MD, April 1994.

[12] Wierenga, P .H., and Holland, G. F., "Developments in and Implementation of Gas Generators for Fire Suppression", *Proceedings of the Halon Options Technical Working Conference*, Albuquerque, NM, April 1999, 453-468.

[13] Mitchell, M., "Hybrid Fire Extinguisher for Occupied and Unoccupied Spaces," *Proceedings of the Halon Options Technical Working Conference*, Albuquerque, NM, April 1999.

[14] G. Jomaas, B.T. Roberts, J. DuBois and J.L.Torero, "A Study of the Mechanisms Leading to Re-ignition in a "Worst Case" Fire Scenario, Final Report, Cooperative Agreement No. 70NANB8H0043

[15] Taylor, B.N. and Kuyatt, C.E., "Guidelines for Evaluating and Expressing the Uncertainty of NIST Measurement Results," NIST Technical Note 1297, National institute of Standards and Technology, 1993.

[16] Yang, J.C., Donnelly, M.K., Prive, N.C., and Grosshandler, W.L., "Dispersed Liquid Agent Fire Suppression Screen Apparatus," NISTIR 6319, National Institute of Standards and Technology, Gaithersburg, MD, July 1999.

[17] Neidert, J., personal communication, Atlantic Research Corporation (ARC), 2000.

[18] Liou, T.M., and Hwang, P.W., "Numerical Visualization and Residence Time Determination of Turbulent Reacting Duct Flow with Mass Bleed and a Backstep on One Wall," *Proceedings of the Twenty-Seventh Symposium (International) on Combustion*, The Combustion Institute, pages 1131-1138, 1998.

[19] Weller, H.G., Tabor, G., Gosman, A.D., and Fureby, C., "Application of a Flame-Wrinkling LES Combustion Model to a Turbulent Mixing Layer," *Proceedings of the Twenty-Seventh Symposium (International) on Combustion, The Combustion Institute*, pages 899-907, 1998.

[20] McGrattan, K.B., Baum, H.R., Rehm, R.G., Hamins, A., and Forney, G.P.,"Fire Dynamics Simulator, Technical Reference Guide," Technical Report NISTIR 6467, National Institute of Standards and Technology, Gaithersburg, Maryland, January 2000.

[21] Reid, R.C., Prausnitz, J.M. and Poling, B.E., *Properties of Gases and Liquids*, McGraw-Hill, Inc., New York, 4th edition, 1987.

[22] Grosshandler, W., Hamins, A., McGrattan, K, Charagundla, S.R., and Presser, C., "Suppression Of A Non-Premixed Flame Behind A Step," *Proceedings of the Twenty-eighth Symposium (International) on Combustion, The Combustion Institute*, in press, 2000.

[23] Rehm, R.G., and Baum, H.R., "The Equations of Motion for Thermally Driven, Buoyant Flows," *Journal of Research of the NBS 83*, 297-308, 1978.

[24] Westbrook, C.K. and Dryer, F.L., "Simplified Reaction Mechanisms for the Oxidation of Hydrocarbon Fuels in Flames," *Combustion Science and Technology 27*, 31-43, 1981.

[25] Pitts, W.M., Mulholland, G.W., Bruel, B.D., Johnsson, E.L., Chung, S., Harris, R.H., and Hess, D., "Real-time Suppressant Concentration Measurement," chap. 11 in *Fire Suppression Syst. Performance of Alter. Agents in Aircraft Engine and Dry Bay Lab. Simulations*, NIST SP 890: Vol. II, Gann, R.G. (ed.), DoC, Washington, DC, Nov. 1995.

[26] Pitts, W.M., and Yang, J.,"Characterization and Identification of Super-Effective Thermal Fire Extinguishing Agents--Final Report," Technical Report NISTIR xxxx, National Institute of Standards and Technology, Gaithersburg, Maryland, in press, 2001.

[27] Satcunanathan, S., and Zaczek, B.J., "The Spontaneous Ignition and Ignition Delay of Liquid Fuel Droplets Impinging on a Hot Surface," Thermodynamics and Fluid Mechanics Convention, Institution of Mechanical Engineers, London, 27-29 March, 1968.

[28] Grosshandler, W.L., Hamins, A., Charagundla, R., and Presser, C., "Suppression Effectiveness Screening for Impulsively Discharged Agents," Proceedings of Halon Options Technical Working Conference, Albuquerque, pp. 15-25, 2000.

[29] Sheinson, R. S., Penner-Hahn, J. E.; Indritz, D., "The Physical and Chemical Action of Fire Suppressants", *Fire Safety Journal* 15, 1989, pp 437-450.

BIBLIOGRAPHY

Grosshandler, W., "Screening Of Transient Agent Effectiveness In Combusting Recirculating/Re-Ignition Zone Burning Gaseous Or Condensed-Phase Fuels (3a/2)," FY1998 Next Generation Program Annual Research Meeting, June 29, 1998, Rockville, MD.

Grosshandler, W.L., Hamins, A., McGrattan, K.B., and Presser, C., "Transient Agent, Recirculating Pool Fire (TARPF) Suppression Screen," in annual Conference on Fire Research: *Book of Abstracts,* Beall, K.A., Editor, NISTIR 6242, National Institute of Standards and Technology, Gaithersburg, MD, pp. 115-116, October 1998.

Grosshandler, W., Donnelly, M., Charagundla, R., and Presser, C., "Suppressant Performance in a Baffle-stabilized Pool Fire," Halon Options Technical Working Conference, University of New Mexico, Albuquerque, April, 1999.

Grosshandler, W.L., "Transient Application Recirculating Pool Fire Agent Effectiveness Screen," FY 1999 Next Generation Program Annual Research Meeting, Gaithersburg, May 1999.

Grosshandler, W.L., "Suppression of Baffle-Stabilized," poster presentation at the Sixth International Symposium on Fire Safety Science, University of Poitiers, France, July 1999.

Grosshandler, W.L., Hamins, A., Charagundla, R., and Presser, C., "Suppression Effectiveness Screening for Impulsively Discharged Agents," Proceedings of Halon Options Technical Working Conference, Albuquerque, pp. 15-25, 2000.

Grosshandler, W., Hamins, A., McGrattan, K, Charagundla, S.R., and Presser, C., "Suppression Of A Non-Premixed Flame Behind A Step," *Proceedings of the Twenty-eighth Symposium (International) on Combustion, The Combustion Institute,* in press, 2001.

Jomaas, G., Roberts, B.T., DuBois, J., and Torero, J.L.,"A Study of the Mechanisms Leading to Re-ignition in a 'Worst Case' Fire Scenario," Final Report, Cooperative Agreement No. 70NANB8H0043, Department of Fire Protection Engineering, University of Maryland College Park, MD20742-3031, June, 2000 (also NIST GCR 01-806, National Institute of Standards and Technology, Gaithersburg, MD, January 2001.

Grosshandler, W., "SPGG Effectiveness Screening Using the NIST Transient Application Recirculating Pool Fire Facility," SPGG Consortium Meeting, Gaithersburg, MD, Sept. 12 2000

Grosshandler, W.L., "Transient Application Recirculating Pool Fire Agent Effectiveness Screen," FY 2000 Next Generation Program Annual Research Meeting, Gaithersburg, November 2000.

Grosshandler, W., Hamins, A., McGrattan, K., and Presser, C., *Transient Application, Recirculating Pool Fire, Agent Effectiveness Screen: Final Report, NGP Project 3A/2/890,* NISTIR 6733, National Institute of Standards and Technology, Gaithersburg, MD, April 2001.

Grosshandler, W., Hamins, A., McGrattan, K., and Presser, C., "Transient Application, Recirculating Pool Fire, Agent Effectiveness Screen: Final Report," Proceedings of Halon Options Technical Working Conference, Albuquerque, in press, 2000.

APPENDIX A. Detailed Mechanical Drawings

TRANSIENT AGENT APPLICATION
EFFECTIVENESS SCREENING FACILITY

HOUSE
AIR
INLET

1 1/2" PIPE

AGENT
INJECTOR

ENTRANCE SECTION
4" SQ. TUBE

TRANSITION SECTION
1.5" RD. TO 4" SQ.

BAFFLE PLATE

4" SQ. TUBE

BURNER ASSEMBLY

INTERNAL RAMP

EXHAUST

FLEXIBLE STEEL DUCT
6" DIA.

2500 mm.

AGENT INJECTOR
(FRONT & TOP VIEWS)
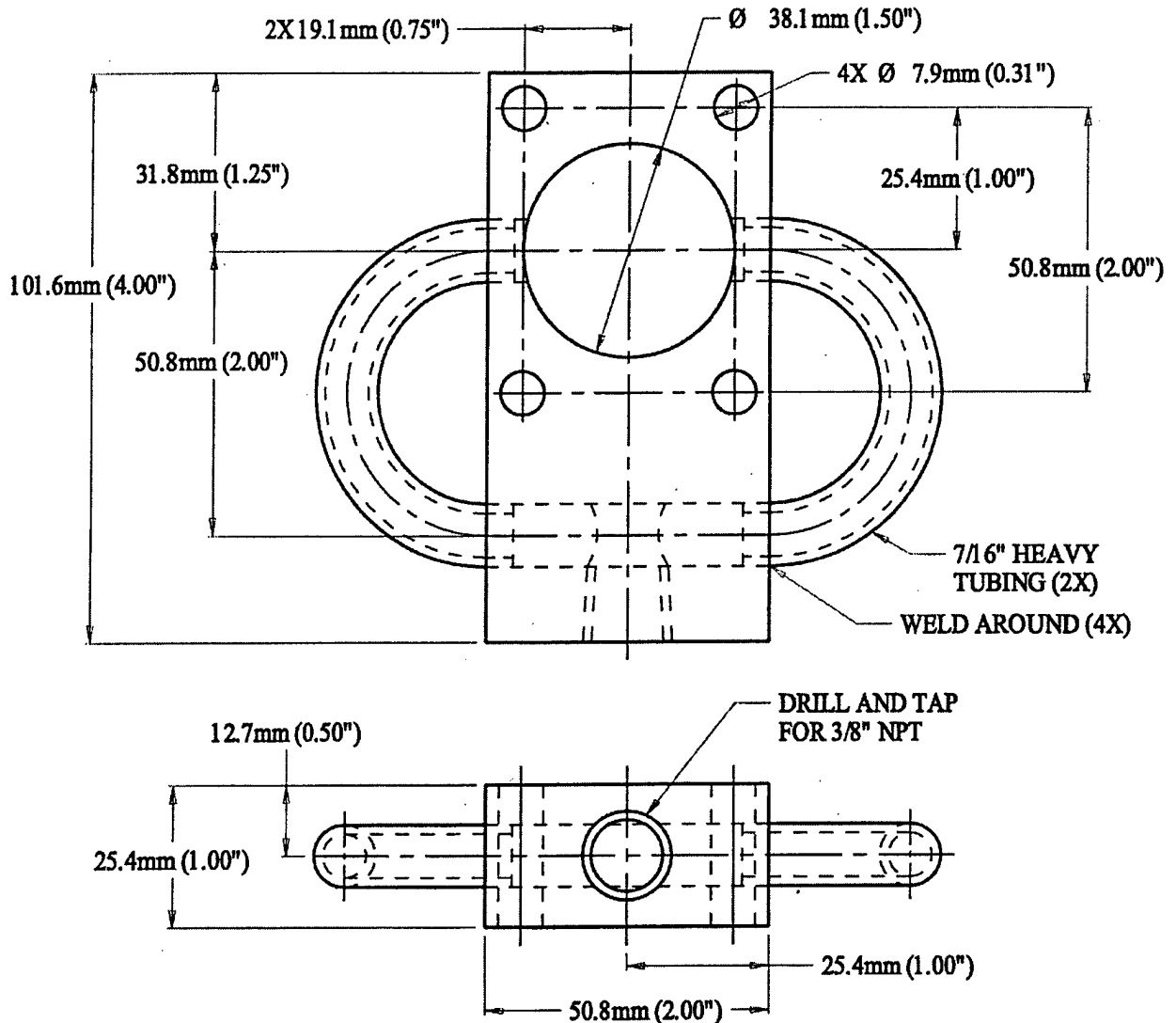
2X 19.1 mm (0.75")

Ø 38.1 mm (1.50")

4X Ø 7.9 mm (0.31")

31.8 mm (1.25")

25.4 mm (1.00")

50.8 mm (2.00")

101.6 mm (4.00")

50.8 mm (2.00")

7/16" HEAVY TUBING (2X)

WELD AROUND (4X)

DRILL AND TAP FOR 3/8" NPT

12.7 mm (0.50")

25.4 mm (1.00")

25.4 mm (1.00")

50.8 mm (2.00")

MATERIAL: STAINLESS STEEL

ASSEMBLY: WELD

TRANSITION SECTION
(FRONT & RIGHT SIDE VIEW)

2X 46.0mm (1.81")

127.0mm (5.00")

8X Ø 7.9mm (0.31")

2X 46.0mm (1.81")

63.5mm (2.50")

2X 58.7mm (2.31")

2X 58.7mm (2.31")

63.5mm (2.50")

2X 4.8mm (0.19")

127.0mm (5.00")

152.4mm (6.00")

3.2mm (0.13") THICK (TYP)

SMOOTH TRANSITION
FROM 38.1mm DIA
TO 92.2mm SQUARE

63.5mm (2.50")
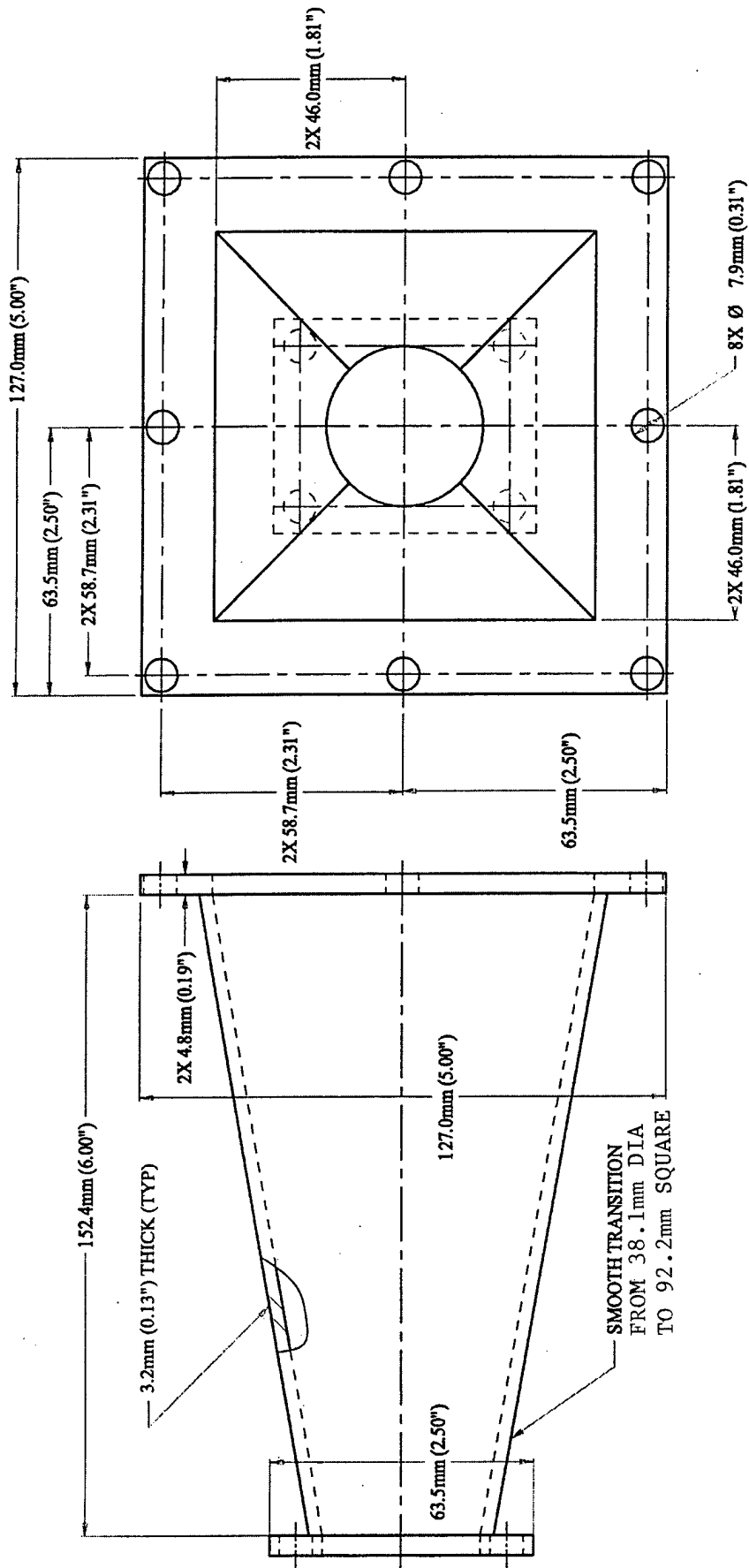
MATERIAL: MILD STEEL

ASSEMBLY: WELD

TRANSITION SECTION
(LEFT SIDE VIEW)

50.8mm (2.00")

25.4mm (1.00")

2X 19.1 mm (0.75")

2X 25.4mm (1.00")

31.8mm (1.25")

Ø 38.1 mm (1.50")

4X Ø 7.9mm (0.31")

ENTRANCE SECTION

4.76mm (0.1875in)

1016mm (40.0in.)

4.76mm (0.1875in)

4x4 TUBING, 4.76mm (0.1875in) WALL

6x Ø6.76mm (2.66in)

38.1mm (1.5in)

38.1mm (1.5in)

63.5mm (2.5in)

4.76mm (0.1875in)

2x Ø5.11mm (0.201in)

127mm (5.0in)

63.5mm (2.5in)

4.76mm (0.1875in)

4.76mm (0.1875in)

5.0in (12.7 cm)

8x Ø6.76mm (0.266in)

127mm (5.0in)

127mm (5.0in)

58.7mm (2.3125in)

58.7mm (2.3125in)

63.5mm (2.5in)

58.7mm (2.3125in)

58.7mm (2.3125in)

63.5mm (2.5in)

MATERIAL: MILD STEEL

BAFFLE PLATES

6x Ø6.76mm (0.266in)

17.46mm (0.688in)

127mm (5in)

A

4.76 (0.188in)

6.35mm (0.25in)

4.76mm (0.188in)

127mm (5in)

63.5mm (2.5in)

4.76mm (0.188in)

17.46mm (0.688in)

92.08mm (3.63in)

4.76mm (0.188in)

38.1mm (1.5in)

38.1mm (1.5in)

25.4mm (1in)

2x Ø5.11mm (0.201 in)

NOTE: A = 81.76mm (3.22in) for 10mm pl
       A = 74.61mm (2.94in) for 17mm pla
       A = 66.78mm (2.63in) for 25mm pla
       A = 56.36mm (2.22in) for 35mm pla
       A = 36.51mm (1.44in) for 55mm pla

Material: Stainless Steel
(5 pieces)

POOL BURNER
(FRONT & TOP VIEW)

203.2mm (8.00")

101.6mm (4.00")

10X Ø 7.9mm (0.31")

4X 47.6mm (1.88")

63.5mm (2.50")

58.7mm (2.31")

A

196.9mm (7.75")
98.4mm (3.88")

127.0mm (5.00")

117.5mm (4.63")

92.1mm (3.63")
184.2mm (7.25")

DRILL HOLE TO CLEAR 3/16" O.D. TUBE
TAP FOR 1/8" NPT
INSTALL SINTERED BRONZE PLATE THEN
INSERT ENDS OF TUBING FROM INSIDE
CAVITY WITH AT LEAST 2" OF THE TUBING
PROTRUDING THROUGH EACH HOLE

3/16" COPPER TUBE
BEND SIMILAR TO
SHOWN SHAPE

A

2X 9.5mm (0.38")

2X 19.1mm (0.75")

SOLDER
ALL AROUND
(2X)

1/4" BRASS
SWAGELOK
TEE

50.8mm (2.00")

2X 38.1mm (1.50")

1/4" COPPER TUBE
BEND SIMILAR TO
SHOWN SHAPE
(2X)

MATERIAL: BRASS PLATE

ASSEMBLY: SOLDER

POOL BURNER
(SECTION A-A)

101.6mm (4.00")

95.3mm (3.75")

50.8mm (2.00")

6.4mm (0.25")

47.6mm (1.88")

19.1 mm (0.75")

25.4mm (1.00")

22.2mm (0.88")

3 3/4" X 7 1/2" X 1/4"
SINTERED BRONZE
PLATE (GRADE 103A)

44.5mm (1.75")

88.9mm (3.50")

BURNER FRAME
(FRONT & TOP VIEW)

212.7mm (8.38")

11.1mm (0.44")

4X 47.6mm (1.88")

46.0mm (1.81")

190.5mm (7.50")

95.3mm (3.75")

92.1mm (3.63")

20X Ø 7.9mm(0.31")

A

NO FILLET (4X)

25.4mm (1.00")

2X 31.8mm (1.25")

50.8mm (2.00")

76.2mm (3.00")

152.4mm (6.00")

A

2X 50.8mm (2.00")

WELD #10-3/4" THREADED
STUDS (16X)

2X 82.6mm (3.25")

BURNER FRAME
(SECTION A-A)

MATERIAL: 3/16" STAINLESS STEEL PLATE

ASSEMBLY: WELD

BURNER WINDOW HOLDER (TOP)

101.2mm
(3.984in)

10x Ø6.756m
(0.266in)

47.63mm
(1.875in)

47.63mm
(1.875in)

47.63mm
(1.875in)

47.63mm
(1.875in)

4.82mm
(.1875in)

19.05mm
(0.75in)

127mm
(5in)

117.60mm
(4.625in)

88.9mm
(3.5in)

177.0mm
(6.969in)

12.7mm
(0.5in)

202.4mm
(7.969in)
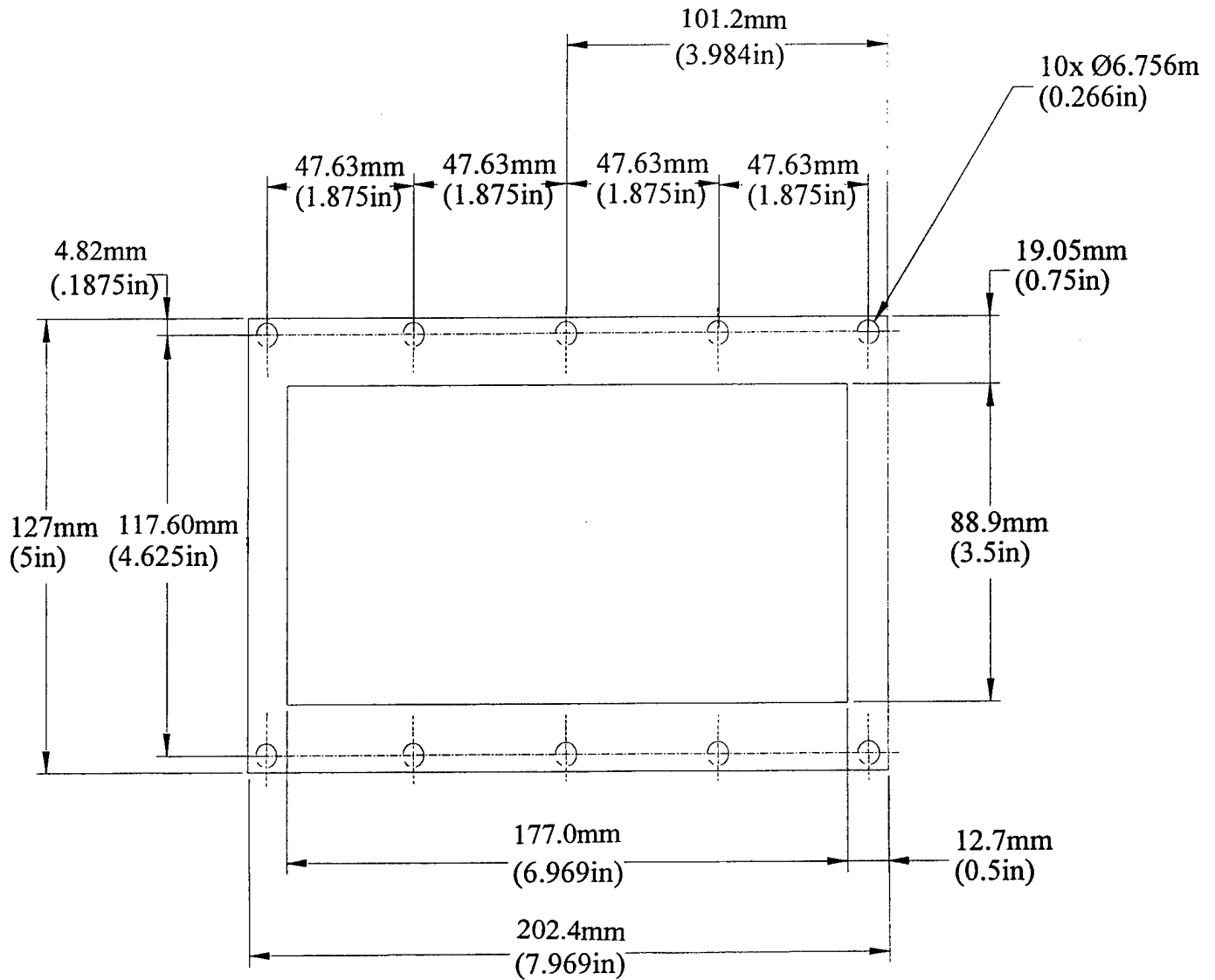
Material: 1.59mm (0.0625in) Stainless Steel

BURNER WINDOW HOLDER (SIDE)

8xØ5.11mm (0.2 in)

177.8mm (7in)

88.9mm (3.5in)

50.8mm (2in)

50.8mm (2in)

6.35mm (.25in)

6.35mm (.25in)

76.2mm (3in)

38.1mm (1.5in)

15.88mm (.625in)

146.1mm (5.75in)

44.45mm (1.75in)

15.8mm (0.625in)

Material: 1.59mm (0.0625in) Stainless Steel Plate

BURNER SIDE PLATE

8xØ5.11mm
(0.2 in)

76.2mm
(3in)

38.1mm
(1.5in)

88.9mm
(3.5in)

50.8mm
(2in)

177.8mm
(7.0in)

50.8mm
(2in)

6.35mm
(.25in)

25.4mm
(1in)

6.35mm
(.25in)

Drill & Tap
for 1/8" NPT

25.4mm
(1in)

Material: 6.35mm (0.25in) Stainless Steel Plate

EXHAUST SECTION
(FRONT & BOTTOM VIEWS)

609.6mm (24.00")

2X 4.8mm (0.19")

2X Ø 50.8mm (2.00")

DRILL THRU AND
TAP FOR #10-32 SCREWS
(8X)

4X 25.4mm (1.00")

4X 25.4mm (1.00")

304.8mm (12.00")

50.8mm (2.00")

101.6mm (4.00")

4" X 4" X 3/16" SQ. TUBING

50.8mm (2.00")

MATERIAL: MILD STEEL

ASSEMBLY: WELD

DRILL AND TAP FOR
#10-32 SCREWS (6X)

50.8mm (2.00")

50.8mm (2.00")

101.6mm (4.00")

25.4mm (1.00")

2X 31.8mm (1.25")

12.7mm (0.50")

2X 34.9 mm (1.38")

2X 31.8mm (1.25")

EXHAUST SECTION
(RIGHT SIDE VIEW)

8X Ø 7.9mm (0.31")
EQUALLY SPACED

Ø 177.8mm (7.00")

Ø 168.3mm (6.63")

46.0mm (1.81")

92.1 mm (3.63")

46.0mm (1.81")

92.1 mm (3.63")
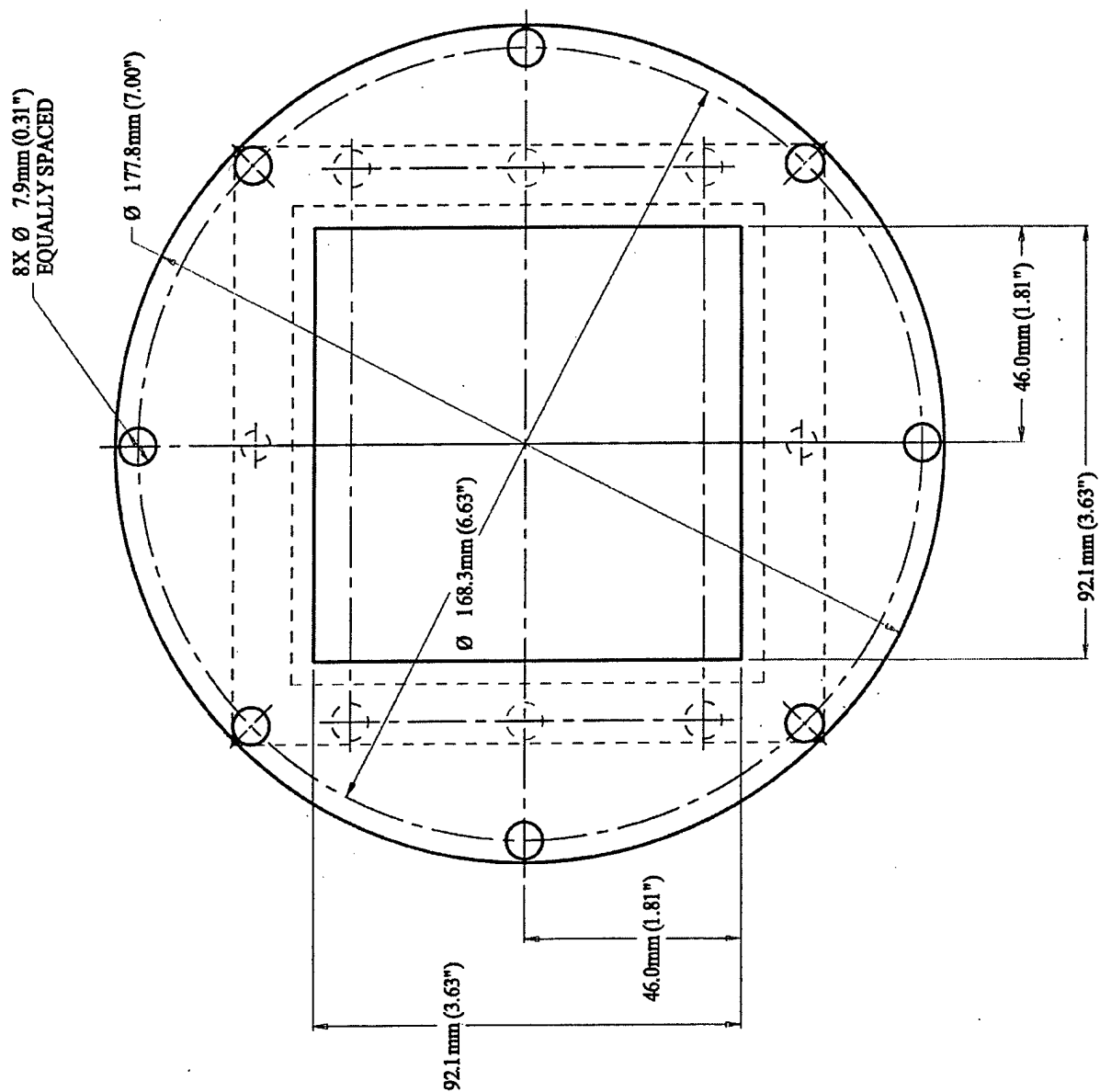
EXHAUST SECTION
(LEFT SIDE VIEW)

127.0mm (5.00")

92.1mm (3.63")

63.5mm (2.50")

2X 58.7mm (2.31")

46.0mm (1.81")

92.1mm (3.63")

127.0mm (5.00")

2X Ø 6.4mm (0.25")

2X 38.1mm (1.50")

46.0mm (1.81")

2X 58.7mm (2.31")

63.5mm (2.50")

6X Ø 7.9mm (0.31")

HOT SURFACE

76.2mm
(3in)

6x Ø5.11mm
(0.201in)

6.35mm
(0.25in)

12.7mm
(0.5in)

A

A

50.8mm
(2in)

82.55mm
(3.25in)

35.05mm
(1.38in)

6.35mm
(0.25in)

16mm
(0.63in)

25.4mm
(1in)

Weld

1.55mm
(0.061in)

25.4mm
(1in)

Section A-A
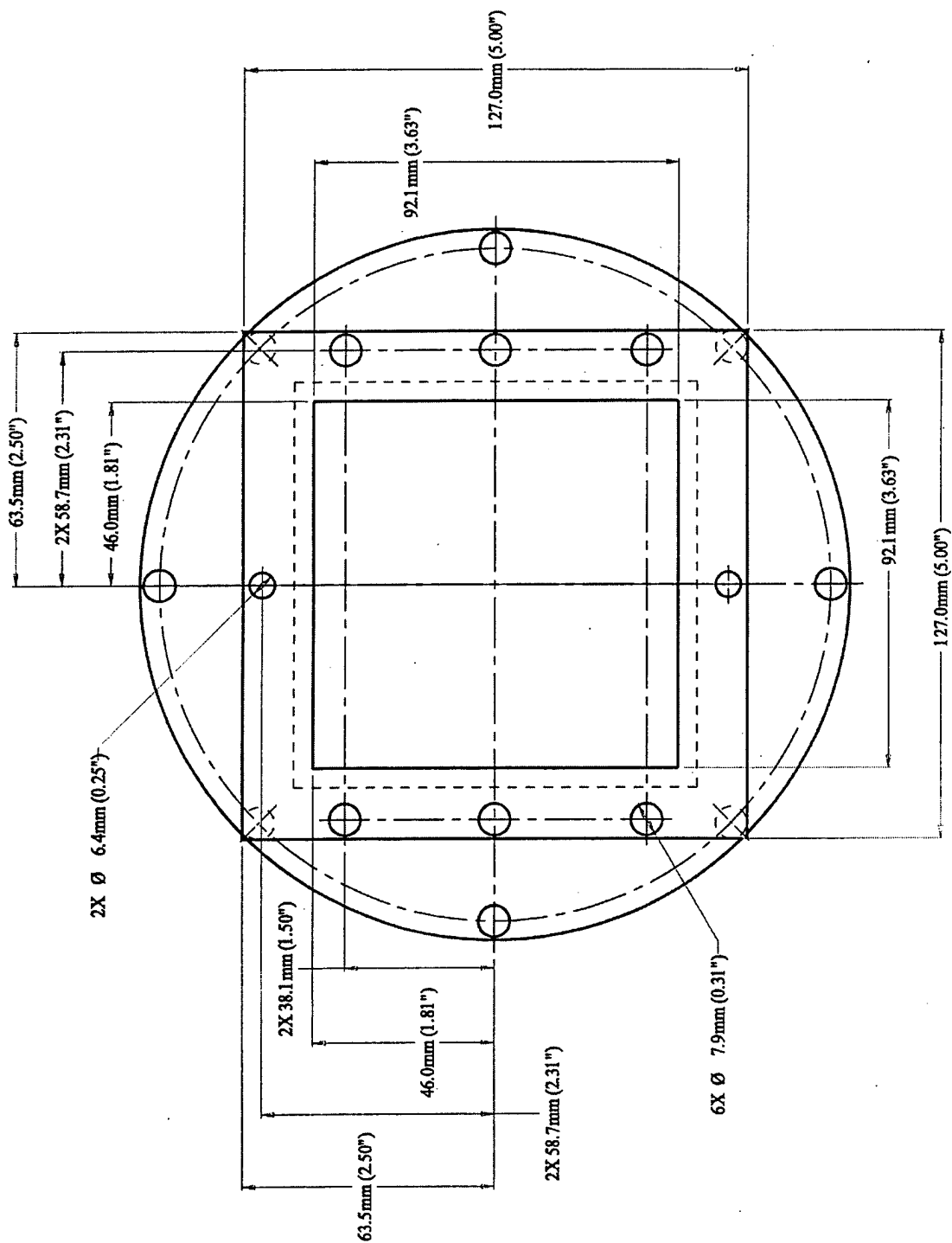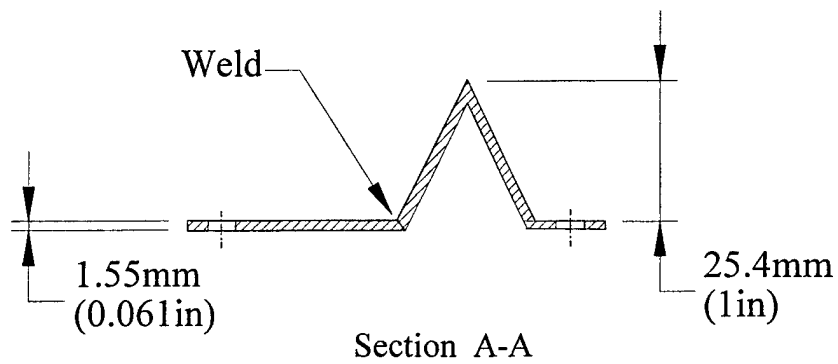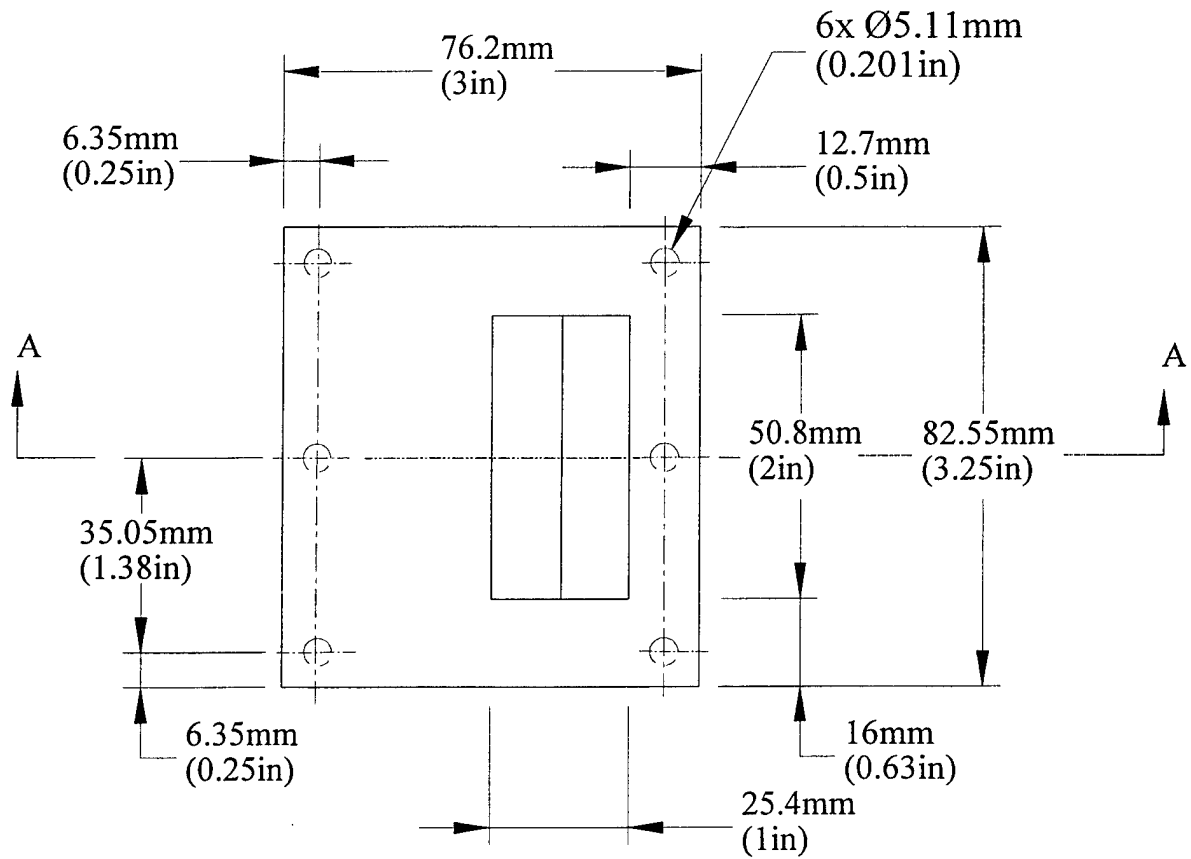
Material: 1.55mm (0.061in) Inconel

SPGG DISCHARGE CHAMBER

MATERIAL: STAINLESS STEEL

SECTION A-A

85.0mm (3.35")

25.0mm (0.98")

5.0mm (0.20")

3/8"-16 UNC TAPPED HOLE (2X)

Ø 50.8mm (2.00")

1/4"-20 UNC TAPPED HOLE 15.9mm (0.63") DEEP (2X)

3/4" NPT DRILL & TAP

Ø 6.4mm (0.25")

2X Ø 6.4mm (0.13")

1/2"-13 UNC TAPPED HOLE 31.8mm (1.25") DEEP (8X)

100.0mm (3.94")

2X 37.3mm (1.47")

50.0mm (1.97")

2X 31.8mm (1.25")

A

38.1mm (1.50")

76.2mm (3.00")

2X 28.1mm (1.11")

38.1mm (1.50")

2X 1/8" NPT DRILL & TAP

A

2X 28.1mm (1.11")

76.2mm (3.00")

SPGG ORIFICE PLATE

10mm
(0.39in)

38.1mm
(1.5in)

Ø1.59mm
(0.063 in)

76.2mm
(3in)

38.1mm
(1.5in)

10mm
(0.39in)

76.2mm
(3in)

4x Ø13.49m
(0.531in)

Material: 3.18mm (0.125in) Stainless Steel

SPGG OUTLET PORT

4x Ø 13.49mm
(0.531in)

Ø12.7mm(0.5 in)
SS Tube 0.065in Wall

Swagelok
Fitting

Weld

50.8mm
(2in)

6.35mm
(0.25in)

38.1mm
(1.5in)

38.1mm
(1.5in)

76.2mm
(3in)

10mm
(0.39in)

10mm
(0.39in)

76.2mm
(3in)
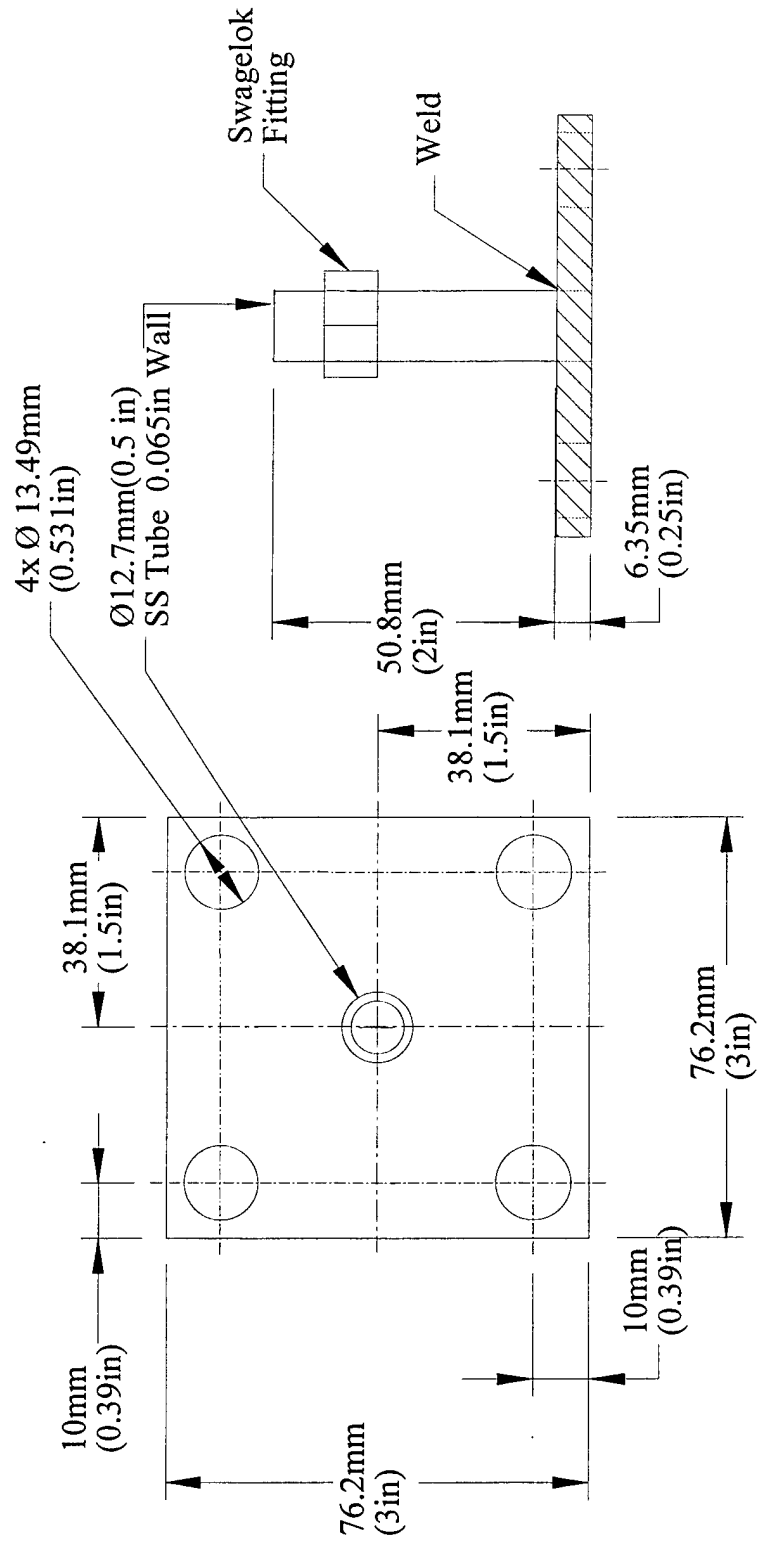
Material: Stainless Steel

SPGG-COPPER-GASKET

10mm
(0.39in)

38.1mm
(1.5in)

Ø 50.8mm
(2in)

76.2mm
(3in)

38.1mm
(1.5in)

10mm
(0.39in)

76.2mm
(3in)

4x Ø13.49m
(0.531in)
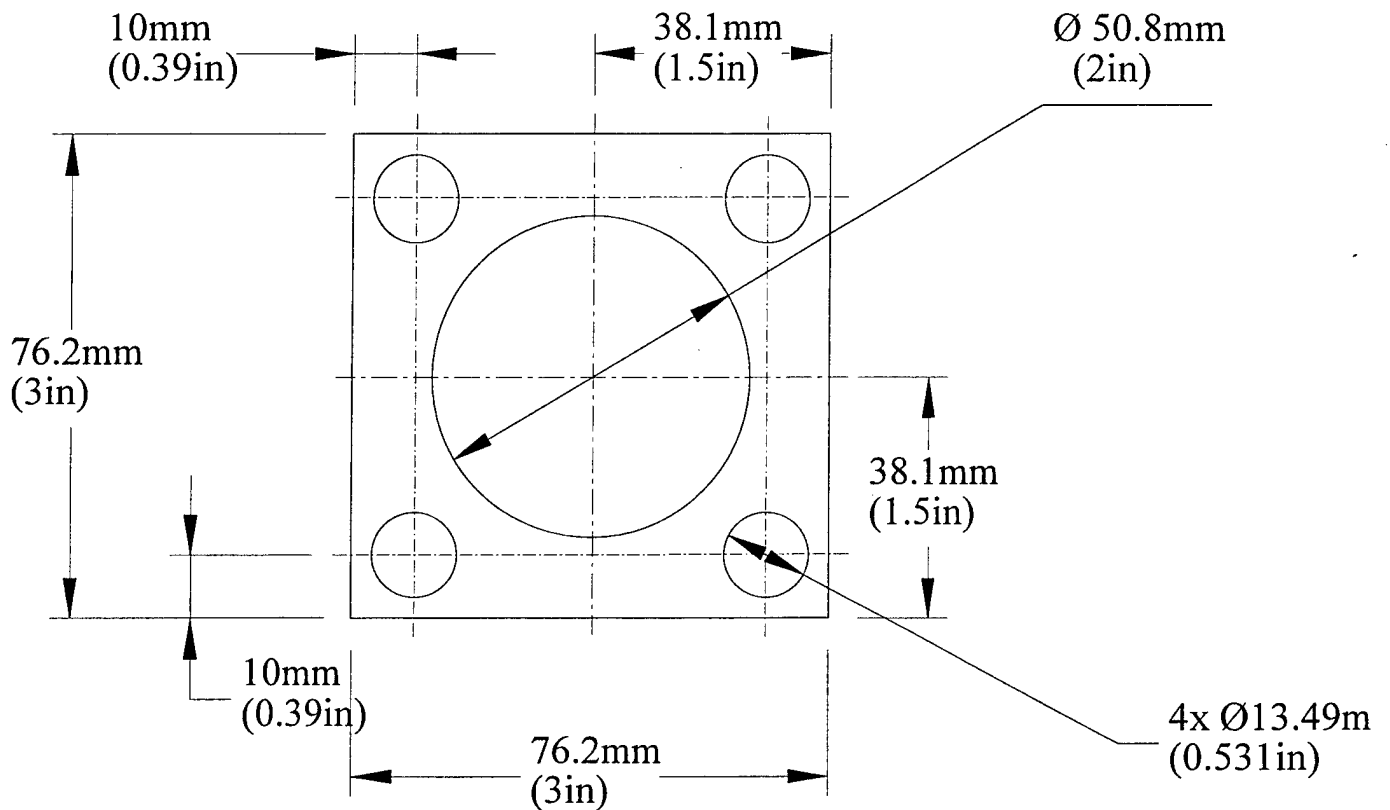
Material: 0.51mm (0.02in) Copper Sheet
3 Pieces

SPGG DISCHARGE CHAMBER BOTTOM PLATE

10mm
(0.39in)

38.1mm
(1.5in)

Drill & Tap
0.75in NPT

76.2mm
(3in)

38.1mm
(1.5in)

10mm
(0.39in)

76.2mm
(3in)

4x Ø13.49m
(0.531in)
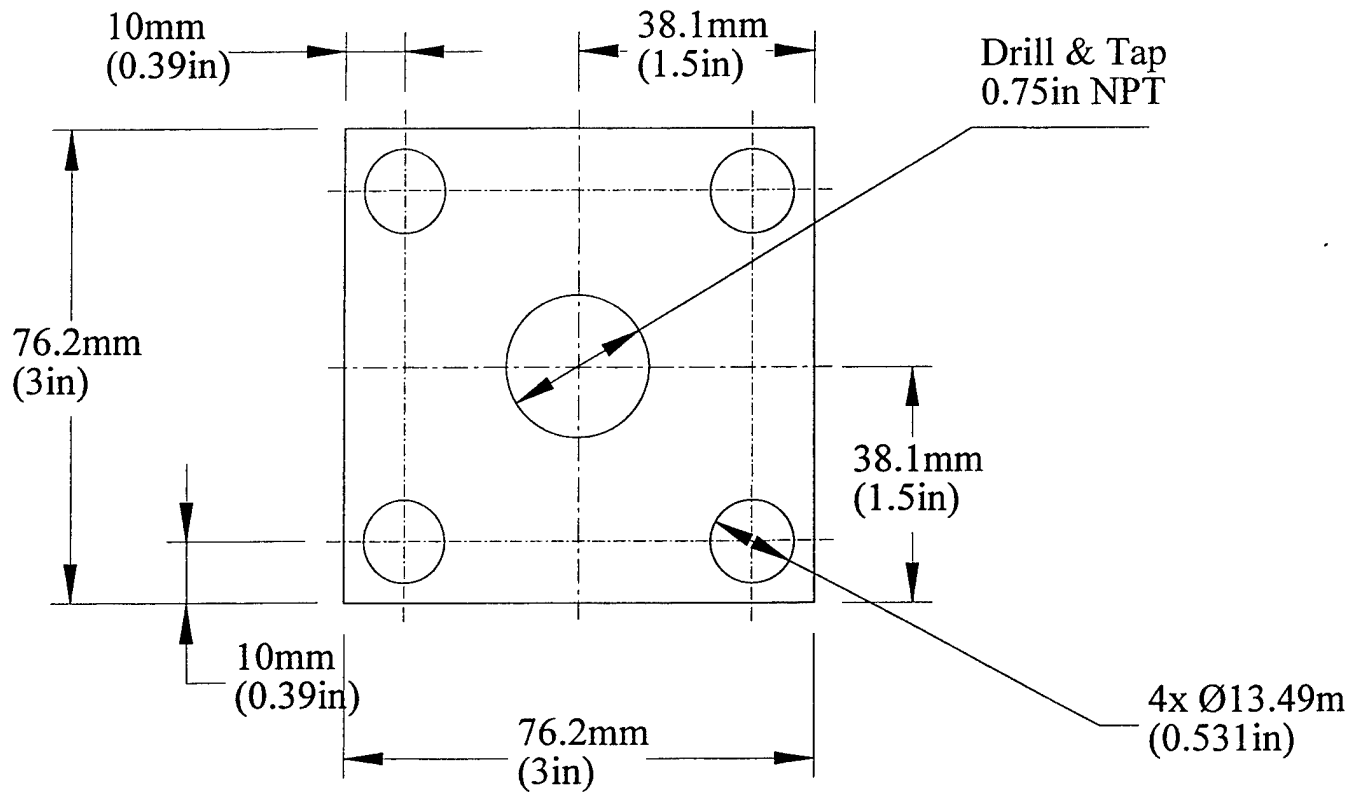
Material: 12.7mm (0.5in) Stainless Steel

APPENDIX B.
A Study of the Mechanisms Leading to Re-Ignition in a "Worst Case" Fire Scenario
Final Report, Cooperative Agreement No. 70NANB8H0043

G. Jomaas, B.T. Roberts, J. DuBois and J.L.Torero
Department of Fire Protection Engineering
University of Maryland
College Park, MD20742-3031

ABSTRACT

A systematic evaluation of the stability of a re-circulation zone behind a backward facing step under conditions expected in an aircraft engine nacelle has been conducted together with the evaluation of the effects of the flow structure on a propane diffusion flame established downstream of the step. The objective being to characterize a "worst case" fire scenario. Characterization of the non-reacting re-circulation zone was performed by means of flow visualization. The parameters varied were the flow velocity, step height and surface temperature. Numerical modeling using a Large Eddie Simulation (LES) code has been contrasted with the experimental results. It was observed that for all conditions studied a flow re-circulation zone appears down-stream of the step and is stable but not stationary. The temperature of the floor of the test section was increased up to 600 °C to explore the effect of buoyancy without the complexity of the reacting flow. Heating of the incoming flow lead to an increase in the dimensions of the re-circulation zone. However, de-stabilization of the flow did not occur. Comparison between the numerical and experimental results shows good qualitative agreement. The caracterization of the flame established behind the backward facing step was followed by a study of the re-ignition potential. The flame was extinguished by separating fuel from oxidizer by means of a plate which was impulsively removed and re-ignition observed. It was established that re-ignition is controlled by cooling and mass transport towards the hot plate. A "worst case scenario" for re-ignition is given by maximizing the fuel mass transfer while keeping the characteristic time for cooling of the fuel surface shorter than the characteristic time to attain a flammable mixture.

1. Introduction

Determination of the efficacy of a suppression agent has been the subject of many studies and an issue of renewed interest after the Montreal Protocol [1]. A general review of the current efforts and literature is provided by Hamins [2]. An area of great concern is that of aircraft where the use of Halon-1301 for fire suppression has been the norm [3]. Different environmentally friendly techniques are under development, among them are solid propellant gas generators.

A gas generator typically consists of a solid propellant tablet, which, upon ignition, rapidly reacts to generate gas phase combustion products and particulate, an igniter to initiate the combustion of the propellant, a filter system, and an exhaust mechanism. This element has been commonly used as a mechanism to inflate air-bags. The principal gas-phase product of the combustion process is nitrogen. Therefore, a logical extension to this technology is fire suppression [3].

If a flame is subject to a fast flow of nitrogen extinction might occur. The advantages of generating this fast flow by means of a solid propellant are many. It is compact, it has a very long storage and service life, it can be used in areas of difficult access, and the response time can be extremely fast. Also, this type of system is considered to have no ozone depletion or global warming potential. One of the main issues that have slowed the development of gas generators as a fire suppression technique is the lack of an adequate test protocol to assess their performance. Estimation of the reliability and efficiency

of this technique depends on a better understanding of the high-speed flow and the fundamental chemical and thermal processes involved in extinction and re-ignition of a fire.

Extinction mechanisms have been a subject of numerous studies and excellent reviews can be found in the literature. A good summary of the existing knowledge is provided by Williams [4]. The process of extinction can be described by means of the Damköhler number (Da=(Residence Time)/(Chemical Time)), by either reducing the residence time or increasing the chemical time a critical Damköhler number for extinction can be attained. The flow originating from burning a solid propellant can reduce the residence time (high velocity flow of products) and increase the chemical time (by directly altering the reactant concentrations, oxygen displacement effect or by decreasing the temperature of the pyrolysis and reaction zones) resulting in sudden extinction of the flame. Furthermore, the interaction between the flame and the flow, coming from the gas generator, can affect the turbulent structure of the system. Local stretch rates can be altered by the nitrogen rich flow resulting in local extinction zones. Depending on the geometry of the system, the type of flame, the characteristics of the gas generator and the distance between the gas generator and the flame the effects of each independent mechanism can be very different. Significant work on the interaction between flames and high speed flow has been reported in the past and have been reviewed by Williams [5] and Blazowski [6] but all the information pertains to scenarios that significantly differ from that of fire flame extinction.

A simple way to increase the residence time is by creating a recirculation zone by means of a backward facing step. This will significantly reduced the strain on the flame and thus provide a "worst case scenario" to test gas generators.

Consider the sudden onset of an enhanced velocity field past a given object. It can be observed that the transient conditions under which the object will continue to burn (or extinguish) differ little from those under which it will continue to burn (or extinguish) in a steady field of equal intensity and distribution. If the flame can not persist after the sudden onset of the velocity it is likely that it will not re-ignite once steady conditions are attained. Cooling down of the fuel will then follow [6]. In the case of solid propellant induced flows the extent and characteristics of the transient and steady state conditions depend on the geometrical configuration. The relative position of the fire with respect to the generator will significantly affect the development and structure of the flow. If the characteristic volume is very large compared to that of the fire and the gas flow induced by the generator, then the transient period will be very short and the flow field will regain its initial characteristics very fast. If the characteristic volume of the flow created by the gas generator is comparable to the volume of the room then a short transient period will be followed by a long steady period (flooding), in this case the flow field will not be expected to regain its initial characteristics. Obstructions in the path between the generator and the fire will significantly affect the velocity and distribution of the flow reaching the fire and will also affect the extent and nature of the transient process.

If flooding occurs it is expected that the critical Damköhler number will be attained permanently and cooling down of the fuel, which is a very slow process (when compared to the chemical and residence times of the flame), will follow. If both transient and steady periods are very short, first scenario depicted above, the flow conditions will provide a Damköhler number that will allow re-ignition if enough gaseous fuel can still be produced when the low velocities and high oxygen concentrations are re-instated [7,8]. Fuel pyrolysis will depend on the surface temperature. When burning, many materials will have a surface temperature much higher than the vaporization temperature (i.e. charring materials). Therefore, fuel pyrolysis will occur even after extinction of the flame. Comparison between the characteristic time of the flow induced by the gas generator and the characteristic cooling time becomes relevant and re-ignition becomes a significant issue when evaluating the performance of gas generators as a suppression mechanisms.

A strong theoretical basis on the areas of ignition and extinction exists but it has never been systematically applied to this type of scenario, therefore, there is a need to evaluate the accuracy of existing theories for a practical situation such as gas generator-fire flame interaction. Addressing all the issues presented is a formidable task that goes far beyond the scope of this study. Suppression is directly linked to the stability and aerodynamic characteristics of the re-circulation zone therefore this work

focuses on the aerodynamic characterization of the flow field behind the backward facing step. A characteristic length scale is defined and used as the main reference parameter. The variables studied are the imposed flow velocity, step height and surface temperature. Reacting flow experiments are conducted and correlated with the different flow conditions to describe the effect that the flow will have on the structure of the flame. Conditions leading to re-ignition are explored as a further parameter that will serve to characterize a "worst case" fire scenario.

2. Experimental Facility

The experimental set-up consists of a wind tunnel and a test section. The dimensions and characteristics of the wind tunnel are defined to guarantee a fully developed flow field, at the entrance to the test section, for all the experimental conditions studied. The test section incorporates a variable height step that can be varied from a step to duct ratio (H/D) of approximately 0.05 to 0.6. Figure 1, below, depicts a global view of the experimental setup where each component of the setup is labeled.
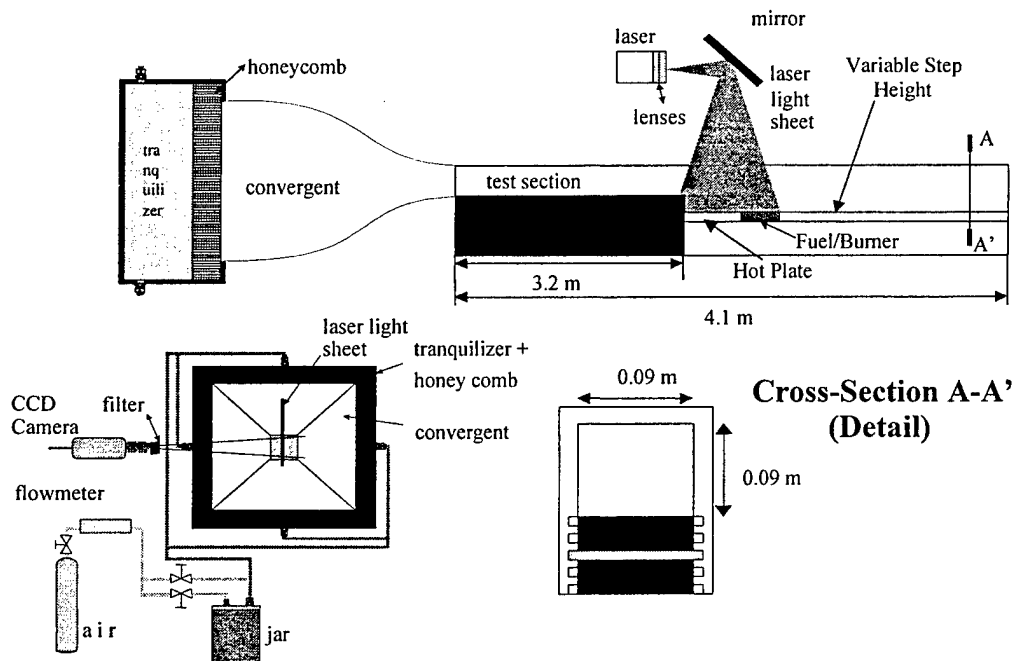
Figure 1 Schematic of the Experimental Apparatus

Air is fed from the compressor to the particle-seeding canister and then to the convergent. A valve from the compressor to the canister allows the mass flow of air to be controlled. From the valve the air flows through a pipe to a tube of diameter 12.7 mm which feeds into the canister. From the canister is another tube, which feeds into the convergent.

The convergent has an 8:1 ratio with a square inlet of dimension 0.72 m by 0.72 m by 0.30 m. A 50 mm thick honeycomb sheet is placed across the entire cross section to help disperse the flow and make it uniform. The convergent leads to a duct of cross section of 90 mm by 90 mm. The duct is 3.2 m long to allow the flow to become fully developed at the outlet.

The test section is attached to the outlet of the wind tunnel. The floor of the test section consists of a stainless steel sheet with dimension 0.090 m by 0.90 m. At the end closest to the wind tunnel outlet, pieces of the sheet can be removed. This creates room for the hot plate and the burner. Also, the step

height can be adjusted from being level to the bottom of the wind tunnel outlet to being 100 mm below the bottom of the wind tunnel outlet. The test section is made of an aluminum frame with glass sides and a glass top. The Robax glass used has a normal operating temperature up to 700°C for long-term usage and an extreme operating temperature of 800°C for short-term usage. It is highly transparent, which allows the laser beam to illuminate particles within the test section and the camera to view the images.

A hot plate is used to characterize the effects of buoyancy on the recirculation zone. The top layer of the hot plate is a sheet of copper. This 1 mm thick sheet fits exactly into the hole left by the removable piece from the stainless steel bottom sheet. Copper is used because of its high thermal conductivity leading to a homogeneous distribution of temperature across its entire surface. Three thermocouples are spaced evenly across the length of the copper plate, and a sheet of stainless steel is placed below them. The stainless steel sheet is resting on a thin layer of cement. Kanthal wire with a diameter of 0.25 mm is coiled evenly covering most of the surface area underneath the cement. An AC voltage source is attached to the ends of the Kanthal wire. The copper plate can reach temperatures up to 600 °C. A 20 mm thick insulation covering is placed below the wire. Total heat flux from the plate to the flow can be evaluated following the methodology presented in references [8,9].

The burner has a fuel inlet at the bottom. A 10 mm thick plate of sintered bronze is placed above the fuel inlet, and serves as a flow rectifier. Glass beads are placed over the bronze filling the inside of the burner. Finally, a lid made of 10 mm thick sintered bronze is placed on top. The lid is held in place with a high temperature gasket sealant. Two different fuels are used for these experiments, gaseous propane and liquid n-heptane. The same burner is used for both fuels.

A red Laser diode with maximum output of 0.5 watts provides a 60 mm by 1 mm thick light sheet. The light sheet is positioned such that the width is parallel to the flow direction of air. The sheet is, for most experiments, positioned at the center of the test section but it can be displaced towards the walls to observe three-dimensional structures.

A monochrome digital camera model 4910 from COHU, Inc. is used to capture the images. The camera resolution is 580 x 350. The electronic shutter is designed for an exposure of 1/60 seconds. A zoom lens with a narrow band filter is attached to the aperture of the digital camera. The zoom lens is attached to achieve a magnification of up to 10 times. For smoke visualization, the zoom lens is adjusted to observe the entire portion of the test section illuminated by the laser beam. Two different video cards are needed to operate the video processing camera and software properly. These cards are a Matrox Graphics Architecture video card and a PIXCI imaging board.

3. Experimental Results

Experiments have been conducted to characterize the re-circulation zone and establish a window of stability. Further experiments will use this window of stability to study the heat transfer mechanisms and the re-ignition process. Experiments have been conducted with step heights less than 55 mm and flow velocities ranging from (0.5 to 5.0) m/s. The flow temperature has been varied between 25 °C and 600 °C by means of the previously described hot plate.

3.1. Flow Visualization Methodology

Flow visualization was conducted by seeding the principal flow and illuminating the particles with a laser sheet. It was initially observed that the re-circulation zone pulsated at a well-established frequency that varied between (3 to 8) Hz, depending on the flow velocity. Entrainment of the seeded particles into the re-circulation zone was found to be weak. Fluctuations together with particle entrainment made visualization difficult. A number of traditional means of visualization were attempted (smoke generation, talc powder, etc.) with no success.

Kanthal wire was placed at the step and 3 mm above the surface. Beads of solder oil were distributed on the wire. Then the wire was heated electrically generating a smoke trace following the streamline closest to the surface. Clearly, the distance between the wire and the surface will represent a

Figure 2 - Sequence of smoke visualization images

minimum error inherent to this methodology. The region of interest was divided into 60 mm sub-sections, and as shown in Figure 2, the smoke traces was detected by means of the CCD camera. Fluctuations of the flow made an averaging process necessary, and the method used is described below.

A sequence of 25 images was captured by means of the EPIX XCAP Software. The images were treated independently, and each one was digitized to a gray level. The sequence was then averaged, and an assigned binary threshold value provided a black and white picture indicating the path of the smoke. The threshold had to be defined carefully since smoke traces changed with increasing distance from the step. At the beginning of the test section the smoke was concentrated in a narrow area (Figure 2), so a high threshold value was needed to obtain adequate contrast. Towards the end of the re-circulation zone the smoke was more dispersed, and a lower limit was needed to obtain a clear picture of the smoke. All sections were assigned several threshold values in the critical regions, and consequently, discrepancies in the manipulation process of the pictures were minimized.

By identifying the locus of the maximum intensity the borderline of the averaged re-circulation zone can be determined, and thus the averaged re-circulation zone length, X_r.

The averaged gray area can be further binarized to obtain the average amplitude of the fluctuations. Figure 3 shows the composition of a sequence of averaged images corresponding to the individual pictures of Figure 2. As can be observed, the flow fluctuates in the horizontal and vertical direction. The length and height of the re-circulation zone can be complemented by the amplitude of the fluctuation (ΔH_r, ΔX_r).
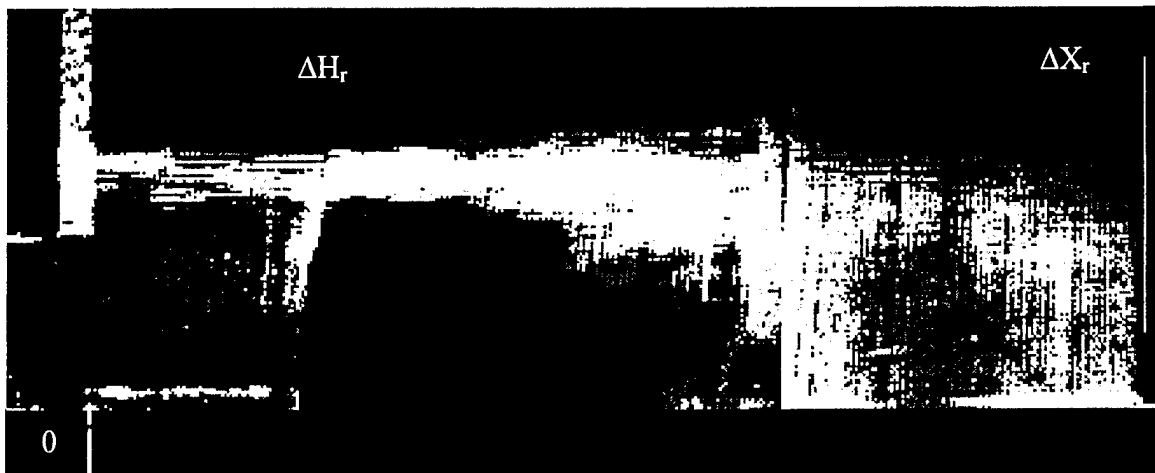

Figure 3 – Sequence of averaged images showing the extent of the re-circulation zone and corresponding to an airflow velocity of 1 m/s with a step height of 57 mm.

3.2. Flow-Visualization Experimental Results

Individual observation of each image obtained in a sequence showed that the re-circulation zone was stable but not stationary for all condition studied. The length and height of the re-circulation zone varied in a periodic fashion. The amplitude of the fluctuations was always less than 20 % of the characteristic length. This can be observed for the particular case presented in Figure 3. The frequency of the fluctuations varied from (3 to 8) Hz and depended on the flow velocity and the step-height. The flow was observed to re-attach after the re-circulation zone without noticeable periodic vortex shedding.
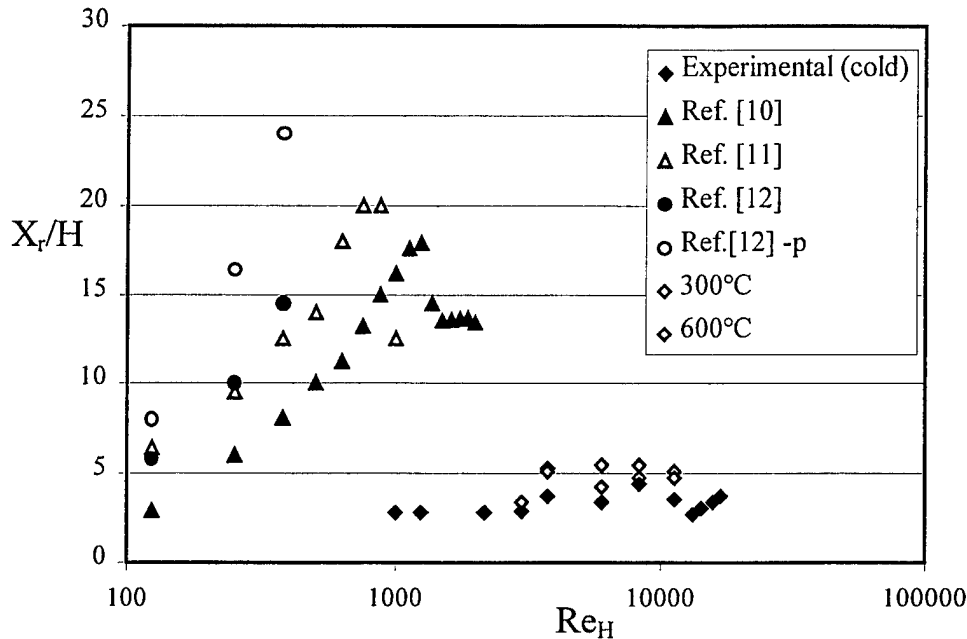

Figure 4 – Evolution of X_r/H as a function of Re_H.

Analysis of the average re-circulation zone showed a weak increase with the Reynold's number as shown in Figure 4. The values are normalized by the step height. Only representative values are presented to avoid overcrowding of the figure. The normalized characteristic length scale increases with Re_H until it reaches a maximum value. A further increase in Re_H leads to a decrease in the re-circulation zone length towards an almost constant value. Although the trends are similar to those previously reported in the literature [10-13], the characteristic length of the re-circulation zone is observed to be much smaller. This is not a surprising observation, since the geometry and characteristic flow velocities typical of this study are much smaller than those used in the references listed.

An increase in the surface temperature results in a larger re-circulation zone (both H_r and X_r) but the stability seems unaffected by the temperature increase. Data is presented for three temperatures: 25°C (ambient), 300 °C, and 600 °C. It can be observed that the surface temperature has a minor effect on the length of the re-circulation zone. Higher temperatures could not be attained due to melting of the Kanthal wire used in the heater.

3.3. Reacting Flow Experiments

Figure 5 shows the different regimes of the flame as a function of both propane flow rate and flow velocity. The images correspond to a step height set at 57 mm but can be generalized to other step heights. For low forced flow velocities and fuel injection the flame established in the re-circulation area is blue and seems to spin with the flow (Regime 1, Figure 5(a)). Increasing the fuel injection velocity or

the forced flow velocity increases the size of the flame and begins to show a yellow glow characteristic of diffusion flames (Regime 2, Figure 5(b)). The flame remains attached to the burner but as the forced flow and fuel injection velocities increase the flame is deflected towards the step (against the flow) indicating the dominant role of the recirculating flow (Figure 5 (c)). When this regime is fully established, the flame becomes attached to the edge of the step and it begins to detach from the burner surface. The entrainment velocity seems to have reached the blow-off limit at the trailing edge of the burner. Regime 3 corresponds to a flame attached to the edge of the step, but totally established at the interface of the main flow and the re-circulation zone. The flame is no longer attached to the burner (Figure 5(d)). The flame is yellow and characteristic of a diffusion flame.

Figure 6 shows the experimental conditions that delimit the three different regimes. An increase in the step height will result in attainment of Regime earlier. The border curves are displaced towards the origin. The burner is placed 100 mm downstream of the step. When the burner was placed closer the regimes were the same but transition towards the final condition was faster. Observation of the streamlines obtained from the smoke visualization showed that air entrainment occurred mostly at the downstream edge of the recirculation zone (Figure 3) therefore Regime 1 was enlarged by placing the burner in this region. It is important to note that the flame seems to displace towards the interface due to lack of oxidizer inside the re-circulation zone. Thus, entrainment seems to be the controlling mechanism behind the flame geometry.

Regime 2 corresponds to what Takahashi et al. [14] label Regime I, the flow limitations of the present configuration did not allow to migrate to their Regime II where enhanced oxidizer supply to the recirculation zone results in a wake stabilized flame. Takahashi et al. [14] do not report the presence of Regime 1 as observed in the present work.
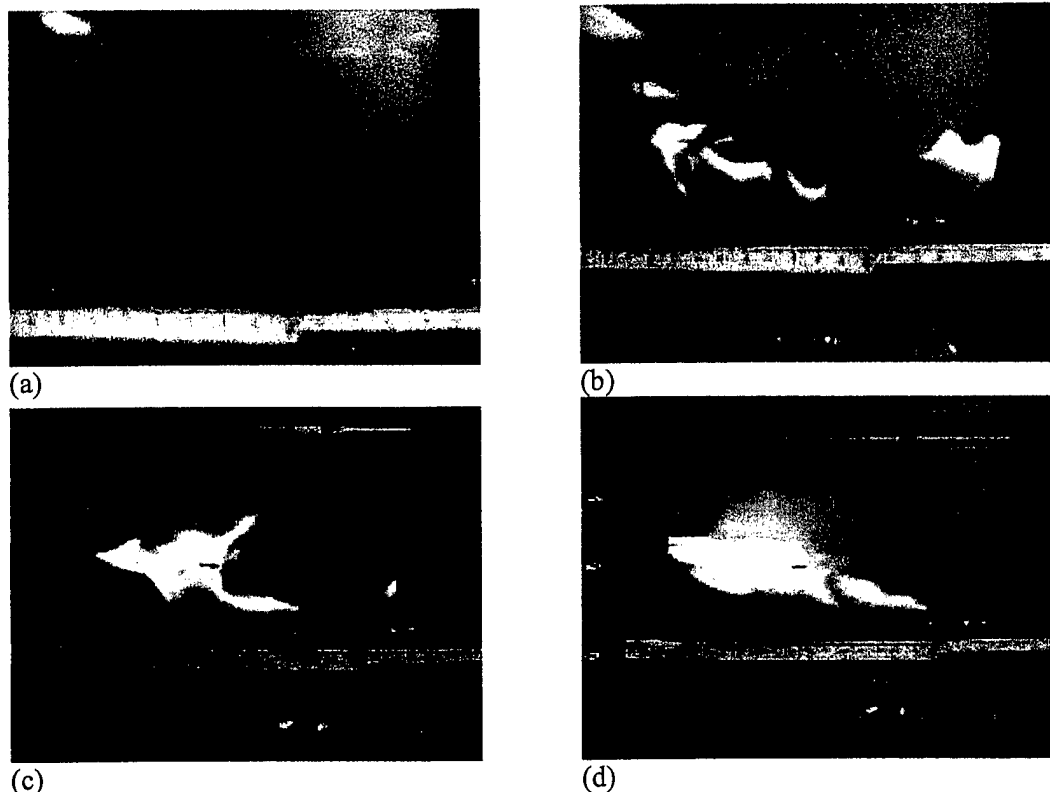

(a)   (b)   (c)   (d)

Figure 5   Sequence of images corresponding to the three different flame regimes observed.
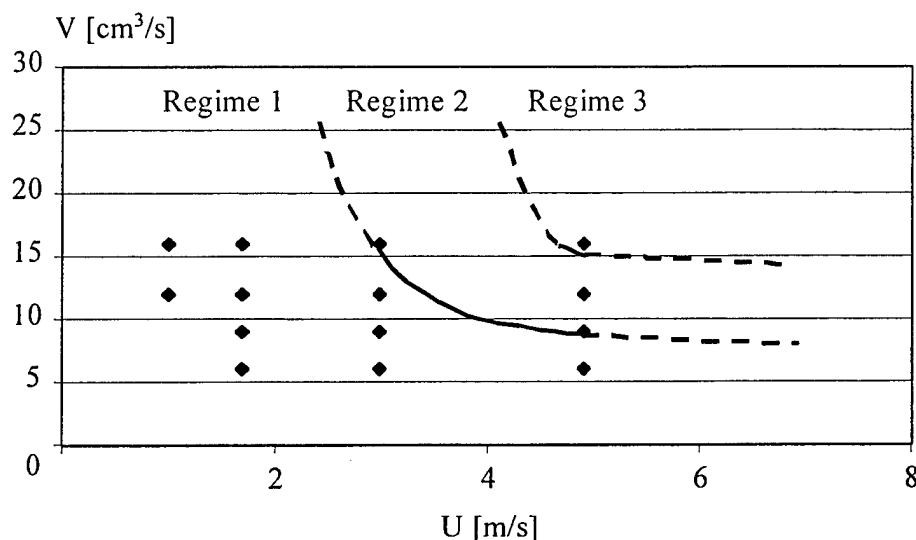
Figure 6 Different regimes of the flame, all tests presented were performed for a 57 mm step height.

3.4 Re-Ignition Experiments

3.4.1 Methodology

The experiments done with smoke and propane indicated that air entrainment towards the re-circulation zone controls the stability and characteristics of the flame therefore, after suppression, re-ignition can only occur upstream of the burner. Fuel and oxidizer will only be present in this region. The hot plate was therefore placed directly adjacent to the step, followed by the burner. This defined the "worst case" scenario for re-ignition. The length of the hot plate was defined based on the characteristic length of the re-circulation zone (X_r). Liquid n-heptane was used as fuel substitute even though jet fuel would have been a more relevant fuel. The quantitative results, thus, only correspond to n-heptane but the general observations can be generalized to other more relevant fuels. Jet fuel was avoided because of the large soot production characteristic of this fuel, which made visualization difficult. Again, experiments were conducted for different step heights, temperatures, and flow velocities. The n-heptane was delivered continuously by the means of a simple gravity tank that guaranteed a constant fuel level at the burner surface.

The experimental procedure was kept consistent for all tests. First the hot plate was heated until a constant temperature was achieved. Once the hot plate temperature varied less than 5 °C/min, supply of fuel and oxidizer was initiated together with data acquisition. At this point the flame was ignited. Finally, the fuel amount and the hot plate temperature were adjusted to be within the desired range.

The porous plate allows heat and fuel transfer to the interior enabling a slight variation of the fuel supply. This was evidenced in larger or smaller flames depending on the position of the gravity tank. The position of the gravity tank was varied within the possible range to allow for a study of the sensitivity of the present observations to the fuel supply.

The presence of the flame generated variations in the hot plate temperature therefore it was necessary to vary the current supply to the Kanthal wire and to wait until steady conditions were resumed.

The data collected during the experiments were temperature, re-ignition delay time, flow velocity, and step height. The temperature was measured with thermocouples placed at three different nodes along the length of the hot plate, where the one furthest from the step was located exactly between the hot plate and the burner frame. Time measurements were taken manually, and due to the uncertainty in the human reaction, recorded in integer values of seconds. The experiments were always run in whole sequences

ranging from 0.5-5.0 m/s at a temperature as consistent as possible. Thus, when something interfered during a sequence, a new sequence was started from scratch.

The auto-ignition temperature of n-heptane ($CH_3(CH_2)_5CH_3$) is 247.2°C [15]. Therefore, a temperature at the hot plate around 400°C was taken as a starting estimate for where re-ignition could occur. The location of the re-ignition point was established setting the origin at the step and with the positive direction following the principal flow direction.

3.4.2. Extinction Protocol

When the flow, the temperature, and the step-height were as specified for the test, the flame was extinguished by sliding a sheet of stainless steel over the burner. This separated fuel and oxygen, and consequently the flame could not sustain. The sheet was removed quickly immediately following visual observation of extinction. The time was recorded from the moment the plate was removed. Sometimes re-ignition occurred immediately, that is, as soon as the sheet was removed, indicating no re-ignition delay time. However, most of the time, there was a delay before re-ignition occurred. For certain combinations of fuel, flow velocity, and temperature the re-ignition delay time approached infinity. Details of these conditions will be presented later.

Here, re-ignition delays longer than forty seconds are considered to approach infinity. This time is significantly longer than any of the reported ignition delay times [16,17].

3.4.3. The Origin of Re-Ignition

To determine the locus of the re-ignition test sequences were videotaped and the re-ignition process was observed frame by frame. The images showed that re-ignition occurred always in the gas above the hot plate. Infra red-imaging of the test section showed no particular hot spots in any of the surfaces so local re-ignition was not considered. By comparing the infra-red data, it could be concluded that the temperature over the hot plate was (10 to 15) % higher than the temperature elsewhere.

3.4.4. Re-Ignition Results

For re-ignition to occur in this particular scenario, several different processes are necessary. The combustible surface needs to remain hot enough to continue producing gaseous fuel. The fuel vapor has to mix with the hot oxidizer gas and form a combustible mixture near the surface of the hot plate and the hot plate has to transfer sufficient heat to lead to initiation of a gas phase combustion reaction. Cooling down of the fuel surface, heat transfer from the hot plate and residence time of the fuel mixture inside the re-circulation zone are all controlled by the flow. The different experimental observations will be described in an attempt to isolate the controlling parameters of the re-ignition process to establish a worst case scenario.

The first experiments were done at a step height of 57 mm, this step height was chosen because it provided a stable re-circulation zone and flame for a broad range of flow conditions. At this height the flame is bright yellow for all flow velocities. For velocities lower than 2.5 m/s the flame flickers down the length of the tunnel, whereas the flame attaches to the tip of the step for higher velocities. Figure 7 shows the flame development as a function of velocity. This indicates a more significant mixing of fuel and oxidizer over the hot plate for the higher flow velocities.

The re-ignition delay times were fairly consistent for a step height of 57 mm, and with few discrepancies, all times were below 3 s. Table 1 contains sample data for a step height of 57 mm. Table 1 shows that the re-ignition delay increases for the low (u_∞ < 3 m/s) and high flow velocities (u_∞ >5 m/s). This pattern is consistent under different experimental conditions. As and example, Figure 8 shows the re-ignition delay time as a function of velocity at five different temperatures. It can be seen that although the above mentioned pattern remains constant the hot plate temperature does not have a consistent effect
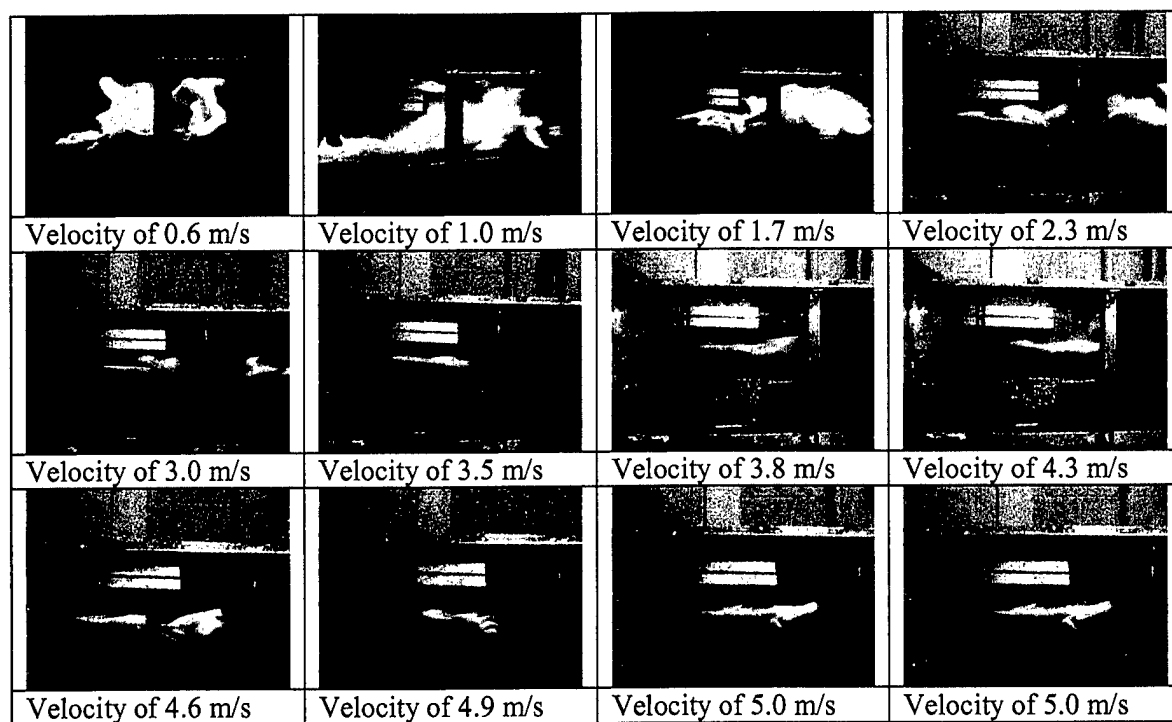
Velocity of 0.6 m/s	Velocity of 1.0 m/s	Velocity of 1.7 m/s	Velocity of 2.3 m/s
Velocity of 3.0 m/s	Velocity of 3.5 m/s	Velocity of 3.8 m/s	Velocity of 4.3 m/s
Velocity of 4.6 m/s	Velocity of 4.9 m/s	Velocity of 5.0 m/s	Velocity of 5.0 m/s

Figure 7   Flame development as a function of velocity for n-heptane

AIR FLOW VELOCITY [M/S]	TEMPERATURE [°C]	IGNITION DELAY TIME [S]
0.6	349	3
1	351	3
1.7	353	2
2.3	353	2
3	354	2
3.5	352	1
3.8	351	1
4.3	350	0
4.6	347	0.5
4.9	347	1
5	345	0
5	344	1.5
5	342	0
5	340	1.5

Table 1   Data sample for step height of 57 mm

on the ignition delay time. The differences seem to be within the experimental error, therefore an average for all different temperatures was taken and is presented in Figure 9.

These results suggest two primary, and competing, mechanisms that control the re-ignition process, convection and induction. The phenomenological explanation that will be provided here is consistent with arguments previously used when addressing ignition of condensed fuels [16,17].

The effect of convection is complex since in this particular case an increase in the flow velocity will result in an increase in the characteristic velocity within the re-circulation zone but will also increase the length of this region. Thus, variations in the characteristic velocity within the re-circulation zone will result in changes in the amount of fuel carried towards the hot plate at the fuel surface. An increase in the velocity will increase cooling at the fuel surface and also mass transfer. In contrast, the induction time can be described in easier terms therefore will be addressed first.

If the ignition temperature of the flammable mixture is assumed to be constant the induction time will only depend on the rate of heat transfer at the hot plate surface. So, if the hot plate has a finite length and constant temperature, a change in velocity will result in a decrease of the time available for the combustible mixture to attain the ignition temperature. The convective heat transfer coefficient being a function of $Re^{1/2}$ and the residence time an inverse function of the characteristic velocity. This effect was made obvious by re-ignition occurring closer and closer to the backward facing step as the velocity increased. The characteristic time available over the hot plate is of the order of a 0.1 s and thus falls within the experimental error, so proper quantification of this effect is not possible. Therefore, the main requirement for the hot plate has to be at a high enough temperature to deliver sufficient heat to the gas mixture faster than the characteristic residence time. In summary, if the induction time (time to for the flammable mixture to attain a temperature were heat losses are smaller than the heat generated by the chemical reaction) is smaller than the residence time (time that the flammable mixture remains over the hot plate) then re-ignition will occur. Definition of an appropriate Damkhöller number is therefore possible.

The above observations explain why the hot plate temperature needs to be much higher than the auto-ignition temperature of the fuel. The auto-ignition temperature of n-heptane is 247.2 °C [15] and as presented in Table 1 the re-ignition temperatures are always above 340 °C. Furthermore, this explains why the re-ignition delay times are not sensitive to the hot plate temperature.

The specific geometry used is responsible for the re-ignition temperature, therefore it is of great importance to note that, for the present configuration, an increase in the plate length should result in a decrease in the re-ignition temperatures only if the flammable mixture supplied from the burner remains constant. Since the flammable mixture is determined by the effects of the re-circulation zone on the burner (as will be detailed later) and this is linked to the flow conditions, and increase in the burner length will not necessarily speed re-ignition. The results presented above correspond to what was found to be the "worst case scenario" and were chosen for presentation because they provided the broadest range of re-ignition conditions.

The above observations justify neglecting the induction time and averaging the data for different hot plate temperatures, as presented in Figure 9. Is in this context that the effect of convection on the fuel surface will be analyzed.

Fuel supply towards the hot plate is controlled by two competing mechanisms, mass transfer and heat transfer at the fuel surface. For low flow velocities the fuel concentration reaches the lean flammability limit before cooling of the fuel surface has been reached, for high flow velocities the fuel surface cools down before the lean flammability limit has been attained.

For $u_\infty < 4$ m/s, mass transfer from the fuel surface to the gas flow controls the re-ignition delay time. Mass transfer is also a function of $Re^{1/2}$ therefore increases with the flow velocity. When the plate covers the fuel the re-circulation zone is filled with air and the fuel is washed away. So when the plate is removed fuel starts migrating towards the hot plate but it will not ignite until the gas phase mixture attains the lean flammability limit. If the induction time can be neglected ignition will occur at this point. Transport of fuel is proportional to the flow velocity therefore the re-ignition time will decrease as the flow velocity increases.
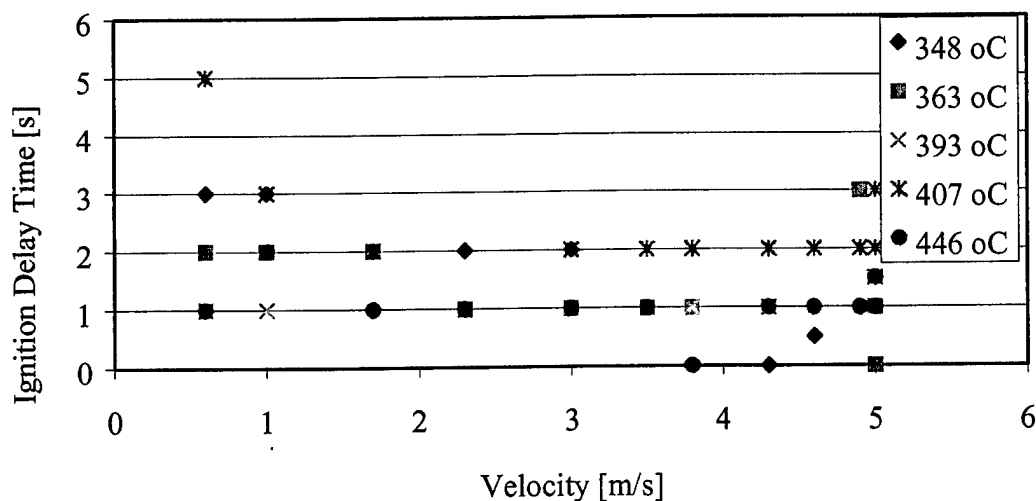
Figure 8 Ignition Delay Time as a Function of Velocity at Different Temperatures for a step height of 57 mm.

For $u_\infty > 4$ m/s, cooling of the fuel surface is the controlling mechanism. Convective heat transfer is also proportional to $Re^{1/2}$ therefore cooling of the fuel surface will be enhanced as the flow velocity increases. The fuel vaporization rate can be considered to follow an Arrhenius law therefore the decrease of the fuel mass flux can be expected to be more abrupt as the surface temperature decreases. The re-ignition delay time is expected to increase abruptly as the velocity increases. A threshold will be attained beyond which the fuel will cool before the lean flammability limit can be attained. The averaged data presented in Figure 9 serves to validate this phenomenological explanation. As observed in Figure 9, re-ignition can not be accomplished for $u_\infty > 5$ m/s.
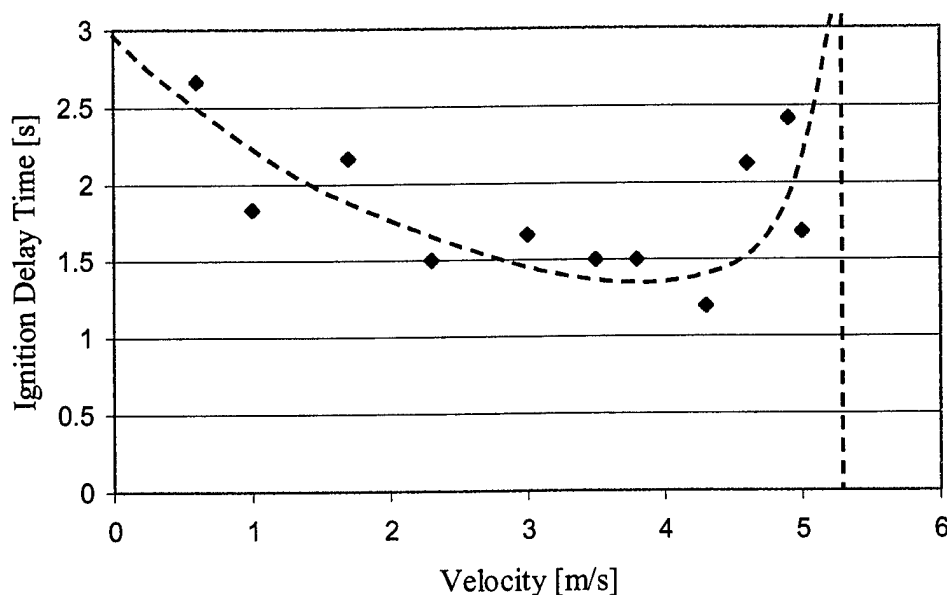

Figure 9 Average Ignition Delay Time as a Function of Velocity

The 57 mm step height corresponded to the shortest re-ignition delay times. If the step height decreases the re-ignition delay times increase significantly because the re-circulation zone ends before the trailing edge of the burner, therefore it requires more time to achieve a flammable mixture. The results at a step height of 32 mm are presented in Figure 10. At flow velocities higher than 4 m/s, the ignition delay time approached infinity (as defined previously) for all temperatures. This maximum flow velocity is lower than that for 57 mm indicating again a minimum evaporation rate necessary to attain a flammable mixture before cooling of the fuel surface dominates. A decrease in the area contributing fuel results in a decrease in the total amount of fuel inside the re-circulation zone, therefore a higher evaporation rate is necessary. At 19 mm, the lowest step height tested, the ignition delay time approached infinity for all flow velocities and all temperatures (as high as 530°C) tested. Similar results can be obtained for larger step heights where the re-circulation zone ends down-stream of the trailing edge of the burner, thus entrains significant amount of excess air before the fuel enter the re-circulation zone.
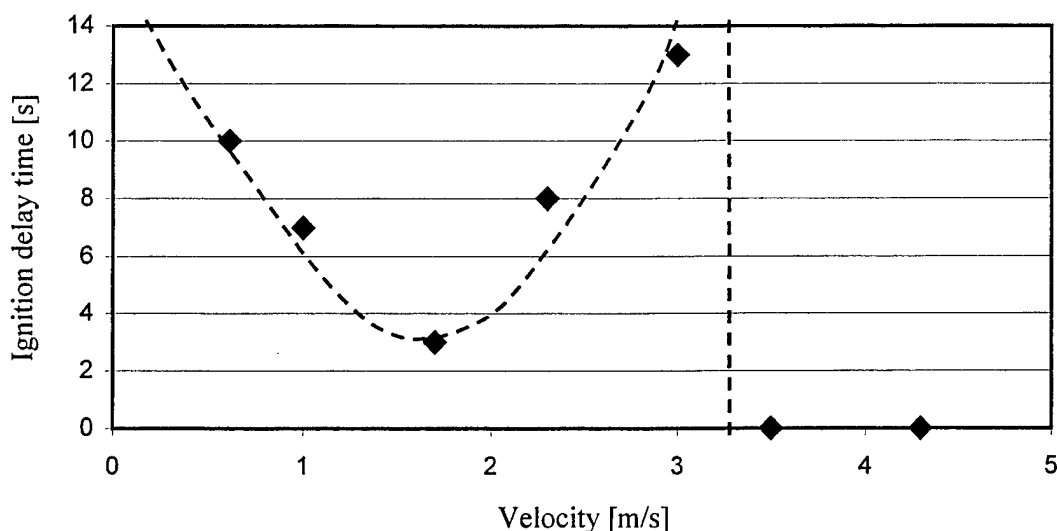

Figure 10   Ignition delay time as a function of flow velocity for a step height of 32 mm, and a temperature of 440 °C

4. Numerical Modeling

The code LES-3D [18] has been implemented on both a Pentium II PC Computer and a DEC-Alpha workstation. Tecplot and Smoke-View provide a visual interface for LES-3D. The code has been used to model the experimental conditions described above. Emphasis has been given to the study of the cold flow. Only a brief summary of this work can be found in reference [19].

Work has focused on using large eddy simulation to model the dynamics taking place in the wind tunnel. Initial work with the code utilized a control volume approach to look at velocity. The boundaries of the computational field were defined as a constant cross section rectangular prism having the dimensions of the actual test section portion of the apparatus. The dimensions of the prism were 0.090 m wide, 0.90 m long and 0.15 m high. The air flowed along the length of the prism. Mass entered normal to the inlet cross sectional area through an 0.090 m by 0.090 m vent extending downward from the top of the prism, and exited through a 0.090 m by (0.090 + H) m vent, where "H" is the step height.

4.1. Preliminary Validation

Prior to running simulations through a mock-up of the test section, a straight 0.90 m duct was modeled with the cross sectional dimensions of the inlet. Specifying a fully developed velocity profile, initial simulations were executed to determine whether both non-slip boundary conditions were preserved, and y- and z- velocities vanished across the domain for a 1.0 m/s flow travelling the length of the duct. This did hold true. Centerline velocities decayed as predicted terminating at the walls. Profiles generated from velocity sampling routines indicated that the flow was symmetric about the y- and z- axes. Likewise, speeds decayed as expected as they traveled down the duct.

4.2 Entry Profile

To generate a computerized flow scenario that could be compared to that moving through the actual apparatus, a means of representing the velocity profile in the coding was necessary. This was done by varying slip conditions, alternating between pre-set velocity profiles (top hat or parabolic), and changing the length of the inlet into the test section. The hope was to generate inlet conditions at the test section entrance that matched the flow through the actual apparatus and accurately predicted the size of the re-circulation zone. An inlet section was added into the computational field by constructing an obstacle a few centimeters into the rectangular prism representing the test section. The test section itself was extended such that the length of the duct after the step remained 0.90 m in length. It was discovered that changes in these parameters significantly changed the length of the average re-circulation zone (X_r). The end of the average re-circulation zone is defined as the location of a zero horizontal velocity vector. A list of the different Test cases is presented in Table 2.

Table 2 shows quantitative differences on the average re-circulation zone length between the different initial conditions studied. The average re-circulation zone length is influenced by the nature of the incoming flow. Allowing the flow to develop (x=-0.25 m and x=-0.90 m) results in a change in the size of the average re-circulation zone that is not a direct function of the developing distance. It was found that beyond x=-0.90 m the average re-circulation zone attained a constant length. The boundary condition (slip, partial-slip, and non-slip) affected the development of the flow, and consequently X_r. A non-slip boundary condition resulted in a shorter developing distance, thus was preferred. Imposing a parabolic profile or specified volume condition at the inlet also had a significant effect on X_r, in both cases the developing distance was much larger than for the Top-Hat profile.

Velocity measurements were compared with the predictions of the LES-3D code for a Top-Hat profile placed at x=-0.90 m. The results are presented in Figure 11. As it can be observed, the velocity

elocity rofile	lip ondition	nlet ength	r	upplied	enterline nlet elocity	verage xit elocity
op Hat	artial	.00 m	.40 m	.0 m/s	.00 m/s	.6 m/s
op Hat	artial	0.25 m	.45 m	.0 m/s	.08 m/s	.7 m/s
op Hat	artial	0.90 m	.43 m	.0 m/s	.13 m/s	.7 m/s
op Hat	on-slip	0.90 m	.41 m	.0 m/s	.30 m/s	.7 m/s
arabolic	artial	.00 m	.40 m	.5 m/s	.50 m/s	.3 m/s
arabolic	artial	0.25 m	.32 m	.5 m/s	.30 m/s	.5 m/s
arabolic	on-slip	0.90 m	.37 m	.5 m/s	.32 m/s	.5 m/s
ol. Flux pecified	on-slip	0.90 m	.46 m	.0 m/s	.08 m/s	.7 m/s

Table 2   Test cases for a specific characteristic inlet velocity of 1.0 m/s and 1.5 m/s.

profile predicted by the LES-3D code corresponds better to that measured for a laminar flow (0.8 m/s), the flattening of the profile, characteristic of initiation of turbulence is not well captured. Vector profiles of the flow were produced in the straight duct study. Top hat flows were found to develop turbulent profiles after travelling 0.40 m. The boundary layer thickness of the profile, however, was slightly greater than what one usually observes for turbulent flows. The speed remained constant by the time it had traveled 0.90 m, a distance equivalent to the entire length of the test section for both the partial and non-slip scenarios.
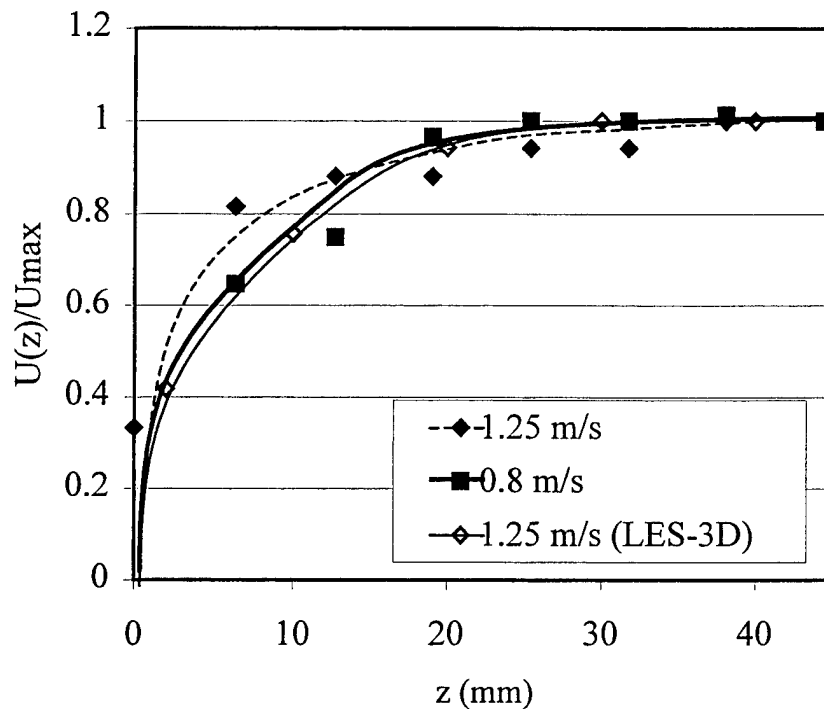

Figure 11   Comparison of normalized velocity profiles

For the particular conditions presented here the experimental re-circulation zone was 0.29 m, as measured with particle laser imaging in the wind tunnel with the same inlet flow speed. Some of the discrepancy in the length of X_r measured in Tecplot could be attributed to averaging of pulsing re-circulating fluid particles behind the step.

As a result, we chose to simulate the problem with the LES-3D/IFS code as a top hat flow through a 1.80 m rectangular prism with non-slip surfaces that featured a 0.90 m obstacle to represent the duct inlet. Consequently, flows were permitted to develop fully and naturally prior to entering the test section. The LES-3D permits the user to specify a velocity profile. Nonetheless, defining an exact equation U (x) for the entire domain of the rectangular closed surface would be an arduous task of questionable value, given the gross nature of the physically measured profile at the walls. Typical profiles for turbulent flows such as $u_{avg.} \propto (y/\delta)^{1/7}$ [10] fail to give reasonable approximations of experimental results near the wall. Running the 1 m/s top hat non-slip flow through the step model yielded a 0.41 m re-circulation zone.

4.3 Re-circulation Zone length (X_r)

The variation in the re-circulation zone length and stability was determined and is presented in Figure 12. All the different step heights assigned were less than 55 mm high. The numerical predictions
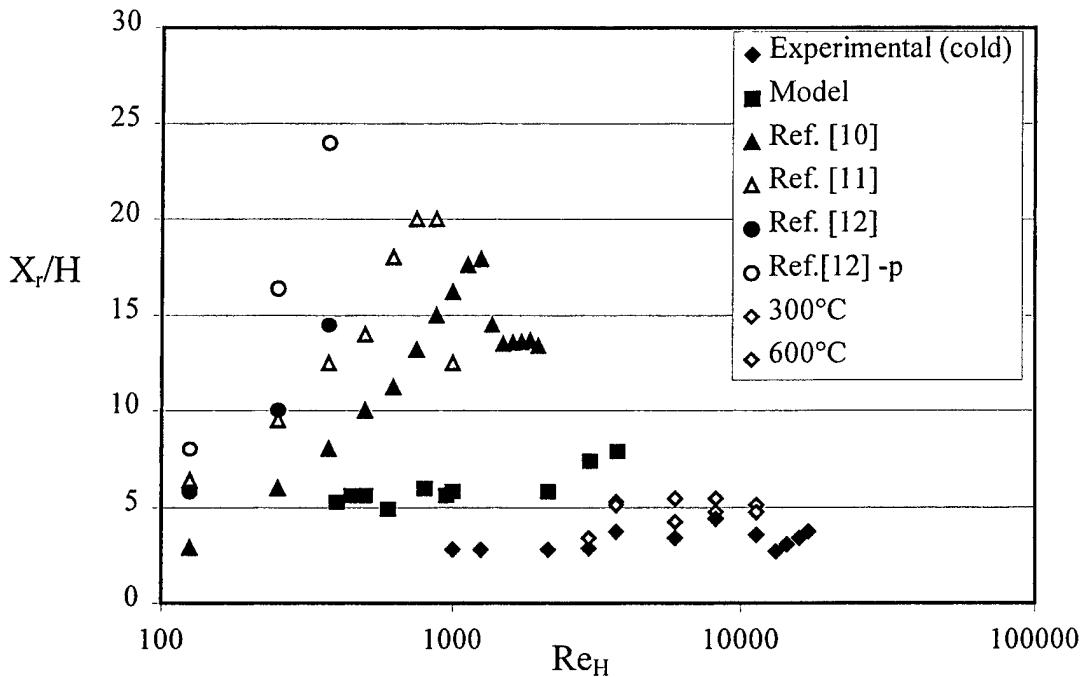
Figure 12 Normalized re-circulation zone length scale as a function of Re_H.

underestimate the data from the literature but the trends correspond well to those observed experimentally.

The experiments available in the literature were conducted under conditions very different from those of the present experiments. In general, velocities were much higher and the aspect ratio significantly larger. The average re-circulation zone does not provide any evaluation of the stability of the re-circulation zone. Therefore, an analysis of the time dependent velocity was conducted to identify vortex shedding.

Velocity measurements were made 76 mm apart down the centerline of the simulated test section at four different heights: test section floor (0 mm), mid-step height (28.6 mm), step height (57.2 mm), and mid inlet (102.1 mm). Time dependent velocity measurements are presented in Figures 13 and 14 for two different positions along the duct. Figure 13 shows the velocity evolution at the inlet. A cross section at a distance smaller than X_r is shown on Figure 14. Strong fluctuations of the velocity around the mean value can be observed. The velocity measurements inside the re-circulation zone are characterized by negative values and by a mean value much smaller than the main flow. Beyond the re-circulation zone (Figure 14) the fluctuations decrease in magnitude and there is a total absence of negative velocities. The absence of negative values and the homogeneity of the flow seem to imply an absence of vortex shedding.

It was assumed that the re-circulation zone would be demarcated by the position where one duct-floor measurement resulted in a negative velocity and its downstream neighbor measured a positive velocity. Pulsing therefore should be traceable by watching where this negative-to-positive phenomenon occurs and noting whether it sweeps back and forth across the computational domain. The LES-3D code was set to take instantaneous measurement of velocity along the duct floor and produce a data file of the speeds recorded as a function of time. It was determined that X_r/H varies from 4 to 12 with a mean value of approximately 6, with these being independent of the Reynolds number. Although larger than the fluctuations observed experimentally these perturbations seem to follow similar trends.
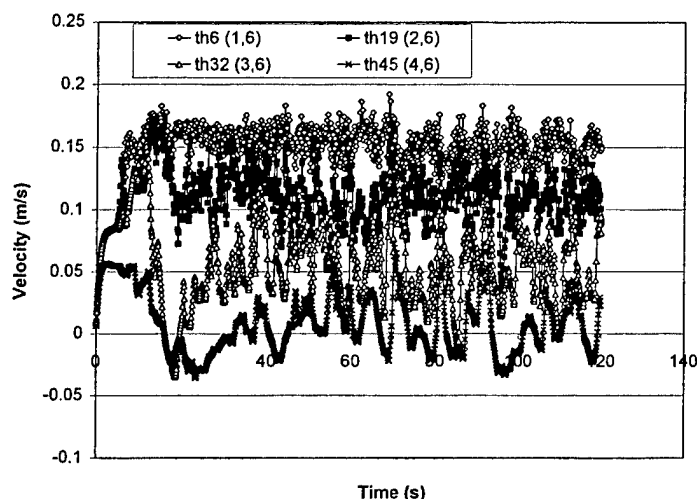
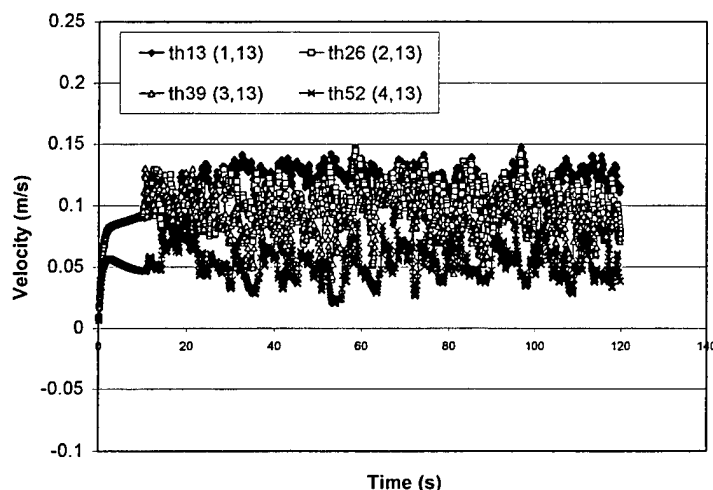**Figure 13** – Time evolution of the velocity for Re=600 measured at x=0.381 m

Figure 14 – Time evolution of the velocity for Re=600 measured at x=0.914 m

5. Conclusions

A systematic evaluation of the stability of a re-circulation zone behind a backward facing step has been conducted. The parameters studied have been the flow velocity, step height, and temperature. Numerical modeling using LES-3D has been contrasted with the cold flow experimental results. It can be concluded that:

- The re-circulation zone is stable but not stationary for all conditions studied.
- Fluctuations occur, and the amplitude is comparable to the step-height. Amplitude and frequency are functions of the velocity and step height.
- Buoyancy has only a minor de-stabilizing effect. Flow temperatures were increased up to 600°C. This increasing the dimensions of the re-circulation zone, without de-stabilizing the flow.
- Comparison between the numerical and experimental results shows good qualitative agreement. The code tends to over-predict the size of the re-circulation zone.
- Numerically simulations showed that the entry profile has a significant effect on the length and characteristics of the re-circulation zone.

- Three different regimes have been established. For low oxidizer and fuel velocity the flame is established inside the re-circulation zone and resembles a premixed flame.
- As the velocities increase the flame undergoes a transitional regime and finally establishes itself at the boundary between the main flow and the re-circulation flow.In this third regime the flame is anchored at the edge of the step.
- Air entrainment seems to determine these three different regimes.
- The worst case scenario for suppression seems to correspond to the regime where the flame is attached to the leading edge and established in the mixing layer between the re-circulation zone and the main flow.
- Re-ignition is controlled by cooling and mass transport towards the hot plate. A "worst case scenario" for re-ignition is given by maximizing the fuel mass transfer while keeping the characteristic time for cooling of the fuel surface shorter than the characteristic time to attain a flammable mixture.
- The worst case scenario is characterized by a minimum re-ignition time.

6. References

1. The 1987 Montreal Protocol on Substances that Deplete the Ozone Layer, as adjusted and amended by the Second Meeting of the Parties (London, June, '90) and by the 4th Meeting of the Parties (Copenhagen, Nov., '92) and further adjusted by the 7th Meeting of the Parties (Vienna, Dec., '95).
2. Hamins, A. "Aspects of Flame Suppression," NIST-IR-5766, 1995.
3. Yang, J.C. and Grosshandler, W.L., "Solid propellant Gas Generators: Proceedings of the 1995 Workshop," 1995.
4. Williams, F.A., *Combustion Theory*, The Benjamin/Cummings Publ. Company, Inc., 2nd Ed., 1985.
5. Williams, F.A., *Applied Mechanics Surveys*, Abramson, H.N., Liebowitz, H., Crowley, J.M. and Juhasz, S. (Eds.), Washington D.C., Spartan Books, 86-91, 1966.
6. Blazowski, W.S., *Progress in Energy and Combustion Science*, **4**, 177, 1978.
7. Fendell, F.A., *Journal of Fluid Mechanics*, **21**, 281-303, 1965.
8. Fendell, F.A., *Chemical Engineering Science*, **22**, 1829-1837, 1967.
9. Ingason, H. and deRis, J., "Flame Heat Transfer in Storage Geometries," Department of Fire Safety Engineering Report, LUTVDG/TVBB-1013, Lund University, Sweden, 1996.
10. Munson, B.R., Young, D.F. and Okiishi, T.H., "Fundamentals of Fluid Mechanics," Third Edition, John Wiley & Sons, Inc., pp.577, 1998.
11. Armaly, B.F., Durst, F., Pereira, J.C.F., Stoning, B. "Experimental and theoretical investigation of backward-facing step flow," J. Fluid Mech., **127**, pp.473-496, 1983.
12. Sinha, S.N., Gupta, A. K., Oberai, M.M., "Laminar separating flow over backsteps and cavities, Part I: Cavities," AIAA J., **19**, pp.1527-1530, 1981.
13. Denham, M.K., Patrick, M.A., "Laminar flow over a down-stream facing step in a two-dimensional flow channel," Trans. Inst. Chem. Engrs. **52**, pp.361-367, 1974.
14. Takahashi, F., Schmoll, W.J., Strader, E.A. and Belovich, V.M., "Suppression of a Nonpremixed Flame Stabilized by a Backward Facing Step," *Combustion and Flame*, **122**, pp.105-116, 2000.
15. Kanury, M., "Ignition of Liquid Fuels", *The SFPE Handbook of Fire Protection Engineering*, 2nd Edition, NFPA, Quincy, 1995
16. Niioka, T., "Ignition time in the stretched-flow field", Eighteenth Symp. (Intl) on Combustion, 1981
17. Fernadez-Pello, Carlos, "The Solid Phase", *Combustion Fundamentals of Fire*, Academic Press Ltd.,1995
18. McGrattan, K.B., Baum, H.R. and Rehm, R.G. "Large Eddie Simulation of Fire Phenomena," NIST Internal Report, Gaithersburg, Maryland, 1997.
19. DuBois, J., "Evaluation of a Large Eddy Simulation's Applicability to a "Worst Case" Fire Scenario" MS Thesis, University of California, Berkeley, California, December 1999.